

Air Force Institute of Technology

AFIT Scholar

Theses and Dissertations

Student Graduate Works

3-2004

An Investigation Relating Longitudinal Pilot-Induced Oscillation Tendency Rating to Describing Function Predictions for Rate-Limited Actuators

Joel B. Witte

Follow this and additional works at: <https://scholar.afit.edu/etd>



Part of the [Aerospace Engineering Commons](#)

Recommended Citation

Witte, Joel B., "An Investigation Relating Longitudinal Pilot-Induced Oscillation Tendency Rating to Describing Function Predictions for Rate-Limited Actuators" (2004). *Theses and Dissertations*. 3934. <https://scholar.afit.edu/etd/3934>

This Thesis is brought to you for free and open access by the Student Graduate Works at AFIT Scholar. It has been accepted for inclusion in Theses and Dissertations by an authorized administrator of AFIT Scholar. For more information, please contact AFIT.ENWL.Repository@us.af.mil.



**AN INVESTIGATION RELATING LONGITUDINAL PILOT-INDUCED
OSCILLATION TENDENCY RATING TO DESCRIBING FUNCTION
PREDICTIONS FOR RATE-LIMITED ACTUATORS**

THESIS

Joel B. Witte, Major, USAF
AFIT/GAE/ENY/04-M16

**DEPARTMENT OF THE AIR FORCE
AIR UNIVERSITY**

AIR FORCE INSTITUTE OF TECHNOLOGY

Wright-Patterson Air Force Base, Ohio

APPROVED FOR PUBLIC RELEASE; DISTRIBUTION UNLIMITED

The views expressed in this thesis are those of the author and do not reflect the official policy or position of the United States Air Force, Department of Defense, or the United States Government

AFIT/GAE/ENY/04-M16

AN INVESTIGATION RELATING LONGITUDINAL PILOT-INDUCED
OSCILLATION TENDENCY RATING TO DESCRIBING FUNCTION
PREDICTIONS FOR RATE-LIMITED ACTUATORS

THESIS

Presented to the Faculty

Department of Aeronautics and Astronautics

Graduate School of Engineering and Management

Air Force Institute of Technology

Air University

Air Education and Training Command

In Partial Fulfillment of the Requirements for the
Degree of Master of Science in Aeronautical Engineering

Joel B. Witte, BS

Major, USAF

March 2004

APPROVED FOR PUBLIC RELEASE; DISTRIBUTION UNLIMITED.

AFIT/GAE/ENY/04-M16

AN INVESTIGATION RELATING LONGITUDINAL PILOT-INDUCED
OSCILLATION TENDENCY RATING TO DESCRIBING FUNCTION
PREDICTIONS FOR RATE-LIMITED ACTUATORS

Joel B. Witte, BS
Major, USAF

Approved:

Bradley S. Liebst (Chairman)

date

Richard G. Cobb (Member)

date

Russell G. Adलगren (Member)

date

Abstract

The purpose of this study was to investigate pilot-induced oscillations (PIO) and determine a method by which a PIO tendency rating could be predicted. In particular, longitudinal PIO in the presence of rate-limited actuators were singled out for examination. Sinusoidal input/triangular output describing function techniques using Nichols charts were used. A new criterion dubbed *Gap Criterion* was calculated for PIO sensitivity. This criterion consists of the product of additional pilot gain and the normalized maximum amplitude of the commanded actuator necessary to cause PIO. These results were paired with simulator and flight test PIO tendency rating data. The PIO rating scale used was the PIO tendency classification of MIL-HDBK-1797. This concept was applied to two historical test databases, HAVE PREVENT and HAVE OLOP. Additional PIO data was gathered in the Large Amplitude Multimode Aerospace Simulator (LAMARS) at the Air Force Research Laboratory (AFRL), Wright-Patterson AFB, Ohio and the USAF NF-16D Variable In-flight Stability Test Aircraft (VISTA) at Edwards AFB, California. Correlation between PIO tendency rating and *Gap Criterion* was determined for each dataset. Most datasets exceeded a confidence level of 95% that a correlation existed. Follow-on analysis for better curve fitting was accomplished; a logarithmic fit was judged best. Datasets were combined with success to demonstrate the universality of the *Gap Criterion* for correlating PIO tendency ratings for longitudinal PIO involving rate-limited actuators.

Acknowledgements

The Air Force Institute of Technology and the United States Air Force Test Pilot School cosponsored this study. I would like to thank the following people for their efforts and contributions: My thesis advisor, Dr Brad Liebst, who proposed this study and offered key insights; Mr. Andy Markofski and Mr. Mike Steen of General Dynamics Advanced Information Systems who programmed the aircraft dynamics for the VISTA NF-16D; the VISTA maintenance team who worked miracles to return the aircraft to flying status; Major Russ Adelgren and Mrs. Cynthia Roell, who made sure the flight test portion succeeded and Mr. Curt Clark and Mr. Jeff Slutz who worked diligently to ready the LAMARS simulator for the simulator test portion.

I'd especially like to thank the members of the MAX GAP test team who made this project succeed: Captain Erik Monsen, Royal Norwegian Air Force; Captain Thomas Washington, USAF; Captain Kris Cowart, USAF and Captain Rich Salasovich, USAF. I'd also like to thank Major James Less, our Test Pilot School staff sponsor, and Major Rick Palo who survived multiple PIO sorties as safety pilot in the VISTA F-16.

Most importantly, I'd like to thank my wife for her support, love and understanding through the trials of the past two and a half years.

Table of Contents

	Page
Abstract.....	iv
Acknowledgements.....	v
Table of Contents.....	vi
List of Figures.....	ix
List of Tables.....	xv
List of Notations and Symbols.....	xvii
I. Introduction.....	1-1
General.....	1-1
Background.....	1-2
PIO Defined.....	1-2
PIO History.....	1-4
PIO Categories.....	1-6
PIO Category II.....	1-7
PIO Scales.....	1-8
PIO Prediction Methods.....	1-10
Gap Criterion.....	1-11
Objectives.....	1-11
Approach.....	1-12
Scope.....	1-12
II. Theory.....	2-1
Describing Function Development.....	2-1
Saturation Nonlinearity Describing Function.....	2-3
Closed Loop Describing Function Approximation.....	2-4
Sinusoidal Input/Triangle Output Describing Function Approximation.....	2-7
Applying Describing Function Results to Predict PIO.....	2-11
Pilot Model.....	2-13
<i>Gap Criterion</i>	2-16
Gap Criterion Formulation.....	2-17
Type I.....	2-19
Type II.....	2-20
Type III.....	2-21
Type IV.....	2-21

	Page
Example of <i>Gap Criterion</i> Application	2-21
III. Analysis of Selected Historical Data	3-1
HAVE PREVENT Analysis	3-1
Gap Criterion Calculation for HAVE PREVENT Datasets.....	3-4
HAVE PREVENT Gap Criterion Summary.....	3-7
HAVE PREVENT Gap Criterion Correlation.....	3-8
HAVE PREVENT Best Curve Fit.....	3-11
HAVE OLOP Analysis.....	3-14
Gap Criterion Calculation for HAVE OLOP Datasets.....	3-15
HAVE OLOP Gap Criterion Summary.....	3-19
HAVE OLOP Gap Criterion Correlation.....	3-19
HAVE OLOP Best Curve Fit.....	3-21
HAVE PREVENT and HAVE OLOP Summary	3-24
IV Analysis of Project MAX GAP (LAMARS) Data	4-1
MAX GAP (LAMARS) Analysis.....	4-1
Gap Criterion Calculation for MAX GAP (LAMARS) Datasets.....	4-2
MAX GAP (LAMARS) Gap Criterion Summary.....	4-5
MAX GAP (LAMARS) Gap Criterion Correlation.....	4-5
MAX GAP (LAMARS) Best Curve Fit.....	4-8
MAX GAP (LAMARS) Summary	4-11
V. Analysis of Project MAX GAP (VISTA) Data.....	5-1
MAX GAP (VISTA) Analysis.....	5-1
Gap Criterion Calculation for MAX GAP (VISTA) Datasets.....	5-2
MAX GAP (VISTA) Gap Criterion Summary.....	5-6
MAX GAP (VISTA) Gap Criterion Correlation.....	5-6
MAX GAP (VISTA) Best Curve Fit.....	5-8
MAX GAP (VISTA) Summary	5-10
VI. Analysis of Combined <i>Gap Criterion</i> Data.....	6-1
LAMARS Combined Datasets	6-1
VISTA Combined Datasets	6-3
LAMARS and VISTA Combined Dataset Correlation	6-4
Combined Dataset Analysis and Observations.....	6-5
VII. Conclusions	7-1

	Page
Appendix A. Matlab/Simulink™ Code	A-1
Appendix B. State-Space Matrices for Project MAX GAP	B-1
Appendix C. Correlation Computation	C-1
Appendix D. MAX GAP Histograms	D-1
Bibliography	BIB-1
Vita.....	VITA-1

List of Figures

Figure	Page
1-1. YF-22A Accident Sequence (Hodgkinson, 1999:128).....	1-4
1-2. Actuator Saturation Example Using an Input = $A \sin(\omega_i t)$	1-8
1-3. Simulink TM Actuator Model	1-8
1-4. PIO Tendency Classification (MIL-HDBK-1797, 1997:152).....	1-9
2-1. Example of a Nonlinear System	2-1
2-2. Saturation Nonlinearity and the Corresponding Input-Output Relationship (Slotine and Li, 1995:173).....	2-3
2-3. Actuator Model Development (Klyde and others, 1995:22)	2-5
2-4. Closed Loop Actuator Transfer Function Diagram.....	2-6
2-5. Rate-Limiting Input and Output (Klyde and others, 1995:42-46).....	2-8
2-6. Describing Function Phase Angle Comparison.....	2-10
2-7. Pitch Tracking Closed Loop System	2-11
2-8. Simplified Pitch Tracking Closed Loop System	2-11
2-9. Neal-Smith Pilot Model Constraints.....	2-15
2-10. Pitch Tracking Closed Loop System for <i>Gap Criterion</i>	2-16
2-11. Four Resulting <i>Gap Criterion</i> Types.....	2-18
2-12. Case I Effective Pilot Gain Increase.....	2-19
2-13. Case II Effective Pilot Gain Decrease	2-20
2-14. Nichols Chart of the Example Problem.....	2-22
3-1. Phase 2 Sum-of-sines Pitch Tracking Task	3-2
3-2. Phase 3 Discrete HUD Pitch Tracking Task	3-2

Figure	Page
3-3. Phase 3 Target Tracking Task	3-3
3-4. Longitudinal State Space Diagram (Matlab/Simulink TM , 2001)	3-4
3-5. HAVE PREVENT Nichols Charts for Cases A, B and C	3-6
3-6. HAVE PREVENT Phase 2 Sum-of-sines Task LAMARS Data	3-9
3-7. HAVE PREVENT Phase 3 Discrete HUD Pitch Tracking Task LAMARS Data ..	3-9
3-8. HAVE PREVENT Phase 3 Target Tracking Task LAMARS Data	3-10
3-9. HAVE PREVENT Phase 2 Sum-of-sines Task LAMARS Data with Logarithmic Curve Fit	3-12
3-10. HAVE PREVENT Phase 3 Discrete HUD Pitch Tracking Task LAMARS Data with Logarithmic Curve Fit	3-13
3-11. HAVE PREVENT Phase 3 Target Tracking Task LAMARS Data with Logarithmic Curve Fit	3-13
3-12. HAVE OLOP Nichols Charts for Cases A, B and C	3-17
3-13. HAVE OLOP Phase 2 Sum-of-sines Task VISTA Data	3-20
3-14. HAVE OLOP Phase 3 Discrete HUD Pitch Tracking Task VISTA Data	3-20
3-15. HAVE OLOP Phase 2 Sum-of-sines Task VISTA Data with Logarithmic Fit ...	3-23
3-16. HAVE OLOP Phase 3 Discrete HUD Pitch Tracking Task VISTA Data with Logarithmic Fit	3-23
4-1. MAX GAP (LAMARS) Nichols Charts for Cases B, N, W and Y	4-3
4-2. MAX GAP (LAMARS) Phase 2 Sum-of-sines Task Data	4-6
4-3. MAX GAP (LAMARS) Phase 3 Discrete HUD Pitch Tracking Task Data	4-6
4-4. MAX GAP (LAMARS) Phase 3 Target Tracking Task Data	4-7
4-5. MAX GAP (LAMARS) Phase 2 Sum-of-sines Task Data with Logarithmic Curve Fit	4-9

Figure	Page
4-6. MAX GAP (LAMARS) Phase 3 Discrete HUD Pitch Tracking Task Data with Logarithmic Fit	4-10
4-7. MAX GAP (LAMARS) Phase 3 Target Tracking Task Data with Logarithmic Fit	4-10
5-1. MAX GAP (VISTA) Nichols Charts for Cases B, N, W and Y	5-4
5-2. MAX GAP (VISTA) Phase 2 Sum-of-sines Task Data	5-7
5-3. MAX GAP (VISTA) Phase 3 Discrete HUD Pitch Tracking Task Data	5-7
5-4. MAX GAP (VISTA) Phase 2 Sum-of-sines Task Data with Logarithmic Curve Fit	5--9
5-5. MAX GAP (VISTA) Phase 3 Discrete HUD Pitch Tracking Task Data with Logarithmic Curve Fit	5-10
6-1. LAMARS Combined Phase2 Sum-of-sines Dataset	6-1
6-2. LAMARS Combined Phase 3 Discrete (HUD) Pitch-Tracking Dataset	6-2
6-3. LAMARS Combined Phase3 Target Tracking Dataset	6-2
6-4. VISTA Combined Phase 2 Sum-of-sines Dataset	6-3
6-5. VISTA Combined Phase 3 Discrete (HUD) Pitch-Tracking Dataset	6-3
6-6. LAMARS and VISTA Combined Phase 2 Sum-of-sines Data	6-4
6-7. LAMARS and VISTA Combined Phase 3 Discrete Pitch-Tracking Data	6-4
A-1. Augmented Dynamics Simulink™ Model	A-4
D-1. LAMARS Phase 2 Sum-of-sines Data, Case B, 15 deg/sec	D-1
D-2. LAMARS Phase 2 Sum-of-sines Data, Case B, 30 deg/sec	D-2
D-3. LAMARS Phase 2 Sum-of-sines Data, Case B, 60 deg/sec	D-2
D-4. LAMARS Phase 2 Sum-of-sines Data, Case N, 15 deg/sec	D-3
D-5. LAMARS Phase 2 Sum-of-sines Data, Case N, 30 deg/sec	D-3

Figure	Page
D-6. LAMARS Phase 2 Sum-of-sines Data, Case N, 60 deg/sec.....	D-4
D-7. LAMARS Phase 2 Sum-of-sines Data, Case W, 15 deg/sec.....	D-4
D-8. LAMARS Phase 2 Sum-of-sines Data, Case W, 30 deg/sec.....	D-5
D-9. LAMARS Phase 2 Sum-of-sines Data, Case W, 60 deg/sec.....	D-5
D-10. LAMARS Phase 2 Sum-of-sines Data, Case Y, 15 deg/sec.....	D-6
D-11. LAMARS Phase 2 Sum-of-sines Data, Case Y, 30 deg/sec.....	D-6
D-12. LAMARS Phase 2 Sum-of-sines Data, Case Y, 60 deg/sec.....	D-7
D-13. LAMARS Phase 3 Discrete HUD Pitch Tracking Data, Case B, 15 deg/sec.....	D-8
D-14. LAMARS Phase 3 Discrete HUD Pitch Tracking Data, Case B, 30 deg/sec.....	D-8
D-15. LAMARS Phase 3 Discrete HUD Pitch Tracking Data, Case B, 60 deg/sec.....	D-9
D-16. LAMARS Phase 3 Discrete HUD Pitch Tracking Data, Case N, 15 deg/sec	D-9
D-17. LAMARS Phase 3 Discrete HUD Pitch Tracking Data, Case N, 30 deg/sec ...	D-10
D-18. LAMARS Phase 3 Discrete HUD Pitch Tracking Data, Case N, 60 deg/sec ...	D-10
D-19. LAMARS Phase 3 Discrete HUD Pitch Tracking Data, Case W, 15 deg/sec... D-11	D-11
D-20. LAMARS Phase 3 Discrete HUD Pitch Tracking Data, Case W, 30 deg/sec... D-11	D-11
D-21. LAMARS Phase 3 Discrete HUD Pitch Tracking Data, Case W, 60 deg/sec... D-12	D-12
D-22. LAMARS Phase 3 Discrete HUD Pitch Tracking Data, Case Y, 15 deg/sec ... D-12	D-12
D-23. LAMARS Phase 3 Discrete HUD Pitch Tracking Data, Case Y, 30 deg/sec ... D-13	D-13
D-24. LAMARS Phase 3 Discrete HUD Pitch Tracking Data, Case Y, 60 deg/sec ... D-13	D-13
D-25. LAMARS Phase 3 Target Tracking Data, Case B, 15 deg/sec	D-14
D-26. LAMARS Phase 3 Target Tracking Data, Case B, 30 deg/sec	D-14
D-27. LAMARS Phase 3 Target Tracking Data, Case B, 60 deg/sec	D-15

Figure	Page
D-28. LAMARS Phase 3 Target Tracking Data, Case N, 15 deg/sec	D-15
D-29. LAMARS Phase 3 Target Tracking Data, Case N, 30 deg/sec	D-16
D-30. LAMARS Phase 3 Target Tracking Data, Case N, 60 deg/sec	D-16
D-31. LAMARS Phase 3 Target Tracking Data, Case W, 15 deg/sec	D-17
D-32. LAMARS Phase 3 Target Tracking Data, Case W, 30 deg/sec	D-17
D-33. LAMARS Phase 3 Target Tracking Data, Case W, 60 deg/sec	D-18
D-34. LAMARS Phase 3 Target Tracking Data, Case Y, 15 deg/sec	D-18
D-35. LAMARS Phase 3 Target Tracking Data, Case Y, 30 deg/sec	D-19
D-36. LAMARS Phase 3 Target Tracking Data, Case Y, 60 deg/sec	D-19
D-37. VISTA Phase 2 Sum-of-sines Data, Case B, 15 deg/sec	D-20
D-38. VISTA Phase 2 Sum-of-sines Data, Case B, 30 deg/sec	D-20
D-39. VISTA Phase 2 Sum-of-sines Data, Case B, 60 deg/sec	D-21
D-40. VISTA Phase 2 Sum-of-sines Data, Case N, 15 deg/sec	D-21
D-41. VISTA Phase 2 Sum-of-sines Data, Case N, 30 deg/sec	D-22
D-42. VISTA Phase 2 Sum-of-sines Data, Case N, 60 deg/sec	D-22
D-43. VISTA Phase 2 Sum-of-sines Data, Case W, 15 deg/sec	D-23
D-44. VISTA Phase 2 Sum-of-sines Data, Case W, 30 deg/sec	D-23
D-45. VISTA Phase 2 Sum-of-sines Data, Case W, 60 deg/sec	D-24
D-46. VISTA Phase 2 Sum-of-sines Data, Case Y, 15 deg/sec	D-24
D-47. VISTA Phase 2 Sum-of-sines Data, Case Y, 30 deg/sec	D-25
D-48. VISTA Phase 2 Sum-of-sines Test Data, Case Y, 60 deg/sec	D-25
D-49. VISTA Phase 3 Discrete HUD Pitch Tracking Data, Case B, 15 deg/sec	D-26

Figure	Page
D-50. VISTA Phase 3 Discrete HUD Pitch Tracking Data, Case B, 30 deg/sec.....	D-26
D-51. VISTA Phase 3 Discrete HUD Pitch Tracking Data, Case B, 30 deg/sec.....	D-27
D-52. VISTA Phase 3 Discrete HUD Pitch Tracking Data, Case N, 15 deg/sec	D-27
D-53. VISTA Phase 3 Discrete HUD Pitch Tracking Data, Case N, 30 deg/sec	D-28
D-54. VISTA Phase 3 Discrete HUD Pitch Tracking Data, Case N, 60 deg/sec	D-28
D-55. VISTA Phase 3 Discrete HUD Pitch Tracking Data, Case W, 15 deg/sec	D-29
D-56. VISTA Phase 3 Discrete HUD Pitch Tracking Data, Case W, 30 deg/sec	D-29
D-57. VISTA Phase 3 Discrete HUD Pitch Tracking Data, Case W, 60 deg/sec	D-30
D-58. VISTA Phase 3 Discrete HUD Pitch Tracking Data, Case Y, 15 deg/sec	D-30
D-59. VISTA Phase 3 Discrete HUD Pitch Tracking Data, Case Y, 30 deg/sec	D-31
D-60. VISTA Phase 3 Discrete HUD Pitch Tracking Data, Case Y, 60 deg/sec	D-31

List of Tables

Table	Page
1-1. Summary of Famous Longitudinal PIO Events (McRuer, 1995:9).....	1-4
1-2. PIO Tendency Rating Scale (MIL-HDBK-1797, 1997:153)	1-10
2-1. Neal-Smith Pilot Models	2-14
3-1. HAVE PREVENT Case Characteristics (Hanley, 2003)	3-3
3-2. HAVE PREVENT Pitch-to-Actuator Transfer Functions (G_c).....	3-4
3-3. HAVE PREVENT Neal-Smith Pilot Models	3-5
3-4. HAVE PREVENT Components for Cases A and B.....	3-6
3-5. Gap Criteria Values for HAVE PREVENT Cases A and B.....	3-7
3-6. <i>Gap Criteria</i> for HAVE PREVENT Case C	3-7
3-7. HAVE PREVENT <i>Gap Criteria</i> Summary.....	3-8
3-8. HAVE PREVENT Correlation Confidence Levels.....	3-11
3-9. HAVE PREVENT Curve Fit Correlation Values.....	3-11
3-10. HAVE OLOP Case Characteristics (Gilbreath, 2001)	3-15
3-11. HAVE OLOP Pitch-to-Actuator Transfer Functions (G_c).....	3-15
3-12. HAVE OLOP Neal-Smith Pilot Models.....	3-16
3-13. HAVE OLOP Components for Cases A and C	3-17
3-14. Gap Criteria Values for HAVE OLOP Case A and C.....	3-18
3-15. HAVE OLOP <i>Gap Criteria</i> Summary	3-19
3-16. HAVE OLOP Correlation Confidence Levels	3-21
3-17. HAVE OLOP Curve Fit Correlation Values	3-22
4-1. MAX GAP (LAMARS) Case Characteristics (Witte and others, 2003).....	4-1

Table	Page
4-2. MAX GAP (LAMARS) Pitch-to-Actuator Transfer Functions (G_c).....	4-2
4-3. MAX GAP (LAMARS) Neal-Smith Pilot Models.....	4-3
4-4. MAX GAP (LAMARS) Components for Cases B, N, W and Y	4-4
4-5. Gap Criteria Values for MAX GAP (LAMARS) Cases B, N, W and Y.....	4-4
4-6. MAX GAP (LAMARS) <i>Gap Criteria</i> Summary	4-5
4-7. MAX GAP (LAMARS) Correlation Confidence Levels	4-8
4-8. MAX GAP (LAMARS) Curve Fit Correlation Values	4-8
5-1. MAX GAP (VISTA) Case Characteristics (Witte and others, 2003).....	5-2
5-2. MAX GAP (VISTA) Pitch-to-Actuator Transfer Functions (G_c)	5-2
5-3. MAX GAP (VISTA) Neal-Smith Pilot Models	5-3
5-4. MAX GAP (VISTA) Components for Cases B and W	5-4
5-5. Gap Criteria Values for MAX GAP (VISTA) Cases B and W	5-5
5-6. MAX GAP (VISTA) Components for Case N.....	5-5
5-7. Gap Criteria Values for MAX GAP (VISTA) Case N.....	5-5
5-8. <i>Gap Criteria</i> for MAX GAP (VISTA) Case Y	5-6
5-9. MAX GAP (VISTA) <i>Gap Criteria</i> Summary	5-6
5-10. MAX GAP (VISTA) Correlation Confidence Levels	5-8
5-11. MAX GAP (VISTA) Curve Fit Correlation Values.....	5-9
C-1. Minimum Values of the Correlation Coefficient for Confidence Level (Wheeler and Ganji, 1996:147).....	C-2

List of Notations and Symbols

<i>Symbol</i>	<i>Definition</i>	<i>Unit</i>
A	Commanded Actuator Deflection	deg
A_{\max}	Maximum Actuator Deflection Available	deg
AFIT	Air Force Institute of Technology	-
AFRL	Air Force Research Laboratories	-
α , Alpha	Angle-of-Attack	deg
dB	Decibels	-
deg	Degrees	-
δ	Actuator Deflection Angle	deg
$\Delta\phi$	Phase Angle	rad
DoD	Department of Defense	-
e, E	Error	-
G(s)	Generic Laplacian Transfer Function	-
G_{actuator}	Actuator Transfer Function	-
$G_{\text{augmented}}$	Augmented Aircraft Transfer Function	-
GC	Gap Criterion	-
$G_c(s)$	Bare Aircraft Transfer Function	-
$G_p(s)$	Neal-Smith Pilot Model Transfer Function	-
HQDT	Handling Qualities During Tracking	-
HUD	Heads Up Display	-
$j\omega$	Imaginary Laplacian Term	-

<i>Symbol</i>	<i>Definition</i>	<i>Unit</i>
k	Feedback Gain Matrix	-
K^*	Intermediate Variable	-
K_p	Neal-Smith Pilot Gain	-
$K_\alpha, K_{\alpha\text{pha}}$	Angle-of-Attack Feedback Gain	-
$K_q, K_{\dot{q}}$	Pitch Rate Feedback Gain	-
LAMARS	Large Amplitude Multimode Aerospace Simulator	-
\ln	Natural Logarithm	-
MIL HDBK 1797	Military Handbook 1797	-
n	Number of Datapoints	-
$N(A, \omega)$	Describing Function	-
OLOP	Open Loop Onset Point	-
\angle	Phase Angle	deg
ω	Frequency	rad/sec
ω_a	Actuator Gain	-
ω_{BW}	Band Width Frequency	rad/sec
ω_{sp}	Short Period Natural Frequency	rad/sec
PIO	Pilot-induced Oscillations	-
PIOR	Pilot-induced Oscillation Tendency Rating	-
q	Aircraft Pitch Rate	deg/sec
R, r_{xy}	Correlation Factor	-
rad	Radians	-
s	Laplacian Operator	-

<i>Symbol</i>	<i>Definition</i>	<i>Unit</i>
sec	Seconds	-
θ , Theta	Aircraft Pitch Angle	deg
T_2	Time to Double Amplitude	sec
T_{Lag}	Neal-Smith Lag Time Constant	sec
T_{Lead}	Neal-Smith Lead Time Constant	sec
USAF TPS	United States Air Force Test Pilot School	-
V	True Velocity	ft/sec
VISTA	Variable In-flight Stability Test Aircraft	-
V_L	Actuator Rate Limit	deg/sec
ζ_{sp}	Short Period Damping Ratio	-

AN INVESTIGATION RELATING LONGITUDINAL PILOT-INDUCED
OSCILLATION TENDENCY RATING TO DESCRIBING FUNCTION
PREDICTIONS FOR RATE-LIMITED ACTUATORS

I. Introduction

General

The purpose of this study was to investigate pilot-induced oscillations (PIO) and determine a new method by which PIO tendency rating could be predicted. In particular, longitudinal PIO in the presence of rate-limited actuators were singled out for examination. The PIO rating scale used in this investigation was the PIO tendency classification of the Department of Defense Interface Standard Flying Qualities of Piloted Aircraft (MIL-HDBK-1797, 1997:152). While there are a number of PIO prediction methods already published, this study will attempt a new approach.

This study was originated at the Air Force Institute of Technology (AFIT), Wright-Patterson AFB, Ohio and was supported by the United States Air Force Test Pilot School (USAF TPS). Research was conducted in both the Large Amplitude Multimode Aerospace Simulator (LAMARS) at the Air Force Research Laboratory (AFRL), Wright-Patterson AFB, Ohio and in the USAF NF-16D Variable In-flight Stability Test Aircraft (VISTA) at Edwards AFB, CA. The VISTA aircraft is operated by USAF TPS and supported by General Dynamics Advanced Information Systems of Buffalo, NY.

Background

Pilot-induced oscillations have been an aviation problem for over 100 years now. The first incidence can be traced back to Wilbur and Orville Wright in 1903. When the two brothers first took to the skies of Kitty Hawk, North Carolina, they experienced “a mild longitudinal oscillation of the Wright Flyer” (Duda, 1995:288). The PIO problem had just begun.

PIO Defined.

Before continuing with the century-long history of PIO, an understanding of the term PIO is in order. A pilot-induced oscillation can be described as “an inadvertent, sustained aircraft oscillation which is the consequence of an abnormal joint enterprise between the aircraft and the pilot” (McRuer, 1995:2). Elaborated, a PIO is a complex interaction between a pilot and his active involvement in an aircraft feedback system (Klyde and others, 1995:14). The United State Department of Defense (DoD) defines PIO as “sustained or uncontrollable oscillations resulting from the efforts of the pilot to control the aircraft” (MIL-HDBK-1797, 1997:151). Although the key causal factor in pilot-induced oscillation seems to be the pilot, it is important to make the assertion that, generally, the pilot is not at fault and that there seems to be embedded in the flight control system of the aircraft some tendencies predisposing the pilot-aircraft system toward PIO occurrence (Klyde and others, 1995:14). In recent times, new terms have been put forth to replace the familiar PIO such that the pilot’s guilt in such events is less likely to be assumed. These include aircraft-pilot coupling (APC), pilot-in-the-loop oscillations and pilot-assisted (or augmented) oscillations (Klyde and others, 1995:14). However, experienced test pilots, including instructors at the US test pilot schools, and people in the

handling qualities community have expressed widespread allegiance to the traditional term PIO and, therefore, this term will be used throughout this study (Mitchell and Hoh, 1995:16; Klyde and others, 1995:14).

In addition to defining what a PIO is, it is just as important to define what it is not. A PIO could mean any oscillation that occurs during manual, piloted control. But some of these situations could be the result of pilot overcontrol such as when a student pilot is learning to land and balloons the aircraft. To an outsider, this could look like a PIO but really is just part of standard pilot compensation lasting no more than one or two cycles and is not a “real” PIO (Mitchell and Hoh 1995:17). Other researchers describe these as “minor bobbles” that are often encountered as pilots get used to a new aircraft and is just part of the learning experience (Klyde and others, 1995:14). It is also important to realize that motions resulting from poor damping of the short period or dutch roll modes are not PIO, when the motion does not result from the “efforts of the pilot to control the aircraft” (Mitchell and Hoh, 1995:17-18).

To distinguish between these examples and a true PIO, some leading researchers propose the following additional definition of PIO: “A PIO exists when the airplane attitude, angular rate, or normal acceleration is 180 degrees out of phase with the pilot’s control inputs” (Mitchell and Hoh, 1995:18). A great example of this phase lag can be seen in Figure 1-1. This is the recorded data of the YF-22A accident which occurred on 25 April 1992 during a planned go-around at low altitude. This stripchart data depict a 180 degree phase difference between the aircraft pitch attitude and stick input.

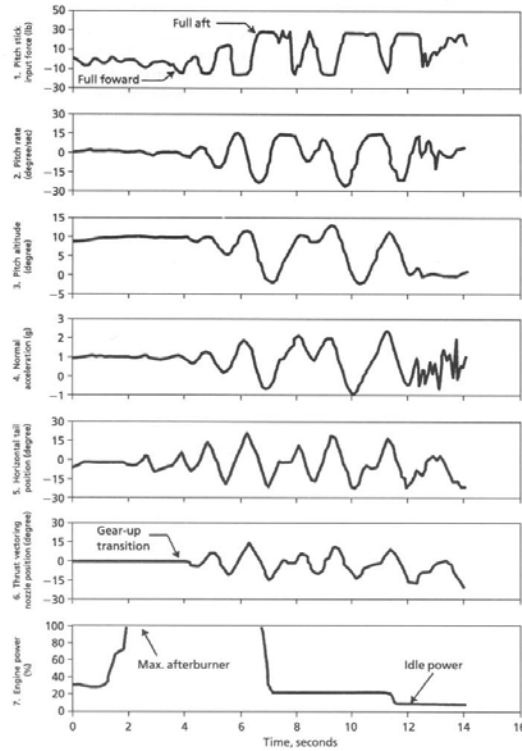


Figure 1-1. YF-22A Accident Sequence (Hodgkinson, 1999:128)

PIO History.

The YF-22A PIO occurrence is just one of the most recent events. There is a long history of PIO events in both operational and test flying as shown in Table 1-1.

Table 1-1. Summary of Famous Longitudinal PIO Events (McRuer, 1995:9)

Aircraft Type	Summary of Incident
XS-1	PIO during gliding approach and landing, 24 Oct 1947
XF-89A	PIO during level off from dive recovery, early 1949
F-100	PIO during tight maneuvering
X-15	Gliding flight approach and landing, 8 Jun 1959; Category II PIO
XF2Y-1	Post-takeoff destructive PIO
YF-12	Mid-frequency severe PIO; Category III PIO
Space Shuttle	ALT-5 during landing approach glide, 26 Oct 1977; Category II PIO
DFBW F-8	PIO during touch and goes, 18 Apr 1978; Category III PIO
YF-22	PIO after touchdown and wave off in afterburner, 25 Apr 1992
JAS 39	PIO during approach, 1990; 1993; Category II – III PIO
MD-11	China Eastern Airlines Flt 583, 6 Apr 1993; Inadvertant slat deployment
F-4	Low altitude record run second pass, 18 May 1961; Destructive PIO

The onset of PIO occurs when the pilot attempts tight control. The DoD defines Category A Flight Phases as “those nonterminal Flight Phases that require rapid maneuvering, precision tracking, or precise flight path control” (MIL-HDBK-1797, 1997:80). Types of maneuvers included in this category are in-flight refueling (receiver), air-to-air combat, and formation flying (MIL-HDBK-1797, 1997:80). Category C Flight Phases also require “accurate flight-path control” and include takeoffs, approaches and landings (MIL-HDBK-1797, 1997:80). Almost all of the events listed in Table 1-1 fall into Category A or Category C.

PIO can range in severity from benign to catastrophic (Anderson and Page, 1995:278). Benign PIO may not lead to loss of aircraft or life, but they can affect operational missions. For example, receiver air-refueling may take longer than expected causing delays in mission progress (Anderson and Page, 1995:278). This is still far easier to accept than the more severe extreme in which aircraft and pilots have both been lost due to PIO. On 18 May 1961, US Navy pilot Cmdr Jack Feldman and his F-4B aircraft were lost when a PIO disintegrated his aircraft during the second pass of a low altitude speed record attempt due to PIO related to low short-period damping (McCruer, 1995:9).

Even worse, the potential for PIO has actually increased due to the evolving use of highly augmented, fly-by-wire aircraft (Liebst and others, 2002:740). Development flight test of the Boeing 777, C-17A and Saab JAS 39 Gripen bear this out. The 777, a fly-by-wire transport, encountered a PIO situation during a Flaps 20 landing. The spoilers automatically deployed upon touchdown and the pilot countered with forward column motion resulting in a PIO that lasted for “about 3 cycles” (Dornheim, 1995:32). C-17 longitudinal PIO tendencies were discovered during dutch roll testing, air-refueling

breakaways and three-engine landings. Additionally, further PIO tendencies were exposed during handling qualities during tracking (HQDT) exercises with an A-37 target aircraft (Preston and others, 1996:20-49). The discovery of PIO tendencies in the JAS 39 was not so uneventful. Two aircraft were lost during different stages of aircraft development. The first accident occurred in 1989 with the test aircraft having had only 5.3 hours of flight time when, during a landing attempt, it experienced “roll pendulums” at low altitude and later “pendular movements in pitch, also” at an altitude of approximately 10 to 15 meters. The mishap pilot attempted a go-around but the aircraft “hit the runway with the left wingtip and main gear as well as the nose portion” (Ahlgren, 1989:12). The pilot survived and returned to test flying the JAS 39. In 1993 while performing in an airshow in Stockholm, Sweden, he experienced a lateral PIO compounded with an uncommanded pitch up to high angle-of-attack. The aircraft diverged from controlled flight but the pilot ejected safely (Jensen and others, undated:12).

PIO Categories.

PIO can be divided into three categories (McRuer, 1995:79-80). Category I PIO are essentially linear pilot-vehicle system oscillations; they are usually the low frequency consequence of excessive high frequency lag in the aircraft’s linear dynamics (Klyde and others, 1996:17). On the other hand, Category III PIO are associated with essentially nonlinear pilot-vehicle systems with transitions; they are the result of abrupt shifts in either the effective controlled-element dynamics or in the pilot’s behavioral dynamics (Klyde and others, 1996:17). Category II PIO are defined as quasi-linear pilot-vehicle system oscillations associated with control surface rate or position limiting (McRuer,

1995:80). In other words, rate-limited actuators. They represent a transition from linear dynamics to nonlinear effects and were the focus of this investigation.

PIO Category II.

One reason for focusing on Category II PIO is that “almost all of the severe PIO time history records available for operational and flight test aircraft ... show surface rate limiting ...in the fully developed oscillation” (Klyde and others, 1996:15). Other researchers have similar opinions: “It seems to be true that all recent PIO have exhibited rate saturation” (Duda , 1995:289). A prime example is the development of the C-17 in which “rate limiting was involved in all the subject [PIO] events and is viewed to be the primary cause of the longitudinal PIO” (Preston and others, 1996:20).

There are two major detrimental effects of rate limiting. One is that it adds to the effective lag in series with the pilot therefore making the effective aircraft dynamics worse and the other is that it exposes the bare aircraft dynamics in stability augmented aircraft. On the positive side, however, rate limiting tends to confine the ultimate amplitude of the pilot-vehicle system oscillation (Klyde and others, 1996:15). Figure 1-2 shows the differences in the output of a typical first-order actuator as the effects of increasing amplitude drive the system toward rate limiting. The figure displays the characteristic triangular wave pattern of the actuator position reversing when equal to the commanded position. The “boxcar-like” rate response is clipped at 40 deg/sec in this example and is also a trait of a rate-limited actuator (Klyde and others, 1996:25). The output was generated using the Matlab™/Simulink™ software model which is shown in Figure 1-3 (Matlab™/Simulink™, 2001).

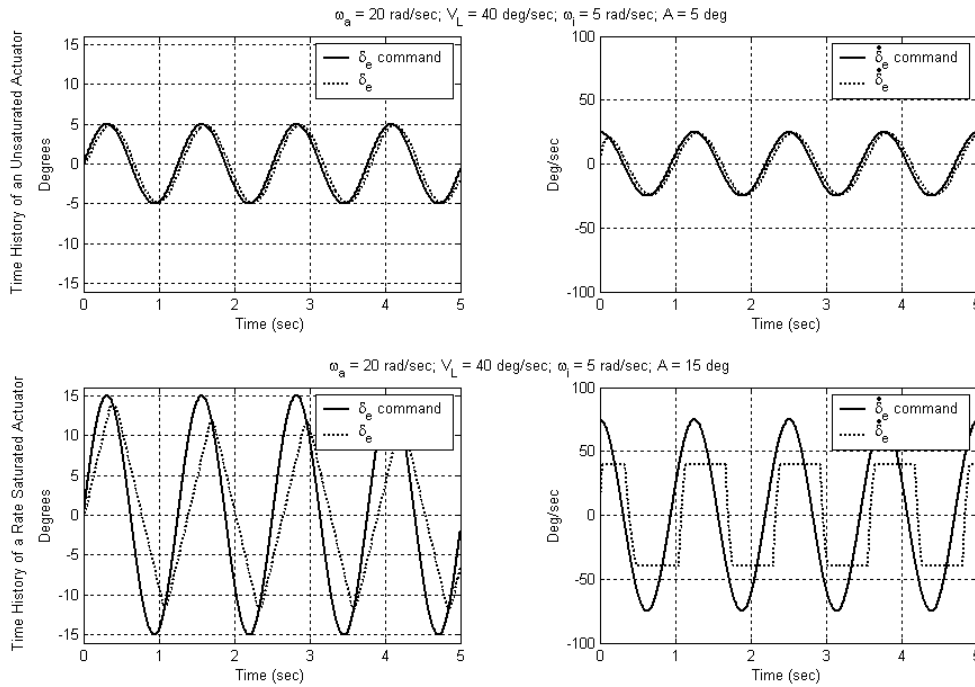


Figure 1-2. Actuator Saturation Example Using an Input = $A \sin(\omega_i t)$

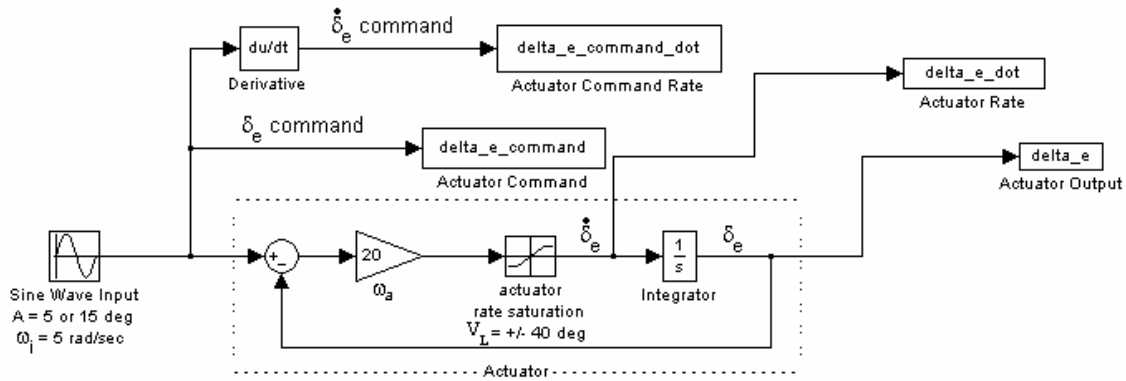


Figure 1-3. Simulink™ Actuator Model

PIO Scales.

Before discussing PIO prediction, a scale must be selected which distinguishes increasing severity of PIO. Figure 1-4 shows just such a scale, the PIO tendency classification (MIL-HDBK-1797, 1997:152). This scale is in common use among test

pilots to rate the susceptibility of aircraft to PIO and a large amount of historical data is available based on this scale. Comparing this scale to Cooper-Harper Handling Qualities Levels, a PIO rating of 1 or 2 is approximately equivalent to a Level 1 aircraft, a PIO rating of 3 or 4 is similar to a Level 2 aircraft, a PIO rating of 5 is Level 3 and a PIO rating of 6 is extremely dangerous (MIL-HDBK-1797, 1997:151). These PIO ratings are more fully described in the PIO tendency rating scale of Table 1-2 (MIL-HDBK-1797, 1997:322).

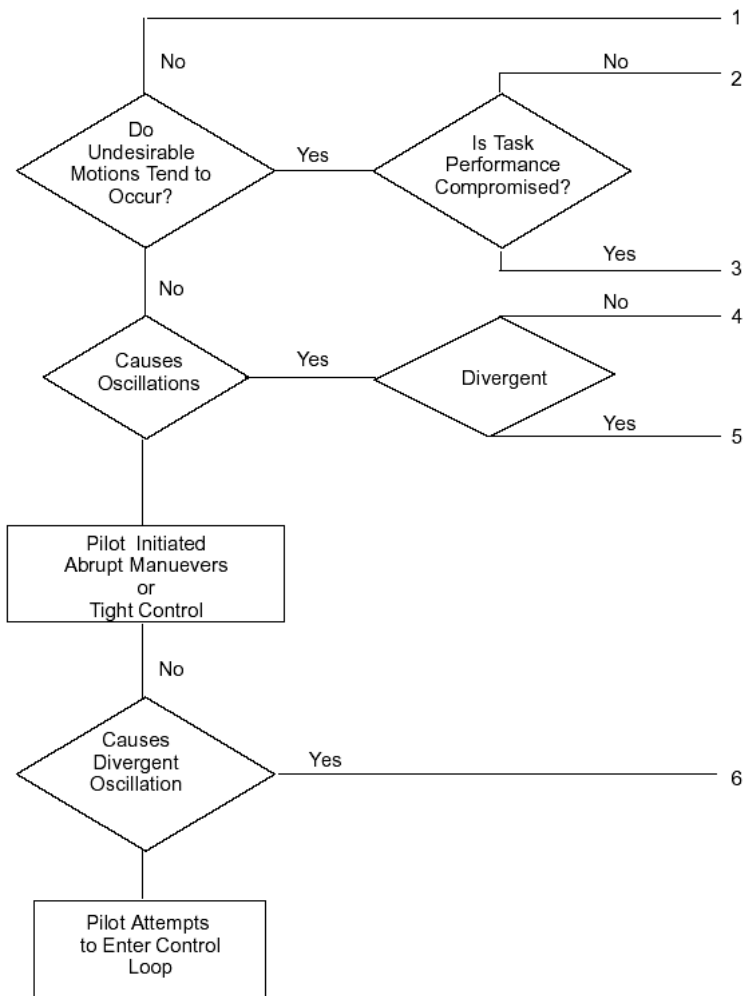


Figure 1-4. PIO Tendency Classification (MIL-HDBK-1797, 1997:152)

Table 1-2. PIO Tendency Rating Scale (MIL-HDBK-1797, 1997:153)

DESCRIPTION	NUMERICAL RATING
No tendency for pilot to induce undesirable motions.	1
Undesirable motions tend to occur when pilot initiates abrupt maneuvers or attempts tight control. These motions can be prevented or eliminated by pilot technique.	2
Undesirable motions easily induced when pilot initiates abrupt maneuvers or attempts tight control. These motions can be prevented or eliminated but only at sacrifice to task performance or through considerable pilot attention and effort.	3
Oscillations tend to develop when pilot initiates abrupt maneuvers or attempts tight control. Pilot must reduce gain or abandon task to recover.	4
Divergent oscillations tend to develop when pilot initiates abrupt maneuvers or attempts tight control. Pilot must open loop by releasing or freezing the stick.	5
Disturbance or normal pilot control may cause divergent oscillation. Pilot must open control loop by releasing or freezing the stick.	6

PIO Prediction Methods.

Using this scale, several criteria for PIO prediction have been developed for Category I and Category II PIO (Mitchell and Klyde, 1998:417-426). Category I PIO prediction methods include the Bandwidth/Pitch Rate Overshoot Method, the original Neal-Smith criteria, the Neal-Smith criteria as modified by the Moscow Aviation Institute, Smith-Geddes PIO criteria, and the Gibson criteria (Mitchell and Klyde, 1998:417-426). A thorough examination of these methods led Mitchell and Klyde to conclude that “we are in reasonably good shape in predicting Category I PIO” (Mitchell and Klyde, 1998:417-426). Satisfactory development of Category II PIO prediction methods, on the other hand, is not as complete.

Some work in Category II prediction methods has been accomplished or is in progress. These efforts include modifying the Bandwidth/Phase Delay criteria to Category II cases, the Time-domain Neal-Smith criteria, the Open Loop Onset Point (OLOP) criteria and a power spectral density method using a structural model of the human pilot (Mitchell and Klyde, 1998:417-426). These efforts continue despite the assertion by Anderson and Page that "...the adaptive nature of the pilot makes such oscillations [PIO] difficult to predict" (Anderson and Page, 1995:278).

Gap Criterion.

The Department of Aeronautical and Astronautical Engineering at the Air Force Institute of Technology (AFIT) now proposes a new criterion for predicting PIO ratings dubbed the *Gap Criterion*. It is based on describing function techniques, modified Neal-Smith pilot models and actuator input amplitude ratios. The goal of this study was to determine if specific relationships between *Gap Criterion* and PIO tendency rating for Category II PIO due to rate-limited actuators exists and, if so, to what extent.

Objectives

The primary objective of this study was to develop a new criterion for predicting PIO tendency rating by:

- 1) Exploiting previously defined describing function methods for determining Category II PIO characteristics based on rate-limited actuators.
- 2) Defining *Gap Criterion*.
- 3) Applying the new method to existing historical data from similar test programs.
- 4) Conducting both simulator and flight tests to expand this database.
- 5) Making recommendations on the implementation of this new criterion.

Approach

The following steps were taken for this project:

- 1) The *Gap Criterion* was applied to data from previous simulator and flight test projects in which rate limiting PIO effects were studied. These included USAF TPS projects HAVE OLOP and HAVE PREVENT (Gilbreath, 2001; Hanley, 2003). The *Gap Criterion* was calculated for each test case of bare aircraft dynamics and rate-limit. These *Gap Criteria* were then matched with their respective PIO tendency ratings and plotted in pairs. Correlation probability confidence level was then determined along with curve fits.
- 2) Based on the observed data from these studies, a broader range of longitudinal flight control system dynamics with varying short period characteristics were chosen to augment the database. These configurations were tested in both the LAMARS simulator and the VISTA NF-16D aircraft.

Scope

This research project was limited in scope and constrained in certain areas:

1. The PIO investigated were strictly longitudinal, Category II PIO due to rate limiting of the actuator.
2. Only three rate limits were chosen: 15 deg/sec, 30 deg/sec and 60 deg/sec.
3. Only four distinct bare aircraft dynamics cases were tested.
4. Tracking tasks were created with HUD generated and target aircraft sorties. No offset landing tasks were planned.
5. Due to schedule and budget, the simulator test portion was limited to two days and three pilots. The flight test portion was limited to eight sorties and 10.8 hour

II. Theory

This chapter will discuss describing functions and how they can be used to understand and predict PIO onset when considered in the context of rate-limited actuators. Further, the Neal-Smith pilot model will be explained followed by an example integrating all of these concepts. The basis of the *Gap Criterion* will then be covered.

Describing Function Development

Observing the time history of the YF-22 PIO from Figure 1-1, it can be seen that the input is approximately sinusoidal. This is true in general of all PIO incidents (Klyde and others, 1996:37). The describing function technique can be used for limit cycle analysis due to the fact that the form of the signals in a limit-cycling system, such as a PIO, is usually approximately sinusoidal (Slotine and Li, 1991:157).

Any system which can be rearranged into the form shown in Figure 2-1, where w and $G(p)$ represent nonlinear and linear elements, respectively, can be studied using describing functions (Slotine and Li, 1991:162). Examples of nonlinear elements include dead-zones, hysteresis or rate saturations. Rate saturations were the focus of this study.

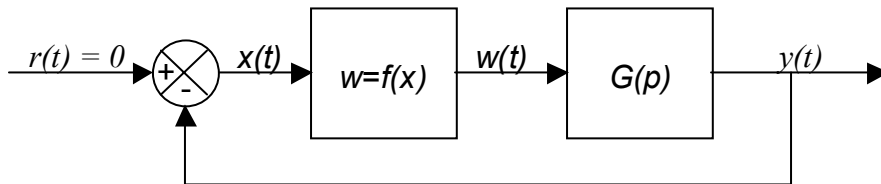


Figure 2-1. Example of a Nonlinear System

For the basic version of the describing function method, the system has to satisfy the following four conditions (Slotine and Li, 1991:164):

- 1) There is only a single nonlinear component
- 2) The nonlinear component is time-invariant
- 3) Corresponding to a sinusoidal input $x = A \sin(\omega t)$, only the fundamental component $w_1(t)$ in the output $w(t)$ has to be considered
- 4) The nonlinearity is odd

Consider a sinusoidal input of the form $x = A \sin(\omega t)$ entering the nonlinear element of the system shown in Figure 2-1. Due to nonlinear effects, the output, $w(t)$, is “often a periodic though non-sinusoidal function” (Slotine and Li, 1991:165). The output function $w(t)$ can be expanded using Fourier series as seen in Equation 1 and the succeeding derivation (Slotine and Li, 1991:165):

$$w(t) = \frac{a_0}{2} + \sum_{n=1}^{\infty} [a_n \cos(n\omega t) + b_n \sin(n\omega t)] \quad (1)$$

where

$$a_0 = \frac{1}{\pi} \int_{-\pi}^{\pi} w(t) d(\omega t) \quad (2)$$

$$a_n = \frac{1}{\pi} \int_{-\pi}^{\pi} w(t) \cos(n\omega t) d(\omega t) \quad (3)$$

$$b_n = \frac{1}{\pi} \int_{-\pi}^{\pi} w(t) \sin(n\omega t) d(\omega t) \quad (4)$$

Applying condition four above, for all odd functions $a_0 = 0$ (Slotine and Li, 1991:166). Further, applying the third assumption means discarding all other terms except $n = 1$ (Slotine and Li, 1991:166). This leaves:

$$w(t) \approx w_1(t) = a_1 \cos(\omega t) + b_1 \sin(\omega t) \quad (5)$$

which can be rewritten as

$$w_1(t) = M \sin(\omega t + \phi) \quad (6)$$

where

$$M = \sqrt{a_1^2 + b_1^2} \quad (7)$$

$$\phi = \tan^{-1} \left(\frac{a_1}{b_1} \right) \quad (8)$$

Rewritten in complex notation leads to:

$$w_1(t) = M e^{j(\omega t + \phi)} = (b_1 + j a_1) e^{j(\omega t)} \quad (9)$$

Finally, the describing function, $N(A, \omega)$, is defined to be the complex ratio of the fundamental component of the nonlinear element to the input sinusoid. This is shown in Equation 10:

$$N(A, \omega) = \frac{M e^{j(\omega t + \phi)}}{A e^{j(\omega t)}} = \frac{M}{A} e^{j\phi} = \frac{1}{A} (b_1 + j a_1) \quad (10)$$

Saturation Nonlinearity Describing Function

Now consider the saturation input-output relationship shown in Figure 2-2 below:

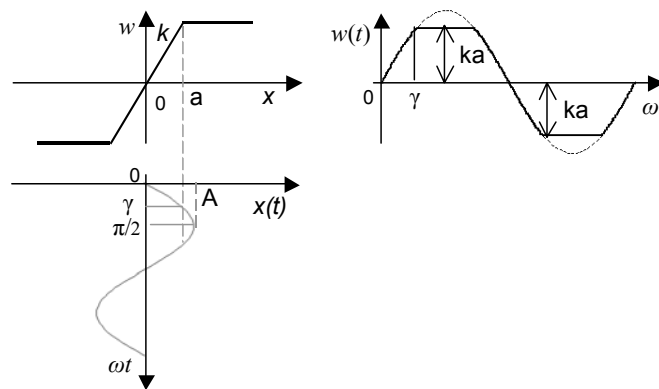


Figure 2-2. Saturation Nonlinearity and the Corresponding Input-Output Relationship (Slotine and Li, 1995:173)

From the figure, it is apparent that if our input, $x(t) = A \sin(\omega t)$, has a maximum amplitude $A \leq a$ then the input remains linear and the output is just $w(t) = kA \sin(\omega t)$. But if the maximum amplitude, A , is greater than a , clipping occurs and the value of $w(t)$ can be split into two sets over the first quarter of the symmetric output (Slotine and Li, 1995:173):

$$w(t) = \begin{cases} kA \sin(\omega t) & 0 \leq \omega t \leq \gamma \\ ka & \gamma < \omega t \leq \pi/2 \end{cases} \quad (11)$$

where $\gamma = \sin^{-1}(a/A)$

The output $w(t)$ is an odd function, implying $a_1 = 0$ in Equation 5. Further, dividing the output into four quarters yields a new equation for b_1

$$b_1 = \frac{4}{\pi} \int_0^{\pi/2} w(t) \sin(\omega t) d(\omega t) \quad (12)$$

$$b_1 = \frac{4}{\pi} \int_0^{\gamma} kA \sin^2(\omega t) d(\omega t) + \frac{4}{\pi} \int_{\gamma}^{\pi/2} ka \sin(\omega t) d(\omega t) \quad (13)$$

$$b_1 = \frac{2kA}{\pi} \left[\gamma + \frac{a}{A} \sqrt{1 - \frac{a^2}{A^2}} \right] \quad (14)$$

Substituting $a_1 = 0$ and Equation 14 into Equation 10 leaves (Slotine and Li, 1995:174):

$$N(A, \omega) = \frac{b_1}{A} = \frac{2k}{\pi} \left[\sin^{-1} \frac{a}{A} + \frac{a}{A} \sqrt{1 - \frac{a^2}{A^2}} \right] \quad (15)$$

Closed Loop Describing Function Approximation

Now, consider the block diagram in Figure 2-3 of a first order actuator system and the derivations which follow (Klyde and others, 1996:36-46).

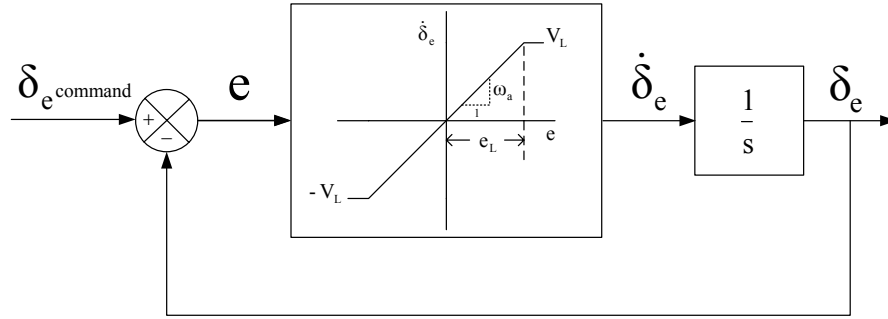


Figure 2-3. Actuator Model Development (Klyde and others, 1995:22)

The nonlinear portion of this model is exactly the same as the saturation nonlinearity discussed previously. Substituting the appropriate new nomenclature and letting $e(t) = E \sin(\omega t + \phi)$ replace $x(t)$, leads to the following describing function for the nonlinear element:

$$N(A, \omega) = \frac{2\omega_a}{\pi} \left[\sin^{-1} \left(\frac{e_L}{E} \right) + \frac{e_L}{E} \sqrt{1 - \frac{e_L^2}{E^2}} \right] \quad (16)$$

Further, by using series expansions for both the arcsine term and the square root, the describing function can be approximated by:

$$N(A, \omega) = \frac{2\omega_a}{\pi} \left[\left(\frac{e_L}{E} + \frac{1}{6} \left(\frac{e_L}{E} \right)^3 + \dots \right) + \frac{e_L}{E} \left(1 - \frac{1}{2} \frac{e_L^2}{E^2} - \dots \right) \right] \quad (17)$$

Keeping only the first order linear terms yields:

$$N(A, \omega) = \frac{2\omega_a}{\pi} \left[\frac{e_L}{E} + \frac{e_L}{E} \right] = \frac{4\omega_a}{\pi} \frac{e_L}{E} \quad (18)$$

Substituting $V_L = \omega_a e_L$ leads to:

$$N(A, \omega) = \frac{4}{\pi} \frac{V_L}{E} \quad (19)$$

Next, consider the revised block diagram shown in Figure 2-4 and determine the closed loop transfer function, treating N as a constant.

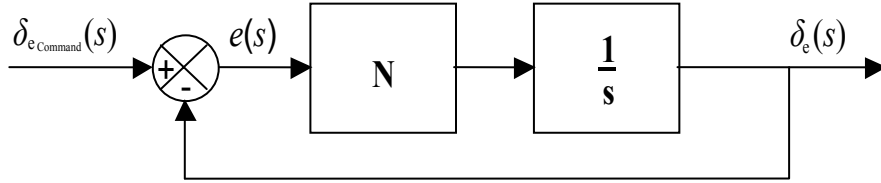


Figure 2-4. Closed Loop Actuator Transfer Function Diagram

Treating N as a constant and utilizing linear block diagram transfer function techniques, the relationship of $e(s)$ to $\delta_{e_{Command}}(s)$ is:

$$\frac{e(s)}{\delta_{e_{Command}}(s)} = \frac{1}{1 + \frac{N}{s}} \quad (20)$$

Assuming $\delta_{e_{Command}}(t) = A \sin(\omega t)$ and $e(t) = E \sin(\omega t + \phi)$ and substituting $j\omega$ for s , the equation for the magnitude of this transfer function becomes:

$$\left| \frac{e(s)}{\delta_{e_{Command}}(s)} \right| = \frac{1}{\sqrt{1 + \frac{N^2}{\omega^2}}} = \left| \frac{E \sin(\omega t + \phi)}{A \sin(\omega t)} \right| = \frac{E}{A} \quad (21)$$

Rearranging Equation 19 in terms of E gives:

$$E = \frac{4 V_L}{\pi N} \quad (22)$$

Substituting Equation 22 into Equation 21 and rearranging terms yields:

$$N = \frac{\omega}{\sqrt{\left(\frac{\pi A \omega}{4 V_L}\right)^2 - 1}} \quad (23)$$

Now, still treating N as a constant and utilizing standard block diagram transfer function techniques, the relationship of $\delta_e(s)$ to $\delta_{e_{Command}}(s)$ is:

$$\frac{\delta_e(s)}{\delta_{e_{Command}}(s)} = \frac{1}{\frac{s}{N} + 1} = \frac{N}{s + N} \quad (24)$$

and its magnitude is

$$\left| \frac{\delta_e(j\omega)}{\delta_{e_{Command}}(j\omega)} \right| = \frac{\sqrt{N^2}}{\sqrt{\omega^2 + N^2}} \quad (25)$$

and substituting Equation 23 into Equation 25 gives

$$\left| \frac{\delta_e(j\omega)}{\delta_{e_{Command}}(j\omega)} \right| = \frac{4 V_L}{\pi A\omega} \quad (26)$$

Solving for the phase angle of Equation 24 yields:

$$\angle \frac{\delta_e(j\omega)}{\delta_{e_{Command}}(j\omega)} = \tan^{-1} \left(\frac{-\omega}{N} \right) \quad (27)$$

and substituting Equation 23 yields

$$\angle \frac{\delta_e(j\omega)}{\delta_{e_{Command}}(j\omega)} = -\tan^{-1} \left(\sqrt{\left(\frac{\pi A\omega}{4 V_L} \right)^2 - 1} \right) \quad (28)$$

Sinusoidal Input/Triangle Output Describing Function Approximation

Another describing function approximation can be made by utilizing the observed characteristics of a saturated actuator. The input, $x_i(t)$, is sinusoidal in nature and the output, $x_o(t)$, takes on the familiar saw tooth triangle shape as shown in Fig 2-5 (Klyde and others, 1995:42-46):

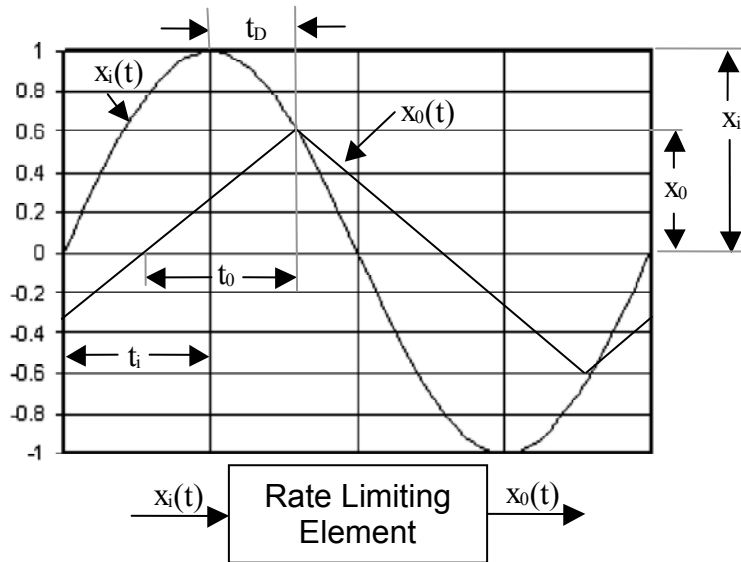


Figure 2-5. Rate-Limiting Input and Output (Klyde and others, 1995:42-46)

As before, let the input be sinusoidal as shown in Equation 29:

$$x_i(t) = x_{i_{\max}} \sin(\omega t) \quad (29)$$

and the derivative or input rate is:

$$\dot{x}_i(t) = x_{i_{\max}} \omega \cos(\omega t) \quad (30)$$

Now, let $\omega = 2\pi/T$ where $T = 4t_i$. Then the maximum input rate is

$$\dot{x}_{i_{\max}} = \frac{\pi}{2} \frac{x_{i_{\max}}}{t_i} \quad (31)$$

The rate of the output, \dot{x}_0 , is equal to the slope of the output and is given by

$$\dot{x}_0 = \pm \frac{x_0}{t_0} \quad (32)$$

Now, take the relationship of the output rate to the input rate in the range of t_0 and solve for the ratio of output to input magnitude as:

$$\frac{\dot{x}_0}{\dot{x}_{i_{\max}}} = \left(\frac{x_0}{t_0} \right) \bigg/ \left(\frac{\pi x_{i_{\max}}}{2 t_i} \right) = \frac{x_0}{t_0} \frac{2t_i}{x_{i_{\max}} \pi} \quad (33)$$

Recognizing t_0 equals t_i , rearranging terms and introducing a new variable K^* gives:

$$\frac{x_0}{x_{i_{\max}}} = \frac{\pi}{2} \frac{\dot{x}_0}{\dot{x}_{i_{\max}}} = K^* \quad (34)$$

Rewriting this expression in terms of the Figure 2-3 variables and recognizing that the output rate when saturated is V_L and the maximum input rate is $A\omega$ leaves

$$K^* = \frac{\pi}{2} \frac{V_L}{A\omega} \quad (35)$$

The describing function magnitude is then expressed using the K^* value multiplied by the Fourier fundamental of the triangle wave as seen in Equation 36 (Klyde and others, 1996:45).

$$\left| \frac{\delta_e(j\omega)}{\delta_{e_{\text{Command}}}(j\omega)} \right| = \frac{8}{\pi^2} K^* = \frac{4}{\pi} \frac{V_L}{A\omega} \quad (36)$$

This is exactly the same expression derived earlier for the closed loop actuator describing function magnitude. To obtain the phase angle of the input/output relationship, the term t_D as shown in Figure 2-5 must be determined. The input and output amplitudes are equal when $t = t_i + t_D$.

$$x_{i_{\max}} \sin[\omega(t_i + t_D)] = x_0 \quad (37)$$

Simplifying this expression by substituting $K^* = x_0/x_{i_{\max}}$, expanding $\sin[\omega(t_i + t_D)]$, and substituting $\omega t_i = \pi/2$ results in (Klyde and others, 1996:45):

$$\cos(\Delta\phi) = K^* \quad (38)$$

where $\Delta\phi = \omega t_D$ is the phase angle between the input and output. Solving for $\Delta\phi$ and noting that it is a phase lag gives Equation 39:

$$-\Delta\phi = -\cos^{-1}(K^*) = \sphericalangle \frac{\delta_e(j\omega)}{\delta_{e_{Command}}(j\omega)} = -\tan^{-1} \left[\sqrt{\left(\frac{1}{K^*}\right)^2 - 1} \right] \quad (39)$$

Now to compare with the closed-loop describing function phase angle, substitute $K^* = (\pi/2)(V_L/A\omega)$ into Equation 39, which results in

$$\sphericalangle \frac{\delta_e(j\omega)}{\delta_{e_{Command}}(j\omega)} = -\tan^{-1} \left[\sqrt{\left(\frac{2A\omega}{\pi V_L}\right)^2 - 1} \right] \quad (40)$$

This is slightly different from the closed loop describing function phase angle expression. These phase angle differences are shown as a function of K^* in Figure 2-6:

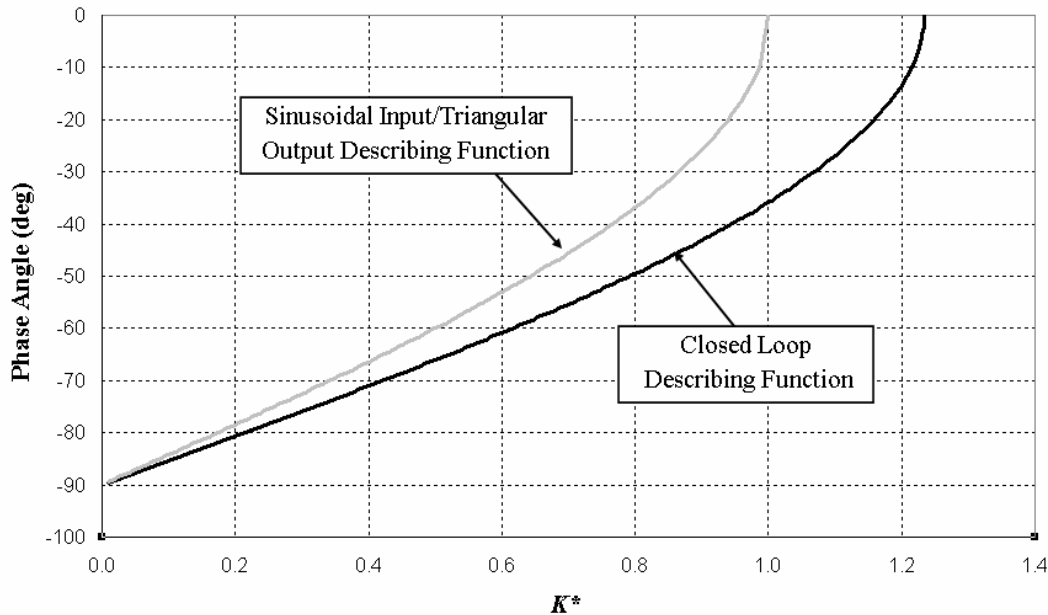


Figure 2-6. Describing Function Phase Angle Comparison

These two describing function approximations were introduced to show that similar results can be derived from different methods. According to Klyde, the more accurate of these two describing function approximations for application to Category II PIO is the sinusoidal input/triangle output solution (Klyde and others, 1996:46). Therefore, this describing function will be used throughout the remainder of this study.

Applying Describing Function Results to Predict PIO

Consider the longitudinal closed-loop system shown in Figure 2-7. $G_p(s)$ represents a model of the pilot and $G_c(s)$ represents a model of the bare aircraft dynamics. The remaining elements are equivalent to the rate-limited actuator model previously discussed in Figure 2-3.

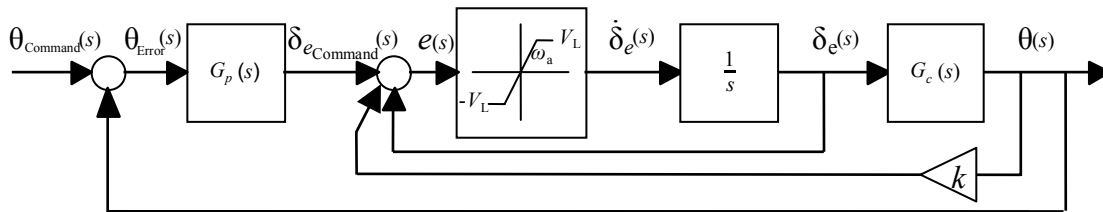


Figure 2-7. Pitch Tracking Closed Loop System

The linear elements $G_p(s)$ and $G_c(s)$ can be combined into one linear element, $G(s)$ and the nonlinear element, $N(A, \omega)$, remains separate as shown in Figure 2-8.

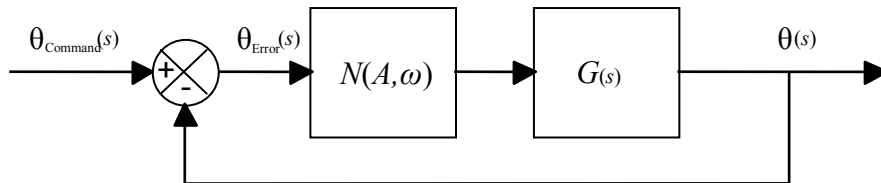


Figure 2-8. Simplified Pitch Tracking Closed Loop System

This model can then be applied to a limit cycle analysis. The requirement for a neutrally damped oscillation is simply that the open-loop amplitude ratio be equal to 1.0 and the phase be -180° (Klyde and others, 1996:54). In order for a PIO to persist, the system shown in Fig 2-8 must satisfy the Nyquist criteria shown in the following equation (Klyde and others, 1996:54):

$$G(j\omega)N(\omega, A) = -1 \quad (41)$$

or rearranged

$$G(j\omega) = \frac{-1}{N(\omega, A)} \quad (42)$$

The easiest way to view the application of this equation is to plot the open-loop magnitude and phase values of the negative inverse describing function, $-1/N(j\omega, A)$, using the K^* solutions from Equations 36 and 39 as well as the open-loop magnitude and phase of $G(j\omega)$. If the two plots intersect, a PIO is predicted (Klyde and others, 1996:63). This will be shown by means of an example later in this chapter. The K^* solutions for the negative inverse describing function are shown below in Equations 43 and 44 (Liebst, 2002):

$$\left| \frac{-1}{N(K^*)} \right| = -20 \text{Log}_{10} \left(\frac{8K^*}{\pi^2} \right) \quad (\text{dB}) \quad (43)$$

$$\angle \frac{-1}{N(K^*)} = \frac{180}{\pi} \cos^{-1} (K^*) - 180 \quad (\text{deg}) \quad (44)$$

Pilot Model

There are many pilot models to choose from in the literature. Some believe that a simple gain with no phase lag best represents the pilot in the PIO situation (Klyde and others, 1996:54). Others believe structural models are better predictors (Mitchell and Klyde, 1998:426). In another recent study, the Neal-Smith pilot model was judged to best represent the pilot model prior to the onset of rate limiting (Gilbreath, 2001:7-3). Therefore, in this study, the Neal-Smith pilot model will be utilized.

The Neal-Smith pilot model is useful for pilot-aircraft pitch attitude control loops with unity-feedback and has the following characteristics (MIL-HDBK-1797, 1997:237):

1. Adjustable gain
2. Time delay
3. Ability to develop lead, or to operate on derivative or rate information
4. Ability to develop lag, or to smooth inputs
5. Ability to provide low-frequency integration

The Neal-Smith pilot model can take on one of two forms. This determination is based on whether constant speed or two-degree-of-freedom equations are used to represent the bare aircraft dynamics. These are typified by noting whether or not a free integrator is contained in the denominator of the aircraft pitch transfer function. Otherwise, three-degree-of-freedom equations or flight control system utilizing attitude stabilization will require a different form. Table 2-1 shows these two transfer functions for the Neal-Smith pilot model (MIL-HDBK-1797, 1997:237; Bailey and BidLack, 1995:8).

Table 2-1. Neal-Smith Pilot Models

Aircraft Transfer Function with a Free Integrator	Aircraft Transfer Function without a Free Integrator
$G_p(s) = K_p \frac{(T_{Lead}s + 1)}{(T_{Lag}s + 1)} e^{-0.25s}$	$G_p(s) = K_p \frac{(5s + 1)(T_{Lead}s + 1)}{s(T_{Lag}s + 1)} e^{-0.25s}$

The theory states that the pilot chooses his gain, K_p , and his lead/lag time constants, T_{Lead} and T_{Lag} , to attain a certain bandwidth. This bandwidth varies with the flight phase category. For example, for Category A flight phase maneuvers such as air-to-air dogfighting, the required bandwidth is 3.5 rad/sec. This is measured at a closed-loop phase of -90 degrees. Further, the pilot adjusts K_p , T_{Lead} and T_{Lag} to minimize droop to no greater than 3 dB for Level 1 performance and no greater than 9 dB for Level 2 over the frequency range from 0 to 10 rad/sec while at the same time minimizing closed loop resonance (MIL-HDBK-1797, 1997:239). The phase lag term, $e^{-0.25s}$, represents delays in the pilot's neuromuscular system (MIL-HDBK-1797, 1997:239). A graphical depiction of these pilot efforts can be seen in Figure 2-9.

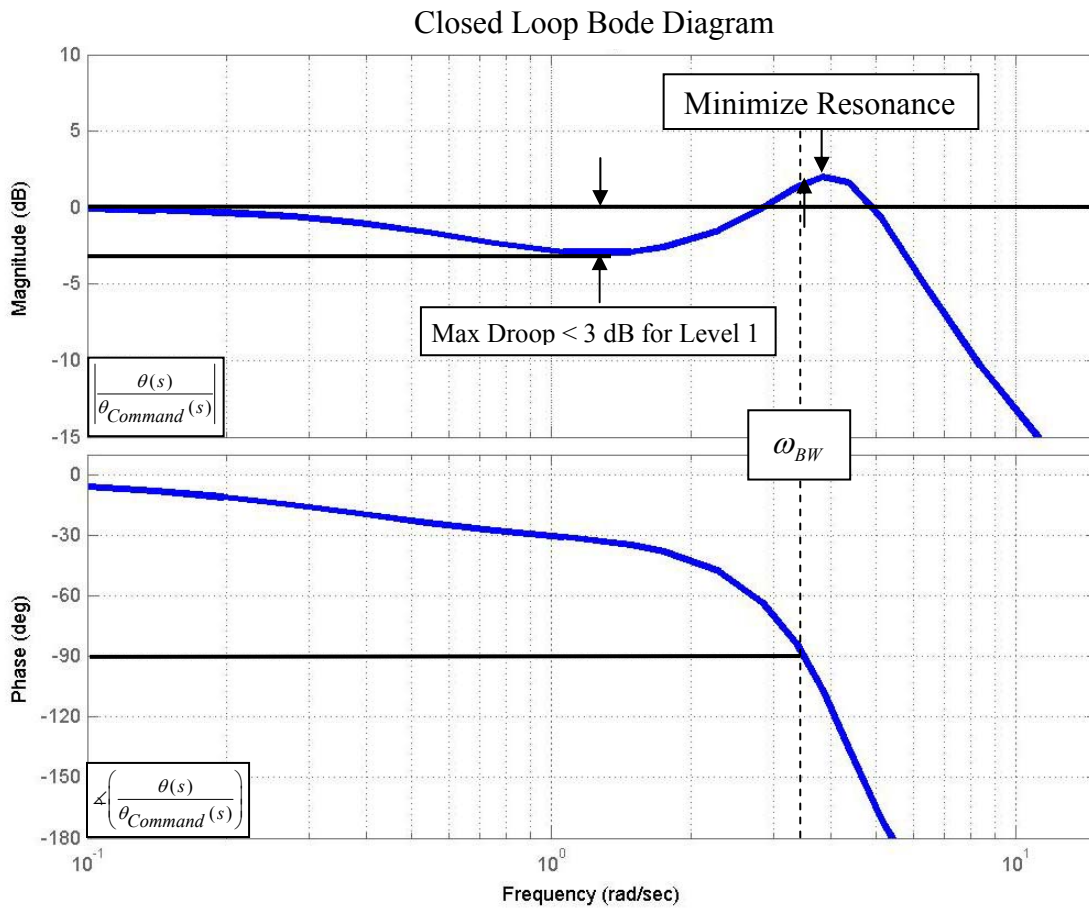


Figure 2-9. Neal-Smith Pilot Model Constraints

Gap Criterion

Utilizing the previous theoretical developments, a systematic process relating aircraft plant dynamics and actuator rate limits to PIO tendency rating will be introduced. The procedure is called the *Gap Criterion* and is based on the block diagram shown in Figure 2-10:

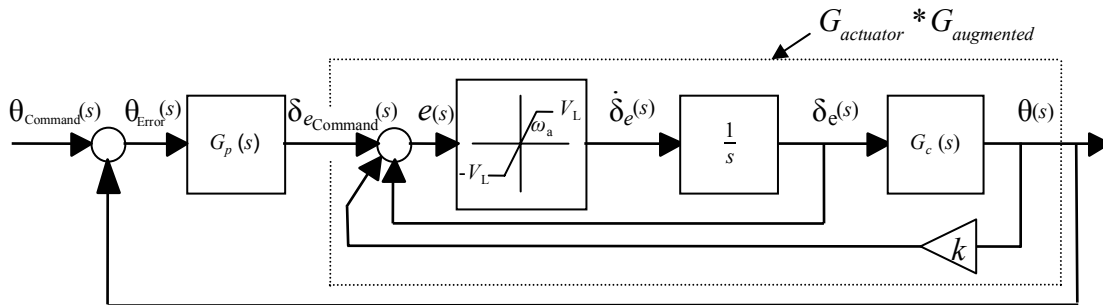


Figure 2-10. Pitch Tracking Closed-Loop System for *Gap Criterion*

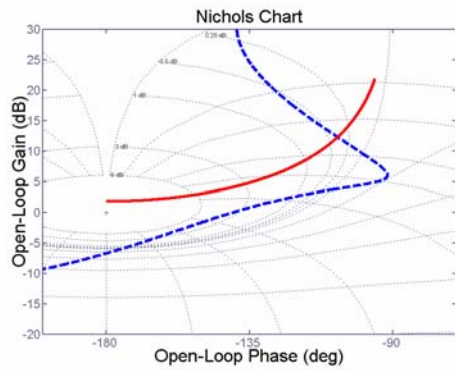
In modern fly-by-wire aircraft, feedback is an integral part of obtaining more desirable closed loop flying qualities. However, as mentioned earlier, rate limiting exposes the unaugmented dynamics and adds phase lag (Hanley, 2003:1-3). A pilot suddenly faced with different flying qualities will not be able to adjust his gain, lead or lag properties instantaneously. He will therefore continue to fly in such a manner as if the augmented aircraft dynamics were still in place. Therefore, the term $G(j\omega)$ from Equation 42 is the product of the bare aircraft dynamics, $G_c(s)$, convolved with the Neal-Smith pilot model, $G_p(s)$. This idea is incorporated in the derivation of the *Gap Criterion*.

When rate limiting is not occurring, the actuator dynamics from Figure 2-10 can be determined from block diagram methods and is $G_{actuator} = \omega_a / (s + \omega_a)$.

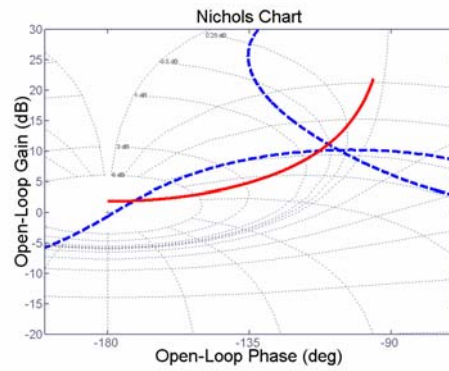
Gap Criterion Formulation.

Computing the *Gap Criterion* consists of the following steps:

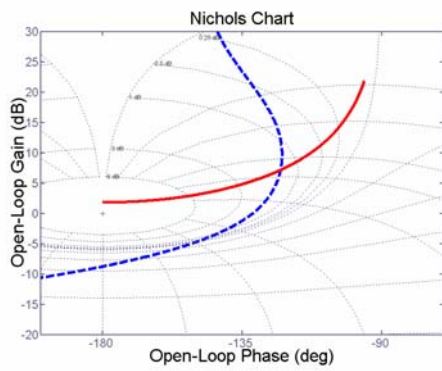
1. Determine the bare aircraft pitch-to-actuator transfer function, $G_c(s) = \frac{\theta(s)}{\delta_e(s)}$.
2. If the short period poles of $G_c(s)$ are unstable then the *Gap Criterion* automatically equals zero. This is due to control amplitudes approaching zero which cause an immediate departure from controlled flight due to dynamic instability resulting from actuator rate saturation.
3. Determine actuator dynamics for the following form: $G_{actuator} = \frac{\omega_a}{s + \omega_a}$.
Typically, $\omega_a = 20$ and this will be used throughout this study (Liebst,2001).
4. Determine an appropriate optimized Neal-Smith pilot model, $G_p(s)$, for the augmented aircraft dynamics plus actuator dynamics, $G_{actuator} * G_{augmented}$.
5. Plot the open-loop magnitude and phase of the bare aircraft dynamics convolved with the Neal-Smith pilot model dynamics, $G_c(s) * G_p(s)$ on a Nichols chart
6. Plot the negative inverse describing function open-loop magnitude and phase on the same Nichols chart using K^* . See Equations 43 and 44.
7. Determine the resulting type by reference to Figure 2-11 and then compute the *Gap Criterion* by following the steps of that type.



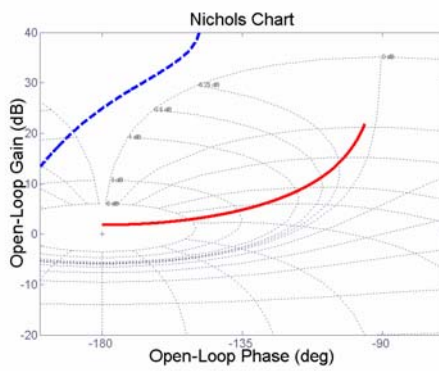
Type I



Type II



Type III



Type IV

Figure 2-11. Four Resulting Gap Criterion Types

Type I.

- 1-1. Determine the minimum amount by which the pilot would need to effectively increase gain, ΔK_p (dB), such that the two magnitude-phase lines just intersect at a frequency greater than the -3 dB Neal-Smith maximum droop frequency as shown in Figure 2-12:

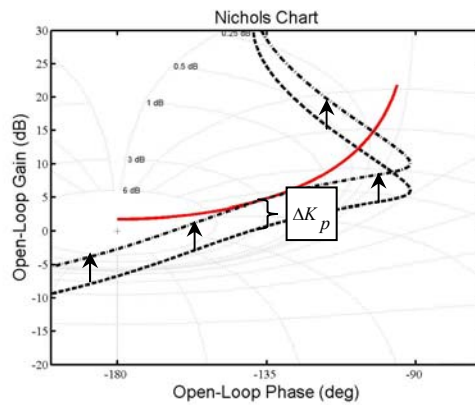


Figure 2-12. Case I Effective Pilot Gain Increase

- 1-2. Determine the values of K^* and ω (rad/sec) at this intersection
- 1-3. Determine the commanded actuator deflection amplitude, A , utilizing the following equation where V_L is the known actuator rate limit in deg/sec:

$$A = \frac{\pi}{2} \frac{V_L}{\omega K^*}$$

- 1-4. Normalize this amplitude by dividing by the maximum available actuator deflection, A_{max}
- 1-5. The *Gap Criterion* is this normalized amplitude multiplied by ΔK_p :

$$Gap\ Criterion = \frac{A}{A_{max}} * 10^{(\Delta K_p / 20)}$$

Type II.

- 2-1. Determine the minimum amount by which the pilot would need to effectively decrease gain, ΔK_p (dB), such that the two magnitude-phase lines only intersect in one place at a frequency greater than the -3 dB Neal-Smith maximum droop frequency as shown in Figure 2-13:

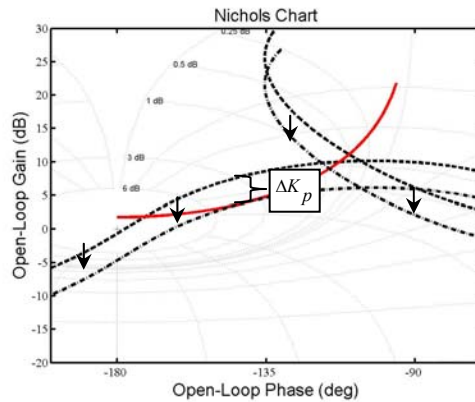


Figure 2-13. Case II Effective Pilot Gain Decrease

- 2-2. Determine the values of K^* and ω (rad/sec) at this intersection
- 2-3. Determine the commanded actuator deflection amplitude, A , utilizing the following equation where V_L is the known actuator rate limit in deg/sec:

$$A = \frac{\pi}{2} \frac{V_L}{\omega K^*}$$

- 2-4. Normalize this amplitude by dividing by the maximum available actuator deflection, A_{max}
- 2-5. The *Gap Criterion* is this normalized amplitude multiplied by ΔK_p .

$$Gap\ Criterion = \frac{A}{A_{max}} * 10^{(\Delta K_p / 20)}$$

Type III.

- 3-1. Determine the values of K^* and ω (rad/sec) at the intersection
- 3-2. Determine the commanded actuator deflection amplitude, A , utilizing the following equation where V_L is the known actuator rate limit in deg/sec:

$$A = \frac{\pi}{2} \frac{V_L}{\omega K^*}$$

- 3-3. Normalize this amplitude by dividing by the maximum available actuator deflection, A_{max}
- 3-4. The *Gap Criterion* is this normalized amplitude.

$$\text{Gap Criterion} = \frac{A}{A_{max}}$$

Type IV.

- 4-1. No determination of Gap Criterion can be made.

Example of Gap Criterion Application

Reconsider the closed loop system of Figure 2-10 with the following characteristics:

- $G_c(s) = \frac{(4.5)(s+1.5)}{s(s^2 + 3s + 6)}$
- $G_{actuator} = \frac{20}{s + 20}$
- $k = 0$ (unaugmented), therefore $G_{augmented} = G_c$
- $V_L = 30$ deg/sec
- Maximum actuator deflection: $\delta_{e_{max}} = 30$ deg
- Category A flight phase, Neal-Smith bandwidth = 3.5 rad/sec

Utilizing the USAF Wright Laboratory Flight Dynamics Directorate's MATLAB™ Interactive Flying Qualities Toolbox for Matlab (Domon and Foringer, 1996), the Neal-Smith pilot model was found to be:

$$G_p(s) = 0.856 \frac{(0.583s + 1)}{(0.0001s + 1)} e^{-0.25s}$$

The open-loop magnitude and phase of $G_{actuator} * G_{augmented}$ are plotted in Figure 2-14 as well as the open-loop magnitude and phase of the negative inverse describing function. It can be seen that an open-loop gain increase (ΔK_p) of 7.502 dB is required for the two lines to meet. At this intersection, the values for K^* and ω are 0.7635 and 3.9418 rad/sec, respectively. After calculating the amplitude, $A = 15.66$ deg, the result is normalized by dividing by 30 deg ($\delta_{e\max}$). This normalized result is multiplied by ΔK_p to yield the Gap Criterion. In this example the *Gap Criterion* equals 1.238.

This example showed how preflight *Gap Criterion* can be calculated. It is expected that matching these values with their respective PIO Tendency Ratings should yield some correlation. This will be accomplished by examining historical databases and then collecting additional data in the LAMARS simulator and VISTA aircraft.

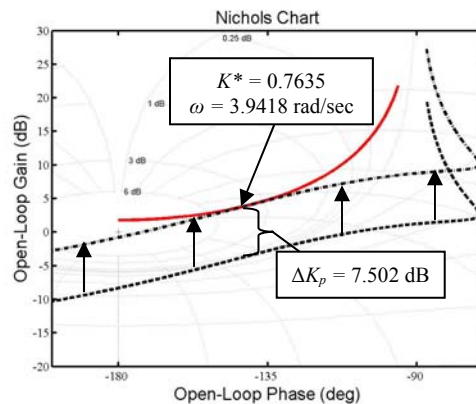


Figure 2-14. Nichols Chart of the Example Problem

III. Analysis of Selected Historical Data

In this section, two previous PIO studies, HAVE PREVENT and HAVE OLOP, will be examined using the *Gap Criterion* (Hanley, 2002; Gilbreath, 2000).

HAVE PREVENT Analysis

HAVE PREVENT was a simulator and flight test study comparing two different PIO prevention filters. The study was conducted as part of a Test Management Project at the USAF Test Pilot School and a thesis sponsored by the Air Force Institute of Technology (Hanley and others, 2002; Hanley, 2003). The two PIO filters examined were the Feedback with Bypass and the Derivative Switching filters. In order to establish a baseline, runs with neither filter engaged were conducted in both the LAMARS simulator and VISTA NF-16D aircraft. However, few no-filter data points were collected during the flight test portion. Therefore, only the simulator data will be examined.

In this simulator, pilot-induced oscillation tendency ratings (PIOR) were gathered in two distinct phases with specific piloting tasks and in which the evaluation pilot was blind to the randomized bare aircraft dynamics and rate limit combinations. In Handling Qualities Phase 2 testing, a precision aimpoint was tracked as “aggressively and assiduously as possible, always striving to correct even the smallest errors” using a piloting technique known as Handling Qualities During Tracking (HQDT) (Brown and others, 2002:21-18). The precision aimpoint involved a sum-of-sines head’s up display (HUD) tracking task, as shown in Figure 3-1 (MIL-HDBK-1797, 1997:108m). Handling Qualities Phase 3 “operational” testing was also accomplished and involved two different tasks (Brown and others, 2002:21-19). These tasks were the discrete HUD pitch tracking task and computer generated aircraft target tracking task shown in Figures 3-2 and 3-3.

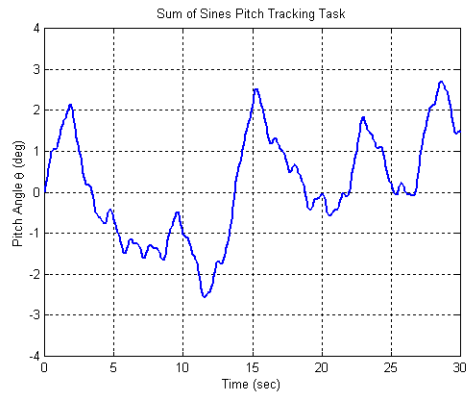
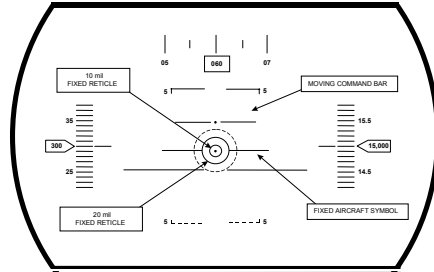


Figure 3-1. Phase 2 Sum-of-sines Pitch Tracking Task

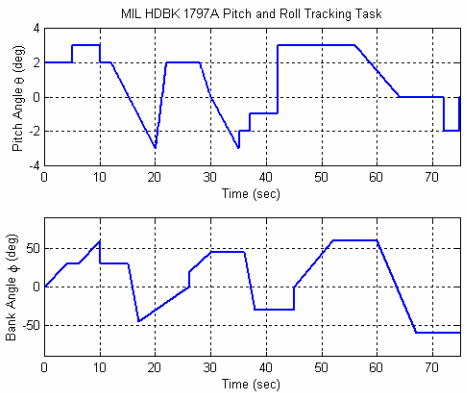
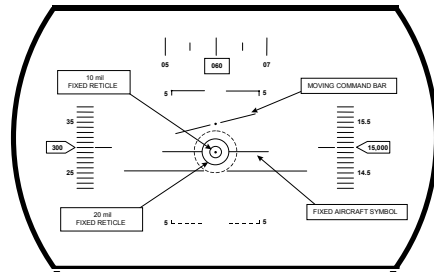


Figure 3-2. Phase 3 Discrete HUD Pitch Tracking Task

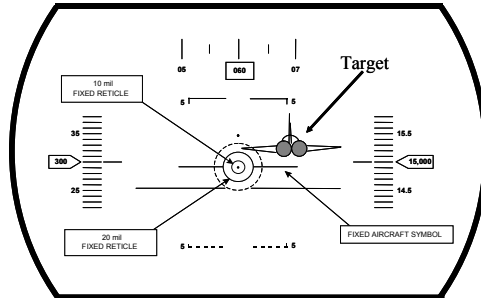


Figure 3-3. Phase 3 Target Tracking Task

The study involved four test cases labeled A through D. Each test case had different bare aircraft dynamics but all were augmented with angle-of-attack and pitch-rate feedback to produce almost identical closed loop dynamics. Table 3-1 shows these dynamics and the augmentation required. Also shown are the bare and augmented short period natural frequencies (ω_{sp}) and damping ratios (ζ_{sp}) for each case except for Case D which is unstable. The time to double amplitude (T_2) is shown instead. The actuator rate limits used in this project were 15 deg/sec, 30 deg/sec, 45 deg/sec and 60 deg/sec. The Matlab/SimulinkTM diagram used to determine the bare and augmented aircraft transfer functions is shown in Figure 3-4. Appendix A contains the fourth order state space model matrices of the linear decoupled small perturbation longitudinal equations of motion.

Table 3-1. HAVE PREVENT Case Characteristics (Hanley, 2003)

Case	Bare Aircraft Poles	ω_{sp}	ζ_{sp}	K_q	K_a	Aircraft Poles with Stability Augmentation
A	$-0.017 \pm 0.074j$ $-2.200 \pm 2.220j$	3.125	0.704	0	0	$-0.017 \pm 0.074j$ $-2.200 \pm 2.220j$
B	$-0.016 \pm 0.079j$ $-1.420 \pm 1.860j$	2.34	0.61	0.14	0.21	$-0.0166 \pm 0.0736j$ $-2.261 \pm 2.359j$
C	$-0.009 \pm 0.097j$ $-0.860 \pm 0.084j$	0.86	0.995	0.24	0.51	$-0.0168 \pm 0.0737j$ $-2.241 \pm 2.517j$
D	$-0.017 \pm 0.033j$ 1.07, -1.67	$T_2 = 2.31$ sec		0.34	0.61	$-0.0169 \pm 0.0737j$ $-2.317 \pm 2.624j$

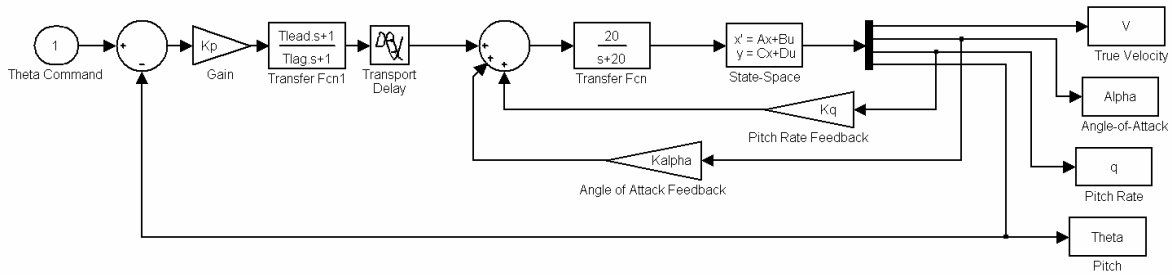


Figure 3-4. Longitudinal State Space Diagram (Matlab/Simulink™, 2001)

Gap Criterion Calculation for HAVE PREVENT Datasets.

Step 1.

The pitch-to-actuator transfer functions for the bare aircraft dynamics are shown in Table 3-2. They were calculated using the Matlab™ code shown in Appendix B.

Table 3-2. HAVE PREVENT Pitch-to-Actuator Transfer Functions (G_c)

Case	G_c
A	$\frac{-11.09s^2 - 14.37s - 0.5277}{s^4 + 4.402s^3 + 9.889s^2 + 0.3562s + 0.05612}$
B	$\frac{-11.09s^2 - 14.37s - 0.5277}{s^4 + 2.887s^3 + 5.573s^2 + 0.1938s + 0.03557}$
C	$\frac{-11.09s^2 - 14.37s - 0.5277}{s^4 + 1.729s^3 + 0.7799s^2 + 0.02955s + 0.007019}$
D	$\frac{-11.08s^2 - 14.37s - 0.5277}{s^4 + 0.634s^3 - 1.765s^2 - 0.05993s - 0.002462}$

Step 2.

Since Case D has unstable short period poles, the *Gap Criterion* is automatically set equal to zero for all rate limits.

Step 3.

Actuator dynamics for this dataset are $G_{actuator} = \frac{20}{s + 20}$.

Step 4.

The Neal-Smith pilot model transfer functions are shown in Table 3-3 along with the augmented dynamics for which they were computed. They were calculated using the Interactive Flying Qualities Toolbox for Matlab provided by the Flying Dynamics Directorate of the Air Force Research Laboratories (Doman and Forringer, 1996).

Table 3-3. HAVE PREVENT Neal-Smith Pilot Models

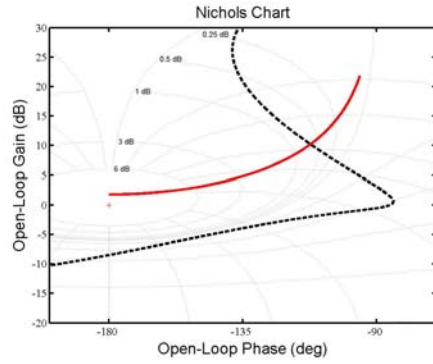
Case	G_p	$G_{actuator} * G_{augmented}$
A	$-0.12533 \frac{(5s+1)(0.31659s+1)}{s(0.0001s+1)} e^{-0.25s}$	$\frac{-221.7s^2 - 287.5s - 10.55}{s^5 + 24.4s^4 + 97.93s^3 + 198.1s^2 + 7.179s + 1.122}$
B	$-0.12652 \frac{(5s+1)(0.28336s+1)}{s(0.0001s+1)} e^{-0.25s}$	$\frac{-221.7s^2 - 287.5s - 10.55}{s^5 + 22.89s^4 + 94.57s^3 + 198.8s^2 + 7.018s + 1.114}$
C	$-0.12618 \frac{(5s+1)(0.25433s+1)}{s(0.0001s+1)} e^{-0.25s}$	$\frac{-221.7s^2 - 287.5s - 10.55}{s^5 + 21.73s^4 + 89.11s^3 + 198.6s^2 + 7.088s + 1.118}$
D	$-0.12659 \frac{(5s+1)(0.23182s+1)}{s(0.0001s+1)} e^{-0.25s}$	$\frac{-221.7s^2 - 287.5s - 10.55}{s^5 + 20.63s^4 + 86.93s^3 + 198.7s^2 + 7.12s + 1.12}$

Step 5 and 6.

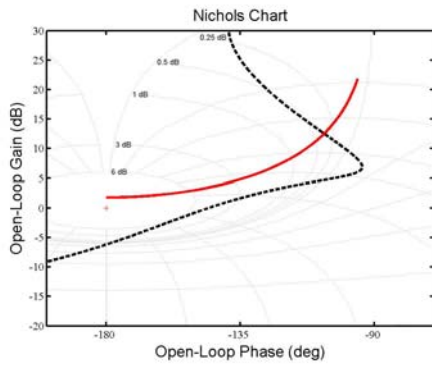
Figure 3-5 shows the Nichols charts for Cases A, B and C.

Step 7.

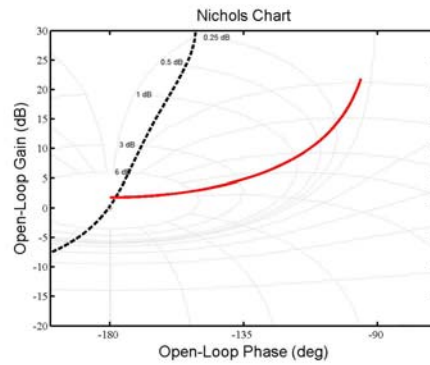
Cases A and B are of Type I. Case C is Type III.



Case A



Case B



Case C

Figure 3-5. HAVE PREVENT Nichols Charts for Cases A, B and C

Type I, Step 1-1 through 1-2.

The minimum amount of effective increase in gain for Cases A and B, along with the determined values for K^* , ω and A_{max} , are shown in Table 3-4:

Table 3-4. HAVE PREVENT Components for Cases A and B

Case	ΔK_p (dB)	K^*	ω (rad/s)	A_{max} (deg)
Case A	8.431	0.829	4.51	30
Case B	3.159	0.726	2.80	30

The final values for the *Gap Criterion* and amplitude for each case and rate limit are shown in Table 3-5:

Table 3-5. Gap Criteria Values for HAVE PREVENT Cases A and B

Case	Maximum Actuator Deflection Rate (V_L , deg/sec)	A (deg)	<i>Gap Criterion</i>
A	15	6.302	0.555
	30	12.604	1.109
	45	18.906	1.664
	60	25.208	2.218
B	15	11.591	0.556
	30	23.182	1.112
	45	34.773	1.667
	60	46.364	2.223

Type III, Step 3-1 through 3-4.

The determined values for K^* , ω , A_{max} and *Gap Criterion* for each rate limit applied to Case C are shown in Table 3-6:

Table 3-6. *Gap Criteria* for HAVE PREVENT Case C

Case	K^*	ω (rad/s)	A_{max} (deg)	Maximum Actuator Deflection Rate (V_L , deg/sec)	A (deg)	<i>Gap Criterion</i>
C	0.999	2.62	30	15	9.002	0.300
				30	18.004	0.600
				45	27.006	0.900
				60	36.008	1.200

HAVE PREVENT Gap Criterion Summary.

Table 3-7 summarizes the *Gap Criteria* for Project HAVE PREVENT. The dataset produced a range of *Gap Criterion* from 0.0 to 2.233. The range was well distributed for attempting to correlate *Gap Criterion* and PIOR.

Table 3-7. HAVE PREVENT *Gap Criteria* Summary

Case	Maximum Actuator Deflection Rate (V_L , deg/sec)	<i>Gap Criterion</i>
A	15	0.555
	30	1.109
	45	1.664
	60	2.218
B	15	0.556
	30	1.112
	45	1.667
	60	2.223
C	15	0.300
	30	0.600
	45	0.900
	60	1.200
D	15	0.0
	30	0.0
	45	0.0
	60	0.0

HAVE PREVENT Gap Criterion Correlation.

The PIOR and *Gap Criterion* data were paired and the results plotted in Figures 3-6 through 3-8. There were cases in which the same bare aircraft dynamics and rate limits and hence the same *Gap Criterion* value were tested multiple times by the same pilot or different pilots. In these cases, the same PIOR was often found. This resulted in multiple pairs of datapoints with the same *Gap Criterion* and PIOR values. In an effort to represent this data density, all plots will use a “bubble chart” style in which bubble size indicates multiple datapoints with the same pair values.

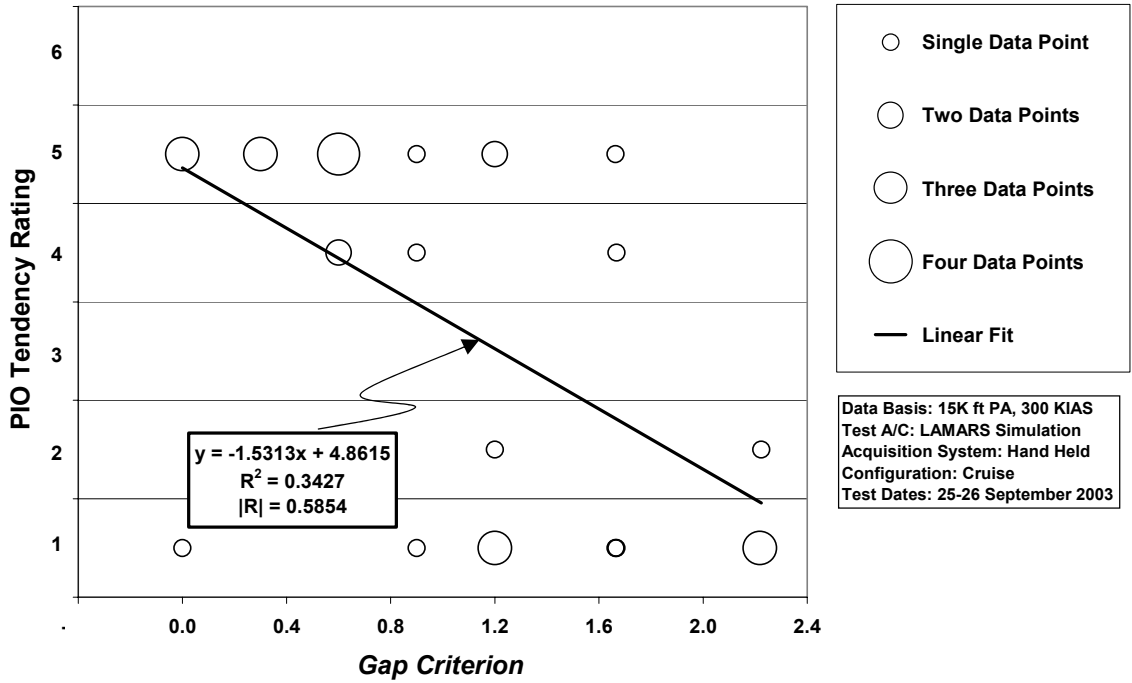


Figure 3-6. HAVE PREVENT Phase 2 Sum-of-sines Task LAMARS Data

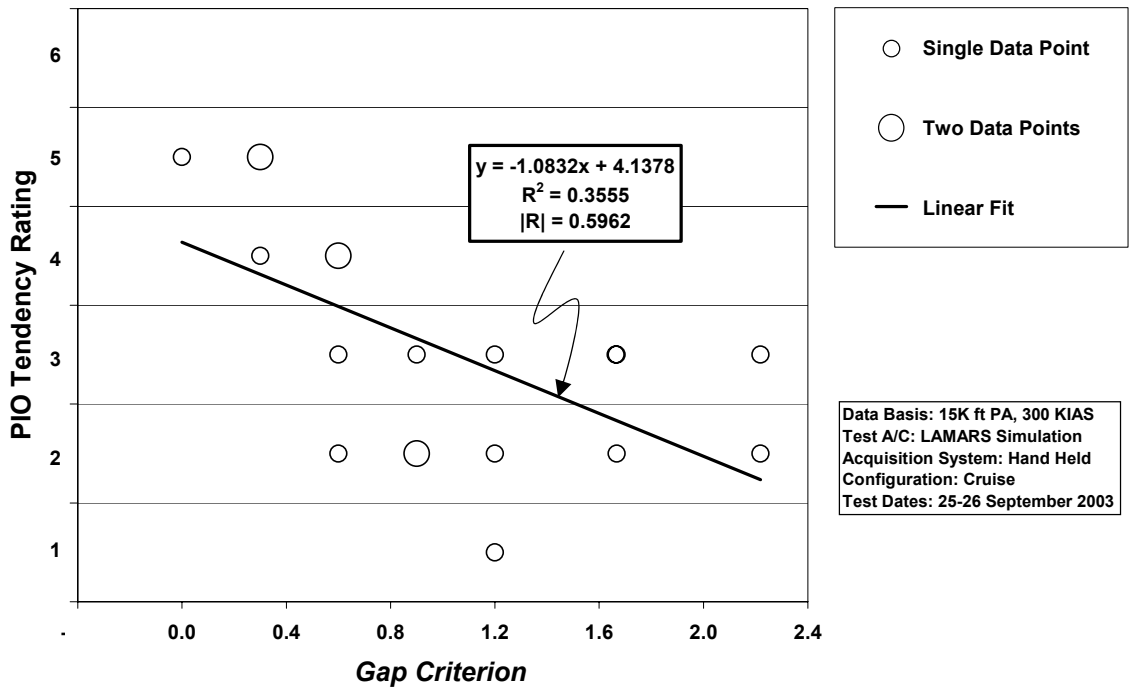


Figure 3-7. HAVE PREVENT Phase 3 Discrete HUD Pitch Tracking Task LAMARS Data

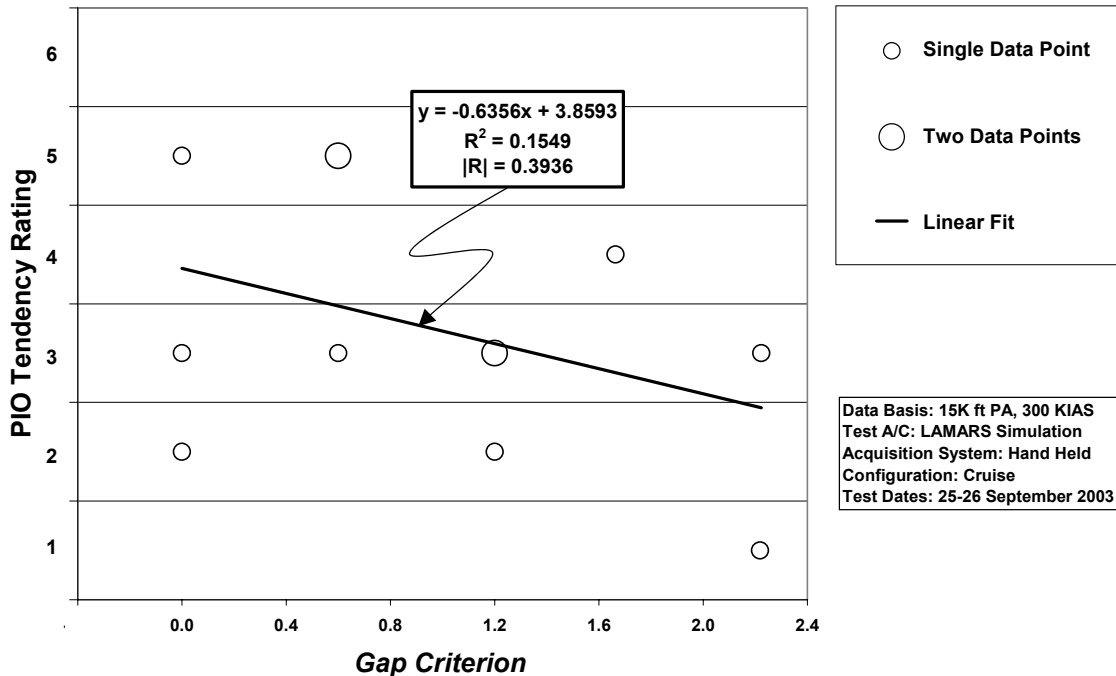


Figure 3-8. HAVE PREVENT Phase 3 Target Tracking Task LAMARS Data

With just a glance, it is difficult to see any readily apparent trend in the data scatter. Therefore, the probability of a linear correlation existing for the data was investigated as described in Appendix C (Wheeler and Ganji, 1996:145-147). The linear fit depicted on the plots displays this correlation.

Confidence level was used to determine if a relationship existed between PIOR and corresponding *Gap Criterion* values. Common engineering practices suggest a confidence level of 95% represents definitive “real” correlation (Wheeler and Ganji, 1996:147). A table listing the linear correlation coefficient, minimum correlation coefficient for 95% confidence and actual confidence level for each dataset is shown below. It can be seen that 2 out of 3 datasets easily met the minimum confidence level. The Phase 3 Target Tracking dataset has fewer datapoints than the other two and hence will be more sensitive to outliers.

Table 3-8. HAVE PREVENT Correlation Confidence Levels

Dataset	Sample Size	95 % Confidence Minimum Correlation	Actual Linear Correlation	Actual Confidence Level
Phase 2 Sum-of-sines	30	0.361	0.585	99.93%
Phase 3 Discrete Pitch Tracking	19	0.456	0.596	99.29%
Phase 3 Target Tracking	12	0.576	0.394	79.49%

HAVE PREVENT Best Curve Fit.

In the previous section, correlation for a linear fit was investigated. This is not necessarily the best curve fit. Multiple curve fits were attempted for each dataset including exponential, natural logarithmic, polynomial and power series interpolations. A least squares method was used to identify the correlation coefficient of each fit using commercial software (Microsoft Excel, 2002). The following table lists these correlation values.

Table 3-9. HAVE PREVENT Curve Fit Correlation Values

Dataset	Linear	Exponential	Logarithmic (Ln (GC+1))	2 nd Order Polynomial	Power Series (GC+1)
Phase 2 Sum-of-sines	0.585	0.561	0.552	0.593	0.525
Phase 3 Discrete Pitch Tracking	0.596	0.507	0.672	0.786	0.577
Phase 3 Target Tracking	0.394	0.426	0.335	0.468	0.357

At first glance, the second order polynomial curve fit gives the best mathematical results. But on further inspection, this curve fit does not match well at higher *Gap Criterion* values. The logarithmic (Ln(GC+1)) seems to be the best case for the

combination of high correlation and endpoint matching. Since *Gap Criterion (GC)* values of zero do not work well with natural logarithmic curve fits, a factor of one was added to these values and the correlation found. Figures 3-6 through 3-8 show the data with this logarithmic curve fit.

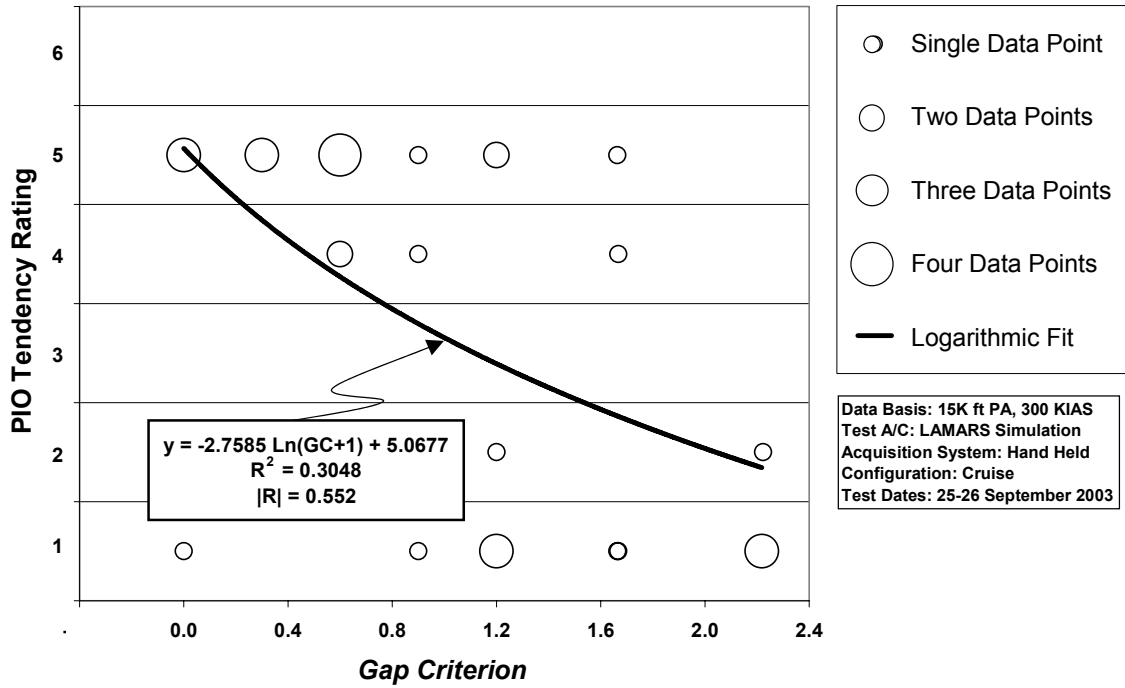


Figure 3-9. HAVE PREVENT Phase 2 Sum-of-sines Task LAMARS Data with Logarithmic Curve Fit

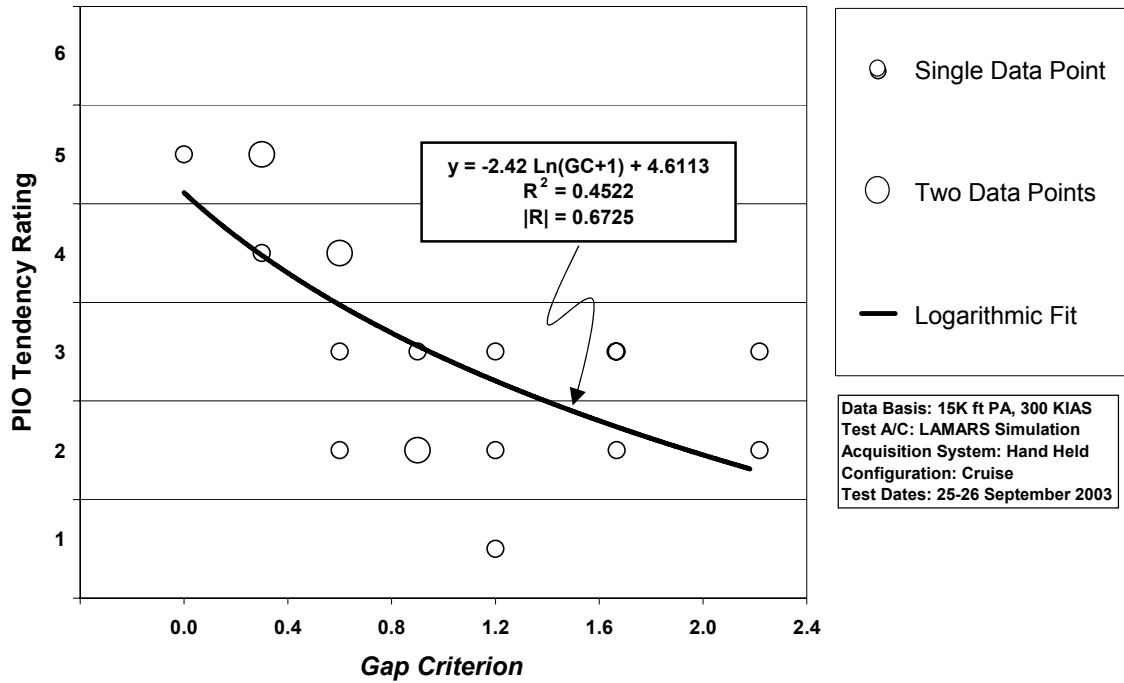


Figure 3-10. HAVE PREVENT Phase 3 Discrete HUD Pitch Tracking Task LAMARS Data with Logarithmic Curve Fit

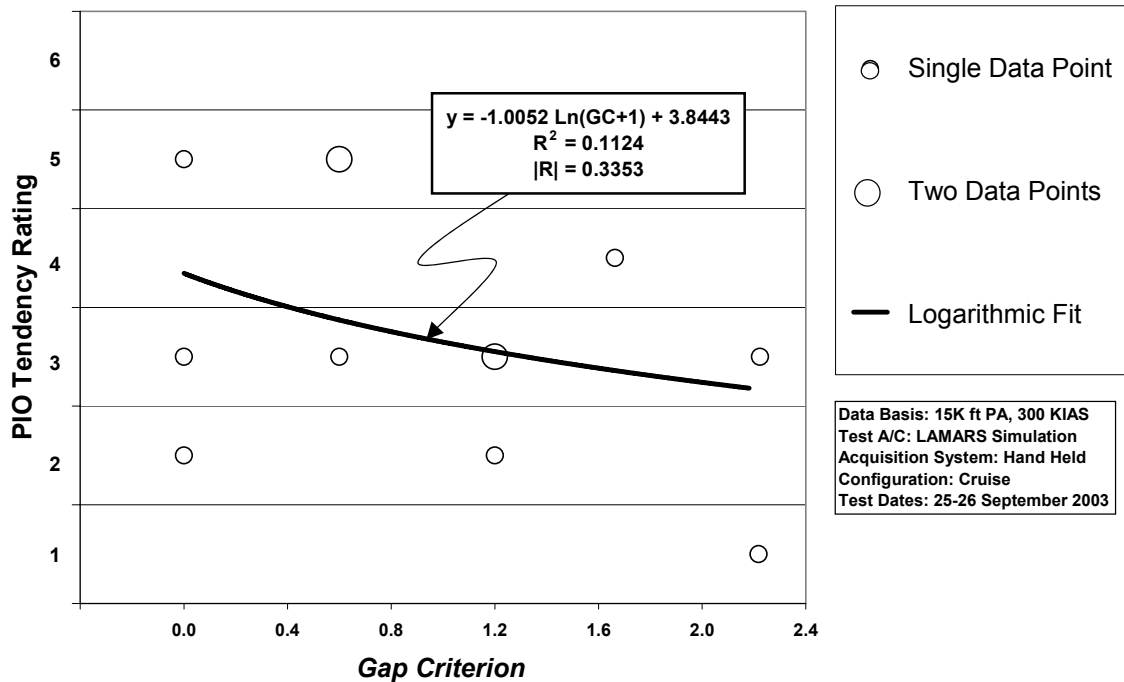


Figure 3-11. HAVE PREVENT Phase 3 Target Tracking Task LAMARS Data with Logarithmic Curve Fit

HAVE OLOP Analysis

HAVE OLOP was a flight test study attempting to validate the Open Loop Onset Point (OLOP) criteria for PIO prediction. The study was conducted in the VISTA NF-16D as part of a Test Management Project at the USAF Test Pilot School and a thesis sponsored by the Air Force Institute of Technology (Gilbreath and others, 2000; Gilbreath, 2001). Just as in Project HAVE PREVENT, PIOR were gathered in two distinct phases with specific piloting tasks. In fact, with the exception of the Phase 3 Target Tracking Task which was not performed, the tasks were identical to those of HAVE PREVENT: Phase 2 Sum-of-sines Tracking Task and Phase 3 Discrete HUD Pitch Tracking Task. The PIOR scale used was the same one previously described in Chapter I.

This study also involved four test cases labeled A through D though each was distinctly different from the identically named HAVE PREVENT cases. Each test case had different bare aircraft dynamics but all were augmented with angle-of-attack and pitch-rate feedback to produce almost identical closed loop dynamics. Table 3-10 shows these dynamics and the augmentation required. Also shown are the bare and augmented short period natural frequencies (ω_{sp}) and damping ratios (ζ_{sp}) for each case except for Case D which is unstable and diverges. Instead, the time to double amplitude (T_2) is shown. The actuator rate limits used in this project were 10 deg/sec, 20 deg/sec, 30 deg/sec, 40 deg/sec, 50 deg/sec and 60 deg/sec. The Matlab/Simulink™ diagram used to determine the bare and augmented aircraft transfer functions is shown in Figure 3-4. Appendix A contains the fourth order state space model matrices of the linear decoupled small perturbation longitudinal equations of motion.

Table 3-10. HAVE OLOP Case Characteristics (Gilbreath, 2001)

Case	Bare Aircraft Poles	ω_{sp}	ζ_{sp}	K_q	K_α	Aircraft Poles with Stability Augmentation
A	$-.017 \pm .074j$ $-.510 \pm 3.36j$	3.40	0.15	0.023	0.412	$-.017 \pm .060j$ $-3.51 \pm 3.58j$
B	$-.017 \pm .074j$ $-.608 \pm 4.88j$	0.78	0.78	0.444	0.984	$-.017 \pm .072j$ $-3.50 \pm 3.58j$
C	$-.017 \pm .074j$ $-1.29 \pm 1.72j$	2.15	0.60	0.897	0.347	$-.017 \pm .074j$ $-3.50 \pm 3.57j$
D	$-.017 \pm .074j$ 1.284, -2.13	$T_2 = 0.6sec$		1.218	0.487	$-.017 \pm .074j$ $-3.55 \pm 3.62j$

Gap Criterion Calculation for HAVE OLOP Datasets.

Step 1.

The bare aircraft dynamics are shown in Table 3-11:

Table 3-11. HAVE OLOP Pitch-to-Actuator Transfer Functions (G_c)

Case	G_c
A	$\frac{-11.08s^2 - 14.37s - 0.5277}{s^4 + 1.054s^3 + 11.60s^2 + 0.3989s + 0.06664}$
B	$\frac{-11.09s^2 - 14.37s - 0.5277}{s^4 + 1.251s^3 + 0.6555s^2 + 0.0277s + 0.003507}$
C	$\frac{-11.08s^2 - 14.37s - 0.5277}{s^4 + 2.614s^3 + 4.716s^2 + 0.172s + 0.02665}$
D	$\frac{-11.08s^2 - 14.37s - 0.5277}{s^4 + 0.88s^3 - 2.7s^2 - 0.08811s - 0.01577}$

Step 2.

Since Case D has unstable short period poles, the *Gap Criterion* is automatically set equal to zero for all rate limits.

Step 3.

Actuator dynamics for this dataset are $G_{actuator} = \frac{20}{s + 20}$.

Step 4.

The Neal-Smith pilot model transfer functions are shown in Table 3-12 along with the augmented dynamics for which they were computed: They were calculated using the Interactive Flying Qualities Toolbox for Matlab (Doman and Forringer, 1996).

Table 3-12. HAVE OLOP Neal-Smith Pilot Models

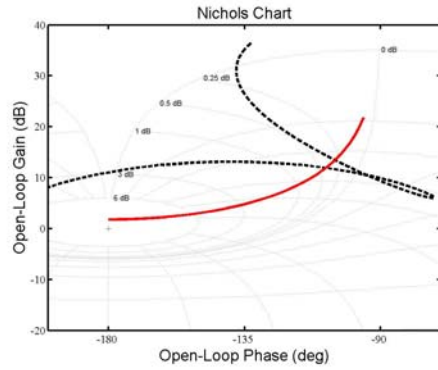
Case	G_p	$G_{actuator} * G_{augmented}$
A	$-0.23108 \frac{(5s+1)(0.07543s+1)}{s(0.0001s+1)} e^{-0.25s}$	$\frac{-221.7s^2 - 287.5s - 10.55}{s^5 + 21.05s^4 + 124.1s^3 + 356.0s^2 + 12.57s + 1.377}$
B	$-0.23398 \frac{(5s+1)(0.074331s+1)}{s(0.0001s+1)} e^{-0.25s}$	$\frac{-221.7s^2 - 287.5s - 10.55}{s^5 + 21.25s^4 + 125.2s^3 + 360.7s^2 + 12.88s + 1.956}$
C	$-0.25267 \frac{(5s+1)(0.068821s+1)}{s(0.0001s+1)} e^{-0.25s}$	$\frac{-221.7s^2 - 287.5s - 10.55}{s^5 + 22.61s^4 + 134.9s^3 + 394.8s^2 + 14.1s + 2.253}$
D	$-0.23213 \frac{(5s+1)(0.072622s+1)}{s(0.0001s+1)} e^{-0.25s}$	$\frac{-221.7s^2 - 287.5s - 10.55}{s^5 + 20.88s^4 + 124.1s^3 + 357.9s^2 + 12.81s + 2.018}$

Step 5 and 6.

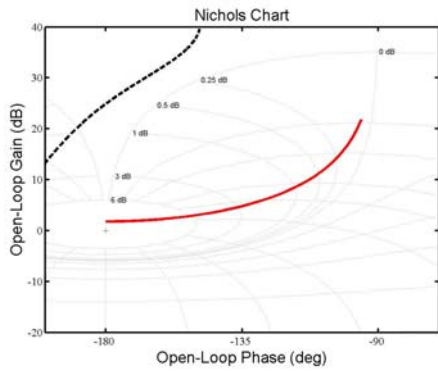
Figure 3-12 shows the Nichols charts for Cases A, B and C:

Step 7.

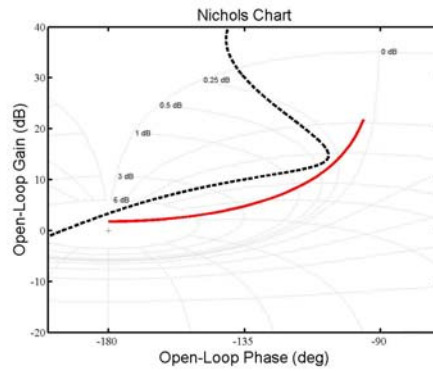
Cases A and C are of Type II. Case B is Type IV.



Case A



Case B



Case C

Figure 3-12. HAVE OLOP Nichols Charts for Cases A, B and C

Type II, Step 2-1 through 2-2.

The minimum amount of effective decrease in gain for Cases A and C, along with the determined values for K^* , ω and A_{max} , are shown in Table 3-13:

Table 3-13. HAVE OLOP Components for Cases A and C

Case	ΔK_p (dB)	K^*	ω (rad/s)	A_{max} (deg)
Case A	-10.290	0.943	3.50	30
Case C	-5.455	0.801	2.05	30

The final values for the *Gap Criteria* and amplitudes for Cases A and C and their respective rate limits are shown in Table 3-14:

Table 3-14. Gap Criteria Values for HAVE OLOP Case A and C

Case	Maximum Actuator Deflection Rate (V_L , deg/sec)	A (deg)	<i>Gap Criterion</i>
A	10	4.76	0.0485
	20	9.52	0.0970
	30	14.28	0.1456
	40	19.04	0.1941
	50	23.80	0.2426
	60	28.55	0.2911
C	10	9.57	0.1702
	20	19.13	0.3403
	30	28.70	0.5105
	40	38.26	0.6806
	50	47.83	0.8508
	60	57.40	1.0210

Type IV, Step 4-1.

HAVE OLOP Case B is a Type IV and has no *Gap Criterion* solution.

HAVE OLOP Gap Criterion Summary.

Table 3-15 summarizes the *Gap Criteria* for Project HAVE OLOP:

Table 3-15. HAVE OLOP *Gap Criteria* Summary

Case	Maximum Actuator Deflection Rate (V_L , deg/sec)	<i>Gap Criterion</i>
A	10	0.0485
	20	0.0970
	30	0.1456
	40	0.1941
	50	0.2426
	60	0.2911
C	10	0.1702
	20	0.3403
	30	0.5105
	40	0.6806
	50	0.8508
	60	1.0210
D	10	0.0
	20	0.0
	30	0.0
	40	0.0
	50	0.0
	60	0.0

HAVE OLOP Gap Criterion Correlation.

The PIOR and *Gap Criterion* data were paired and the results plotted in Figures 3-13 and 3-14:

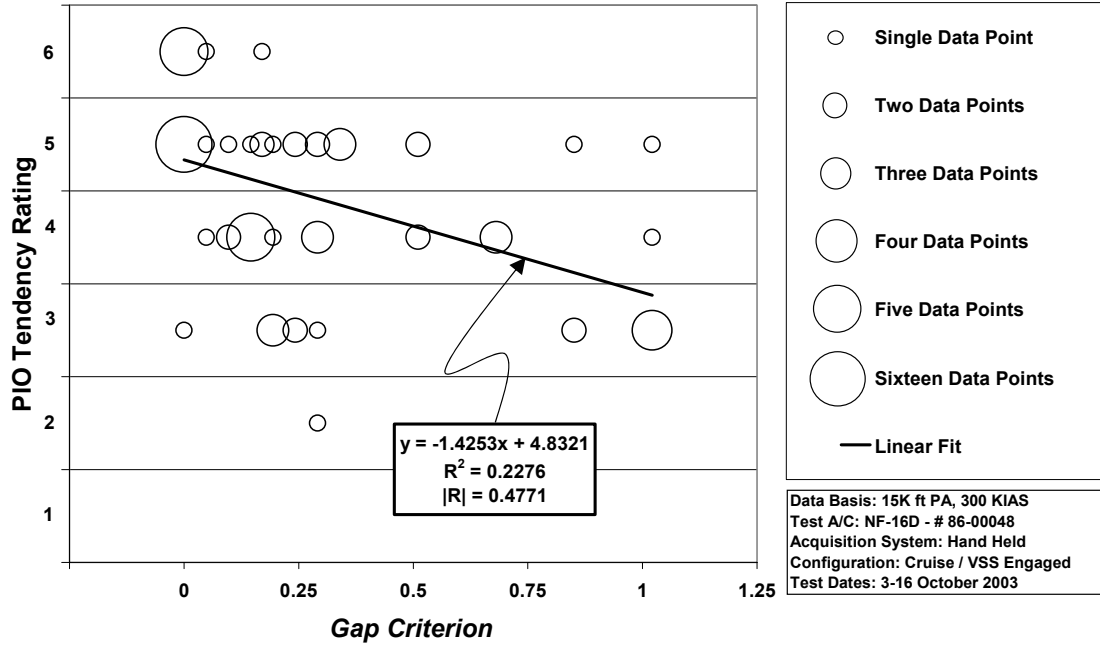


Figure 3-13. HAVE OLOP Phase 2 Sum-of-sines Task VISTA Data

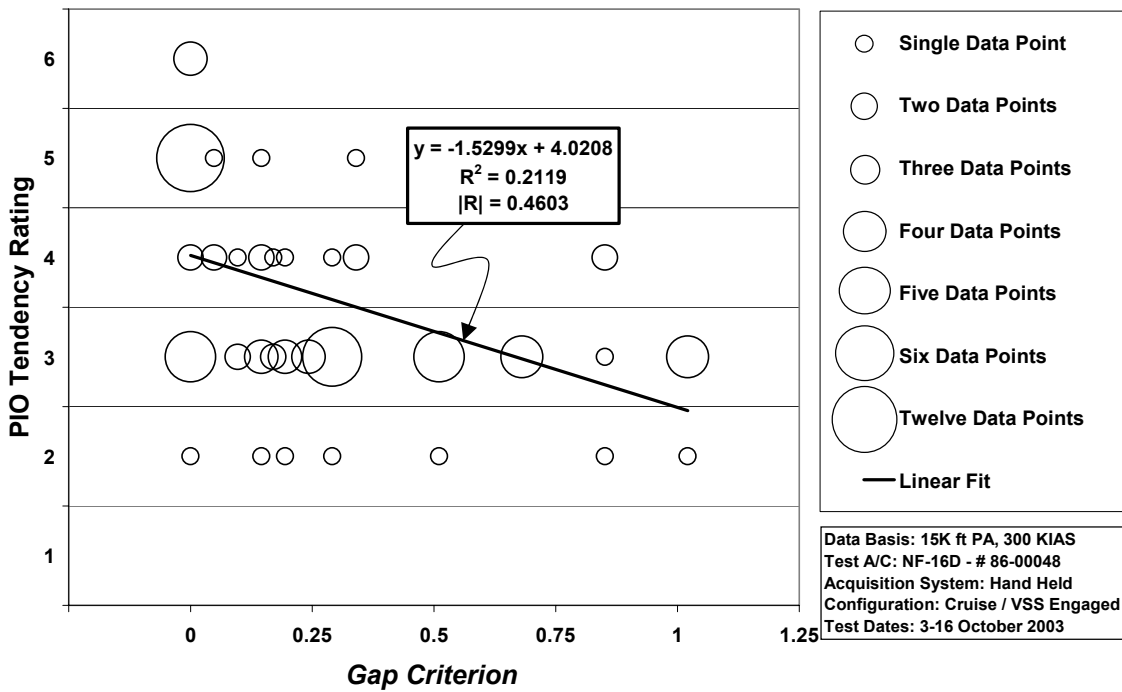


Figure 3-14. HAVE OLOP Phase 3 Discrete HUD Pitch Tracking Task VISTA Data

As in the HAVE PREVENT data analysis, the probability of a linear correlation existing was investigated as described in Appendix C. The linear fit depicted on the plots displays this correlation.

Confidence level was used to determine if a relationship existed between PIOR and corresponding *Gap Criterion* values with a confidence level of 95% representing definitive “real” correlation (Wheeler and Ganji, 1996:147). A table listing the linear correlation coefficient, minimum correlation coefficient and confidence level for each dataset is shown below. It can be seen that both datasets easily met the “real” confidence level.

Table 3-16. HAVE OLOP Correlation Confidence Levels

Dataset	Sample Size	95 % Confidence Minimum Correlation	Actual Linear Correlation	Actual Confidence Level
Phase 2 Sum-of-sines	72	0.232	0.477	99.99%
Phase 3 Discrete Pitch Tracking	77	0.224	0.460	99.99%

HAVE OLOP Best Curve Fit.

In the previous section, correlation for a linear fit was investigated. This is not necessarily the best curve fit. As in the HAVE PREVENT data analysis, multiple curve fits were attempted for each dataset including exponential, natural logarithmic, polynomial and power series interpolations. A least squares method was used to identify the correlation coefficient of each fit as calculated for the HAVE PREVENT data. The following table lists these correlation values:

Table 3-17. HAVE OLOP Curve Fit Correlation Values

Dataset	Linear	Exponential	Logarithmic (Ln (GC+1))	2 nd Order Polynomial	Power Series (GC+1)
Phase 2 Sum-of-sines	0.477	0.463	0.495	0.507	0.479
Phase 3 Discrete Pitch Tracking	0.460	0.444	0.493	0.560	0.472

Again, the second order polynomial curve fit gives the best mathematical results. But on further inspection, this curve fit still does not match well at higher *Gap Criterion* values. The natural logarithmic (Ln(GC+1)) seems to be the best case for the combination of high correlation and endpoint matching. For the same reasons as in the HAVE PREVENT curve fitting, a factor of one was added to the *Gap Criterion* values and the correlation found. Figures 3-15 and 3-16 show the data with this logarithmic curve fit.

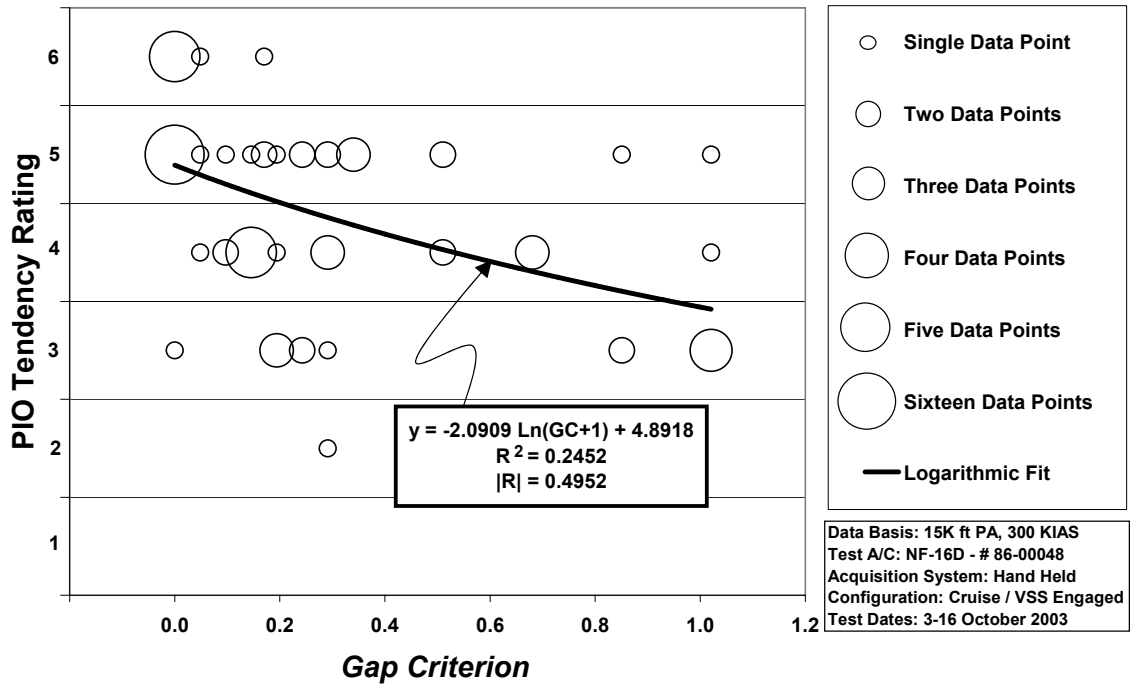


Figure 3-15. HAVE OLOP Phase 2 Sum-of-sines Task VISTA Data with Logarithmic Fit

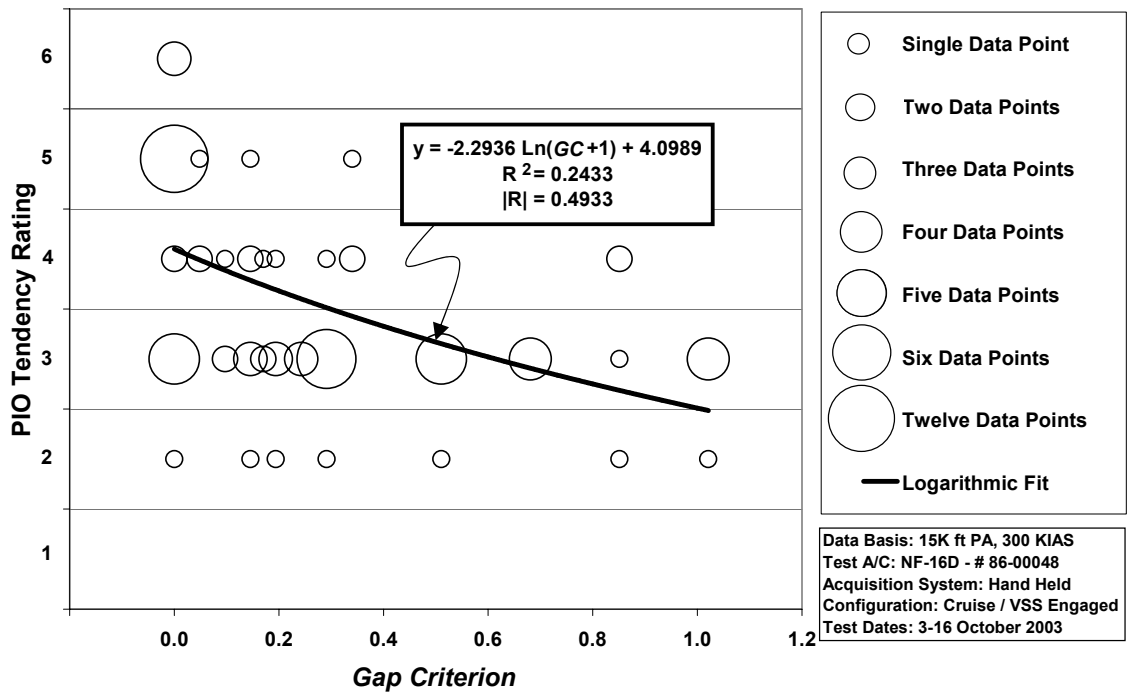


Figure 3-16. HAVE OLOP Phase 3 Discrete HUD Pitch Tracking Task VISTA Data with Logarithmic Fit

HAVE PREVENT and HAVE OLOP Summary

Each dataset from both studies shows correlation. All Phase 2 Sum-of-sines and Phase 3 Discrete HUD Pitch Tracking Task datasets had linear correlation confidence levels better than 99%. The HAVE PREVENT Phase 3 Target Tracking Task dataset had the worst correlation confidence level, never exceeding 87.5% for any of the curve fits.

IV Analysis of Project MAX GAP (LAMARS) Data

Project MAX GAP sought to augment the HAVE PREVENT and HAVE OLOP datasets. The same Phase 2 Sum-of-sines Tracking Task, Phase 3 Discrete HUD Pitch Tracking Task and Phase 3 Target Tracking Task described in Chapter III were used in the LAMARS simulator. The PIOR scale used was the same one previously described.

MAX GAP (LAMARS) Analysis

The study involved one previous test case, Case B from HAVE PREVENT, and three new test cases labeled N, W and Y. A series of bare aircraft dynamics with varying short-period characteristics were chosen (26 in all). The *Gap Criterion* was applied to each of these. Cases B, N, W and Y were chosen for their *Gap Criterion* distribution.

Each test case was augmented with angle-of-attack and pitch-rate feedback which produced almost identical closed-loop dynamics. Table 4-1 shows these dynamics and the augmentation required. Also shown are the bare and augmented short period natural frequencies (ω_{sp}) and damping ratios (ζ_{sp}) for each case. The actuator rate limits used in this project were 15 deg/sec, 30 deg/sec and 60 deg/sec. See Appendix A for the fourth order state space model matrices.

Table 4-1. MAX GAP (LAMARS) Case Characteristics (Witte and others, 2003)

Case	Bare Aircraft Poles	ω_{sp}	ζ_{sp}	K_q	K_α	Aircraft Poles with Stability Augmentation
B	-1.43±1.85j -.017±.074j	2.34	0.61	0.156	0.123	-2.17±-2.22j -.017±.070j
N	-.939±2.99j -.017±.074j	3.13	0.30	-0.335	0.177	-2.18±2.22j -.018±.050j
W	-4.24±2.05j -.017±.074j	4.71	0.90	-0.501	-0.345	-2.18±2.24j -.017 ±.081j
Y	-2.09±1.01j -.017±.074j	2.32	0.90	0.346	0.0334	-2.19±2.24j -.017±.080j

Gap Criterion Calculation for MAX GAP (LAMARS) Datasets.

Step 1.

The pitch-to-actuator transfer functions for the bare aircraft dynamics are shown in Table 4-2 and were computed using the Matlab™ code in Appendix B.

Table 4-2. MAX GAP (LAMARS) Pitch-to-Actuator Transfer Functions (G_c)

Case	G_c
B	$\frac{-11.08s^2 - 14.37s - 0.5277}{s^4 + 2.889s^3 + 5.578s^2 + 0.2026s + 0.03157}$
N	$\frac{-11.09s^2 - 14.37s - 0.5277}{s^4 + 1.912s^3 + 9.867s^2 + 0.3439s + 0.05648}$
W	$\frac{-11.09s^2 - 14.37s - 0.5277}{s^4 + 8.512s^3 + 22.48s^2 + 0.8031s + 0.1279}$
Y	$\frac{-11.08s^2 - 14.37s - 0.5277}{s^4 + 4.21s^3 - 5.53s^2 - 0.2071s - 0.03103}$

Step 2.

Does not apply; all four cases have stable poles for their bare aircraft dynamics.

Step 3.

Actuator dynamics for this dataset were $G_{actuator} = \frac{20}{s + 20}$.

Step 4.

The Neal-Smith pilot model transfer functions are shown in Table 4-3 along with the augmented dynamics for which they were computed. They were calculated using the Interactive Flying Qualities Toolbox for Matlab provided by the Flying Dynamics Directorate of the Air Force Research Laboratories (Doman and Forringer, 1996).

Table 4-3. MAX GAP (LAMARS) Neal-Smith Pilot Models

Case	G_p	$G_{actuator} * G_{augmented}$
B	$-0.11483 \frac{(5s+1)(0.32699s+1)}{s(0.0001s+1)} e^{-0.25s}$	$\frac{-221.7s^2 - 287.5s - 10.55}{s^5 + 22.89s^4 + 90.88s^3 + 182.1s^2 + 6.597s + 0.9303}$
N	$-0.10919 \frac{(5s+1)(0.32699s+1)}{s(0.0001s+1)} e^{-0.25s}$	$\frac{-221.7s^2 - 287.5s - 10.55}{s^5 + 21.91s^4 + 86.89s^3 + 173.2s^2 + 6.186s + 0.4845}$
W	$-0.15254 \frac{(5s+1)(0.30311s+1)}{s(0.0001s+1)} e^{-0.25s}$	$\frac{-221.7s^2 - 287.5s - 10.55}{s^5 + 28.51s^4 + 116.3s^3 + 239.7s^2 + 8.681s + 1.596}$
Y	$-0.12528 \frac{(5s+1)(0.31318s+1)}{s(0.0001s+1)} e^{-0.25s}$	$\frac{-221.7s^2 - 287.5s - 10.55}{s^5 + 24.21s^4 + 97.5s^3 + 197.9s^2 + 7.218s + 1.286}$

Step 5 and 6.

Figure 4-1 shows the Nichols charts for Cases B, N, W and Y:

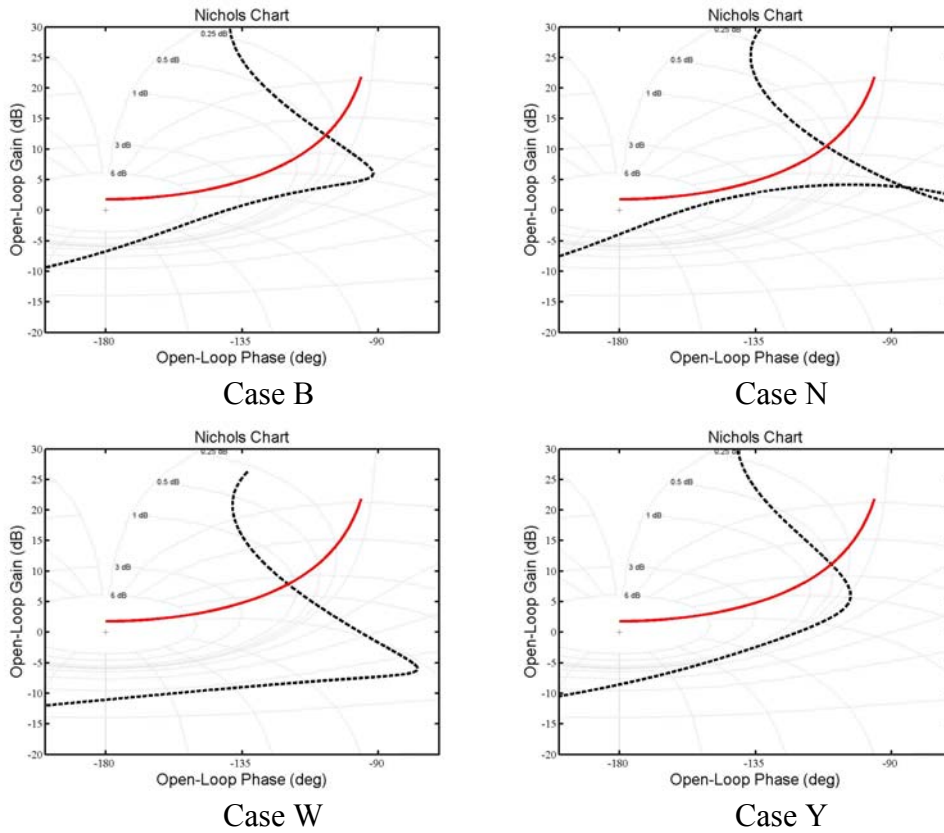


Figure 4-1. MAX GAP (LAMARS) Nichols Charts for Cases B, N, W and Y

Step 7.

Cases B, N, W and Y are all of Type I.

Type I, Step 1-1 through 1-2.

The minimum amount of effective increase in gain for Cases B, N, W and Y, along with the determined values for K^* , ω and A_{max} are shown in Table 4-4. The final values for the *Gap Criterion* and amplitude for each case and rate limit are shown in Table 4-5

Table 4-4. MAX GAP (LAMARS) Components for Cases B, N, W and Y

Case	ΔK_p (dB)	K^*	ω (rad/s)	A_{max} (deg)
Case B	4.065	0.719	2.93	30
Case N	1.661	0.806	3.70	30
Case W	12.450	0.955	7.07	30
Case Y	7.230	0.664	2.95	30

Table 4-5. Gap Criteria Values for MAX GAP (LAMARS) Cases B, N, W and Y

Case	Maximum Actuator Deflection Rate (V_L , deg/sec)	A (deg)	<i>Gap Criterion</i>
B	15	11.18	0.5953
	30	22.37	1.1907
	60	44.72	2.3814
N	15	7.90	0.3189
	30	15.80	0.6377
	60	31.60	1.2754
W	15	3.49	0.4880
	30	6.98	0.9760
	60	13.95	1.9520
Y	15	12.03	0.9276
	30	24.06	1.8552
	60	48.12	3.7104

MAX GAP (LAMARS) Gap Criterion Summary.

Table 4-6 summarizes the LAMARS *Gap Criteria* for Project MAX GAP:

Table 4-6. MAX GAP (LAMARS) *Gap Criteria* Summary

Case	Maximum Actuator Deflection Rate (V_L , deg/sec)	<i>Gap Criterion</i>
B	15	0.5953
	30	1.1907
	60	2.3814
N	15	0.3189
	30	0.6377
	60	1.2754
W	15	0.4880
	30	0.9760
	60	1.9520
Y	15	0.9276
	30	1.8552
	60	3.7104

MAX GAP (LAMARS) Gap Criterion Correlation.

The MAX GAP test team recognized that some outlier datapoints were included in the LAMARS datasets. In these cases, poor pilot recognition of PIO cues such as aircraft lag response had resulted in improper PIOR assessment. Post-test analysis revealed these datapoints which were then omitted from the “reduced dataset” findings (Witte and others, 2003:8). These reduced LAMARS datasets were used for this study.

The remaining PIOR and *Gap Criterion* data were paired and the results plotted in Figures 4-2 through 4-4:

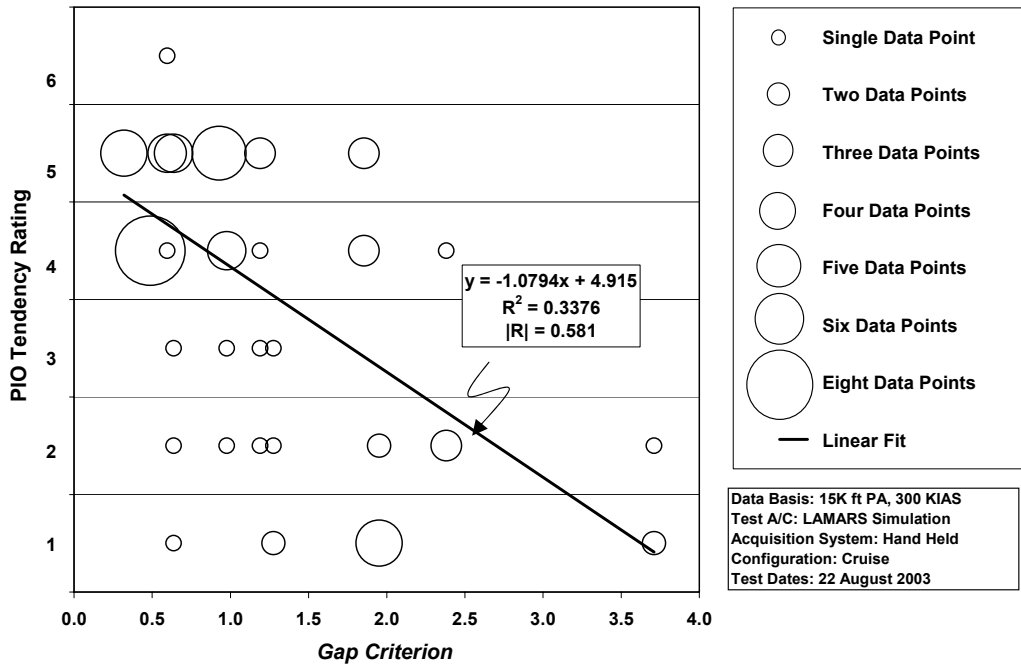


Figure 4-2. MAX GAP (LAMARS) Phase 2 Sum-of-sines Task Data

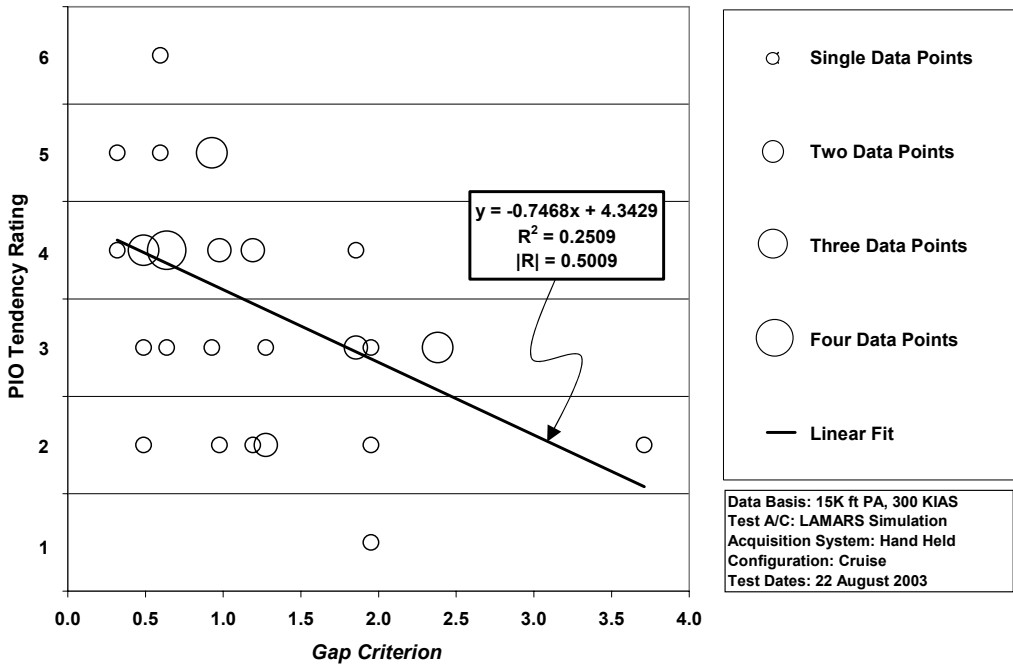


Figure 4-3. MAX GAP (LAMARS) Phase 3 Discrete HUD Pitch Tracking Task Data

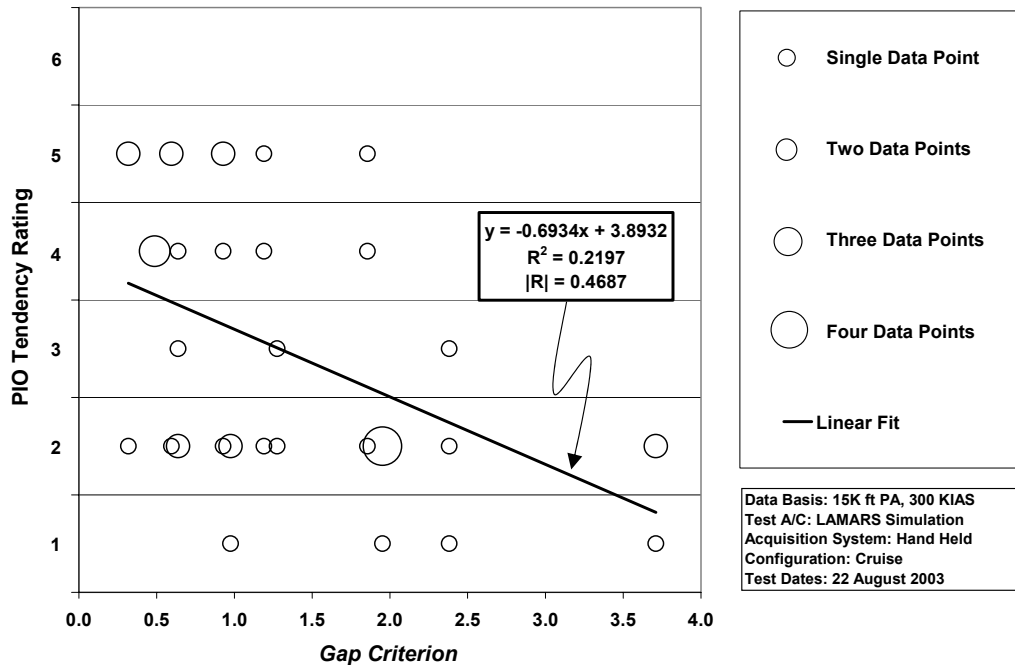


Figure 4-4. MAX GAP (LAMARS) Phase 3 Target Tracking Task Data

As in the HAVE PREVENT and HAVE OLOP data analyses, the probability of a linear correlation existing for the data was investigated and is described in Appendix C. The linear fit depicted on the plots displays this correlation.

Again, confidence level was used to determine if a relationship existed between PIOR and corresponding *Gap Criterion* values with a confidence level of 95% representing definitive “real” correlation (Wheeler and Ganji, 1996:147). A table listing the linear correlation coefficient, minimum correlation coefficient and confidence level for each the datasets of the LAMARS portion of Project MAX GAP is shown below. It can be seen that all three datasets exceeded the necessary confidence level.

Table 4-7. MAX GAP (LAMARS) Correlation Confidence Levels

Dataset	Sample Size	95 % Confidence Minimum Correlation	Actual Linear Correlation	Actual Confidence Level
Phase 2 Sum-of-sines	60	0.254	0.581	99.99%
Phase 3 Discrete Pitch Tracking	47	0.288	0.501	99.97%
Phase 3 Target Tracking	44	0.297	0.469	99.87%

MAX GAP (LAMARS) Best Curve Fit.

In the previous section, correlation for a linear fit was investigated. This is not necessarily the best curve fit. Multiple curve fits were attempted for each dataset including exponential, natural logarithmic, polynomial and power series interpolations just as in the HAVE PREVENT and HAVE OLOP data analyses. A least squares method was used to identify the correlation coefficient of each fit. Table 4-9 lists these correlation values:

Table 4-8. MAX GAP (LAMARS) Curve Fit Correlation Values

Dataset	Linear	Exponential	Logarithmic	2 nd Order Polynomial	Power Series
Phase 2 Sum-of-sines	0.581	0.580	0.573	0.587	0.564
Phase 3 Discrete Pitch Tracking	0.501	0.481	0.507	0.516	0.487
Phase 3 Target Tracking	0.469	0.485	0.482	0.482	0.489

Again, the second order polynomial curve fit gives the best mathematical results. But this curve fit still does not match well at higher *Gap Criterion* values. Just as in the

HAVE PREVENT and HAVE OLOP analyses, the natural logarithmic curve fit seems to be the best case for the combination of high correlation and endpoint matching. There were no *Gap Criterion* values of zero in this analysis and therefore simple natural logarithmic curve fitting was accomplished. Figures 4-5 and 4-6 show the data with this logarithmic curve fit.

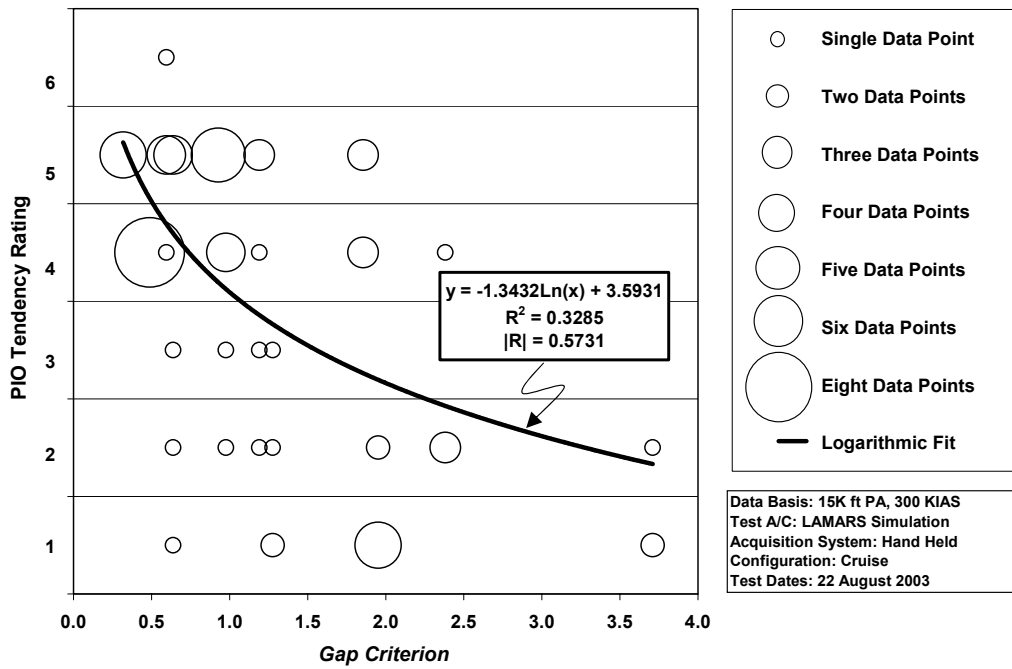


Figure 4-5. MAX GAP (LAMARS) Phase 2 Sum-of-sines Task Data with Logarithmic Curve Fit

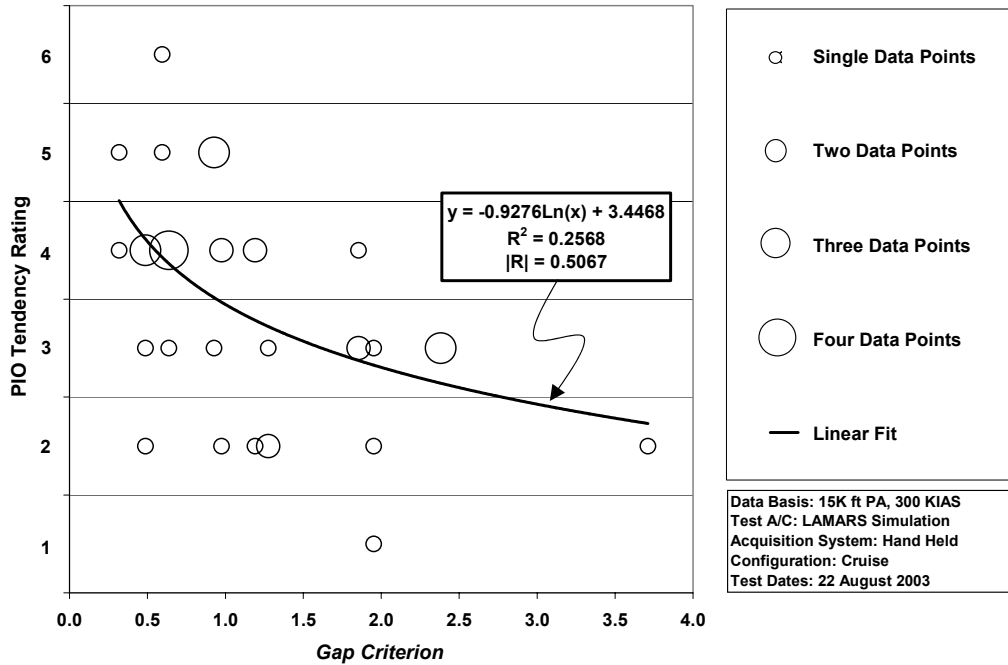


Figure 4-6. MAX GAP (LAMARS) Phase 3 Discrete HUD Pitch Tracking Task Data with Logarithmic Fit

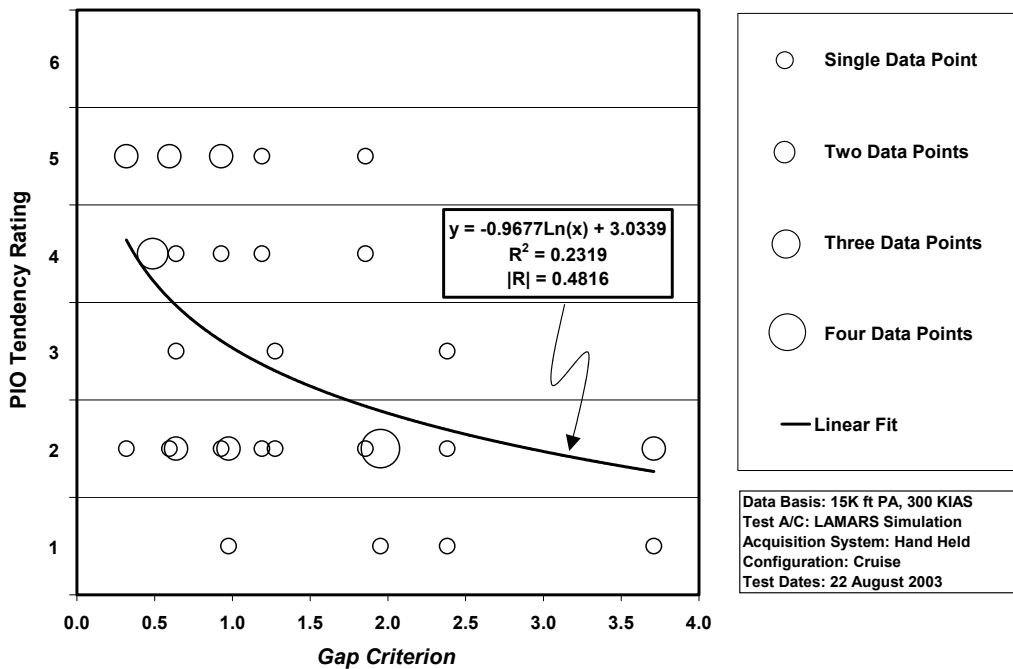


Figure 4-7. MAX GAP (LAMARS) Phase 3 Target Tracking Task Data with Logarithmic Fit

MAX GAP (LAMARS) Summary

Each dataset shows correlation and each linear correlation confidence level is better than 99%. The HAVE PREVENT and HAVE OLOP data analyses bore out the fact that correlation exists between the *Gap Criterion* and PIOR and the LAMARS portion of Project MAX GAP reinforces this assertion.

V. Analysis of Project MAX GAP (VISTA) Data

More *Gap Criterion* and PIO tendency rating was acquired in the flight test portion of Project MAX GAP. The VISTA NF-16D was used to accomplish this. Again, the same Phase 2 Sum-of-sines Tracking Task, Phase 3 Discrete HUD Pitch Tracking Task and Phase 3 Target Tracking Task described in Chapter III were used. The PIOR scale used was the MIL-HDBK-1797 one previously described in Chapter I.

MAX GAP (VISTA) Analysis

The same four sets of bare aircraft dynamics and the same three actuator rate limits used in the MAX GAP LAMARS test were requested for the VISTA aircraft. The actuator rate limits were easily programmed, but, unfortunately, obtaining exact matches in the VISTA NF-16D is as much an art as a science. Compounding the problem, only one calibration sortie was accomplished due to project time constraints. The bare aircraft dynamics for Cases B and N were suitably close to the specified values, but the augmented dynamics for Case B were significantly different. The bare aircraft dynamic damping ratio for Case N was almost perfect, but the requested natural frequency was less by 1 rad/sec. Case Y proved to be an overdamped though stable system. The short period characteristics of these cases were used for the actual *Gap Criterion* analysis and are shown in Table 5-1.

As described in the test report for Project MAX GAP, poor task setup and execution were experienced in the Phase 3 Target Tracking Task. The T-38A target aircraft was allowed to develop too much angle away from the VISTA prior to an engagement being conducted. As a result of this initial offset and less than expected turn performance in the VISTA, the gross acquisition task turned into a low gain task, rather

than the high gain task of a Category A maneuver (Witte and others, 2003:10). For these reasons, this dataset was ignored in this study. Additionally, the MAX GAP test team found instances where the evaluation pilots missed critical PIO cues such as aircraft lag response and assessed improper PIOR. These data points were omitted in the “reduced dataset” results of Project MAX GAP. These reduced datasets were used for this study.

Table 5-1. MAX GAP (VISTA) Case Characteristics (Witte and others, 2003)

Case	Bare Aircraft Poles	ω_{sp}	ζ_{sp}	Kq	K α	Aircraft Poles with Stability Augmentation
B	-1.42±1.85j -.017±.074j	2.33	0.61	-0.0212	0.0877	-1.98±-1.69j -.017±.065j
N	-.493±2.86j -.017±.074j	2.90	0.17	-0.408	0.254	-2.29±1.95j -.018±.031j
W	-3.26±1.77j -.017±.074j	3.70	0.88	-0.0946	-0.185	-2.10±2.14j -.017 ±.082j
Y	-3.02, -0.96 -.017±.074j	1.70	1.17	0.485	0.0400	-2.09±2.14j -.017±.083j

Gap Criterion Calculation for MAX GAP (VISTA) Datasets.

Step 1.

The pitch-to-actuator transfer functions for the bare aircraft dynamics are shown in Table 5-2:

Table 5-2. MAX GAP (VISTA) Pitch-to-Actuator Transfer Functions (G_c)

Case	G_c
B	$\frac{-11.08s^2 - 14.37s - 0.5277}{s^4 + 2.877s^3 + 5.531s^2 + 0.201s + 0.0313}$
N	$\frac{-11.08s^2 - 14.37s - 0.5277}{s^4 + 1.02s^3 + 8.449s^2 + 0.2916s + 0.04848}$
W	$\frac{-11.09s^2 - 14.37s - 0.5277}{s^4 + 6.546s^3 + 13.92s^2 + 0.503s + 0.07892}$
Y	$\frac{-11.08s^2 - 14.37s - 0.5277}{s^4 + 4.012s^3 + 3.031s^2 + 0.1212s + 0.01666}$

Step 2.

Does not apply; all four cases have stable poles for their bare aircraft dynamics.

Step 3.

Actuator dynamics for this dataset were $G_{actuator} = \frac{20}{s + 20}$.

Step 4.

The Neal-Smith pilot model transfer functions are shown in Table 5-3 along with the augmented dynamics for which they were computed (Doman and Forringer, 1996):

Table 5-3. MAX GAP (VISTA) Neal-Smith Pilot Models

Case	G_p	$G_{actuator} * G_{augmented}$
B	$-0.078997 \frac{(5s+1)(0.53135s+1)}{s(0.0001s+1)} e^{-0.25s}$	$\frac{-221.7s^2 - 287.5s - 10.55}{s^5 + 22.88s^4 + 82.48s^3 + 131.3s^2 + 4.811s + 0.5853}$
N	$-0.09531 \frac{(5s+1)(0.42704s+1)}{s(0.0001s+1)} e^{-0.25s}$	$\frac{-221.7s^2 - 287.5s - 10.55}{s^5 + 21.02s^4 + 84.65s^3 + 151.1s^2 + 5.496s + 0.5768}$
W	$-0.12846 \frac{(5s+1)(0.34451s+1)}{s(0.0001s+1)} e^{-0.25s}$	$\frac{-221.7s^2 - 287.5s - 10.55}{s^5 + 26.55s^4 + 103.6s^3 + 204.4s^2 + 7.448s + 1.397}$
Y	$-0.11293 \frac{(5s+1)(0.35487s+1)}{s(0.0001s+1)} e^{-0.25s}$	$\frac{-221.7s^2 - 287.5s - 10.55}{s^5 + 24.01s^4 + 92.64s^3 + 180.6s^2 + 6.626s + 1.263}$

Step 5 and 6.

Figure 5-1 shows the Nichols charts for Cases B, N, W and Y:

Step 7.

Cases B and W are of Type I, Case N is Type II and Case Y is Type III.

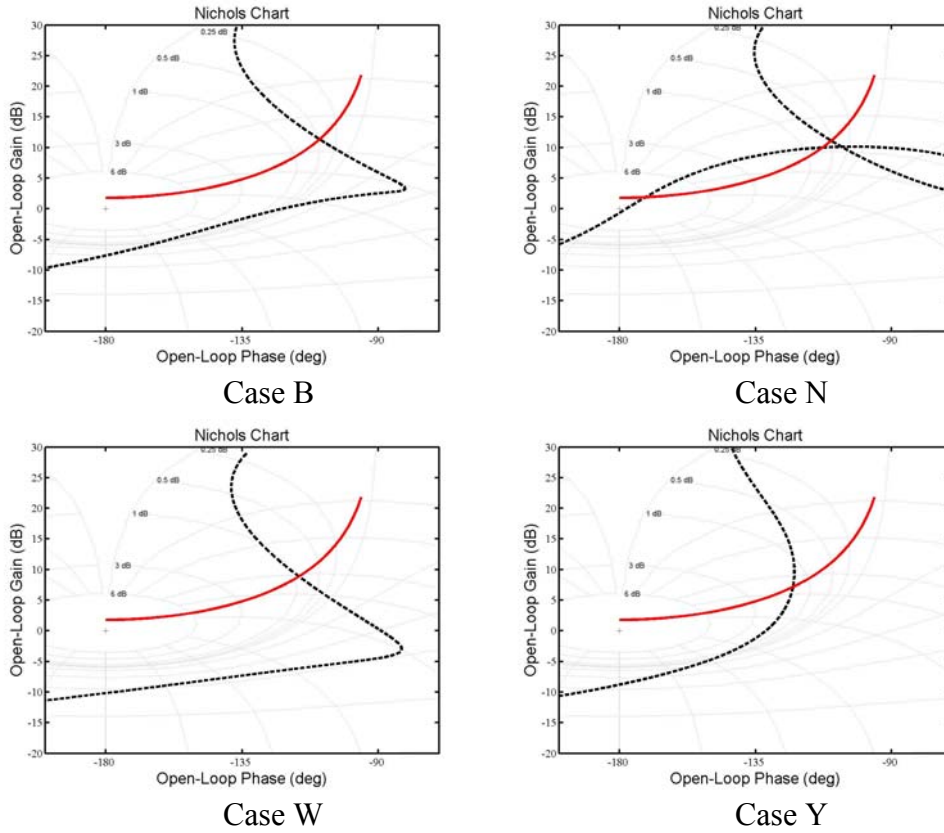


Figure 5-1. MAX GAP (VISTA) Nichols Charts for Cases B, N, W and Y

Type I, Step 1-1 through 1-2.

The minimum amount of effective increase in gain for Cases B and W along with the determined values for K^* , ω and A_{max} , are shown in Table 5-4:

Table 5-4. MAX GAP (VISTA) Components for Cases B and W

Case	ΔK_p (dB)	K^*	ω (rad/s)	A_{max} (deg)
Case B	6.457	0.736	3.57	30
Case W	11.257	0.922	6.12	30

The final values for the *Gap Criterion* and amplitude for these two cases and rate limits are shown in Table 5-5:

Table 5-5. Gap Criteria Values for MAX GAP (VISTA) Cases B and W

Case	Maximum Actuator Deflection Rate (V_L , deg/sec)	A (deg)	<i>Gap Criterion</i>
B	15	8.97	0.6287
	30	17.93	1.2573
	60	35.87	2.5146
W	15	4.18	0.5129
	30	8.35	1.0257
	60	16.70	2.0515

Type II, Step 2-1 through 2-2.

The minimum amount of effective decrease in gain for Case N, along with the determined values for K^* , ω and A_{max} , are shown in Table 5-6:

Table 5-6. MAX GAP (VISTA) Components for Case N

Case	ΔK_p (dB)	K^*	ω (rad/s)	A_{max} (deg)
Case N	-3.998	0.784	3.26	30

The final values for the *Gap Criteria* and amplitudes for Case N and its respective rate limits are shown in Table 5-7:

Table 5-7. Gap Criteria Values for MAX GAP (VISTA) Case N

Case	Maximum Actuator Deflection Rate (V_L , deg/sec)	A (deg)	<i>Gap Criterion</i>
N	15	9.22	0.1939
	30	18.44	0.3879
	60	36.88	0.7758

Type III, Step 3-1 through 3-4.

The determined values for K^* , ω , A_{max} and *Gap Criterion* for each rate limit applied to Case Y are shown in Table 5-8:

Table 5-8. *Gap Criteria* for MAX GAP (VISTA) Case Y

Case	K^*	ω (rad/s)	A_{max} (deg)	A (deg)	Maximum Actuator Deflection Rate (V_L , deg/sec)	<i>Gap Criterion</i>
Y	0.540	1.08	30	40.40	15	1.3467
				80.80	30	2.6934
				161.60	60	5.3868

MAX GAP (VISTA) Gap Criterion Summary.

Table 5-9 summarizes the *Gap Criteria* for the flight test portion of Project MAX GAP.

Table 5-9. MAX GAP (VISTA) *Gap Criteria* Summary

Case	Maximum Actuator Deflection Rate (V_L , deg/sec)	<i>Gap Criterion</i>
B	15	0.6287
	30	1.2573
	60	2.5146
N	15	0.1939
	30	0.3879
	60	0.7758
W	15	0.5129
	30	1.0257
	60	2.0515
Y	15	1.3467
	30	2.6934
	60	5.3868

MAX GAP (VISTA) Gap Criterion Correlation.

The PIOR and *Gap Criterion* data were paired and plotted in Figures 5-2 and 5-3:

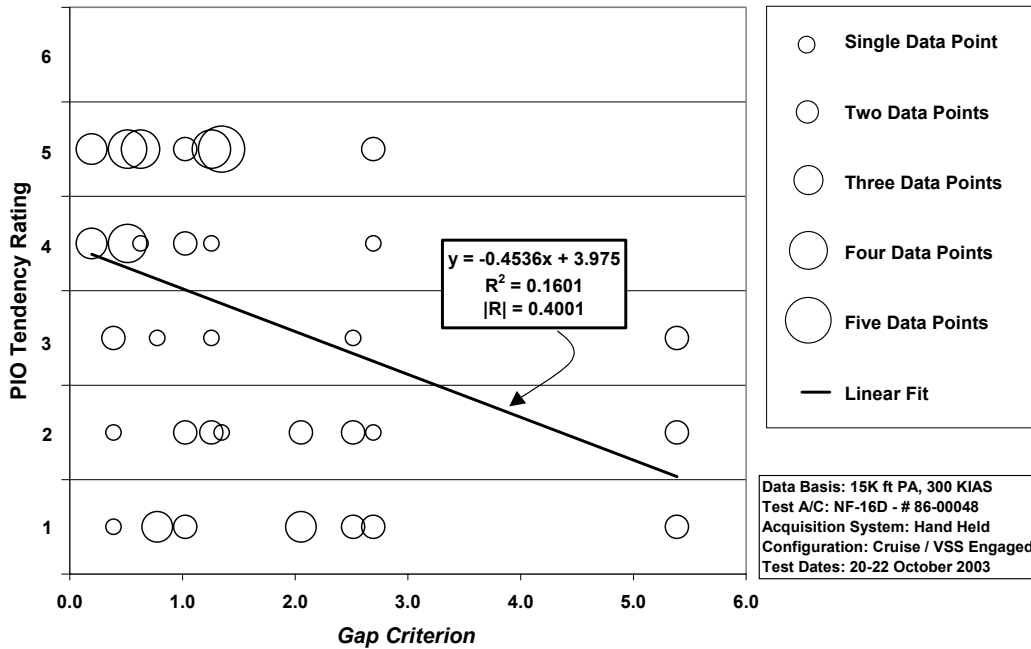


Figure 5-2. MAX GAP (VISTA) Phase 2 Sum-of-sines Task Data

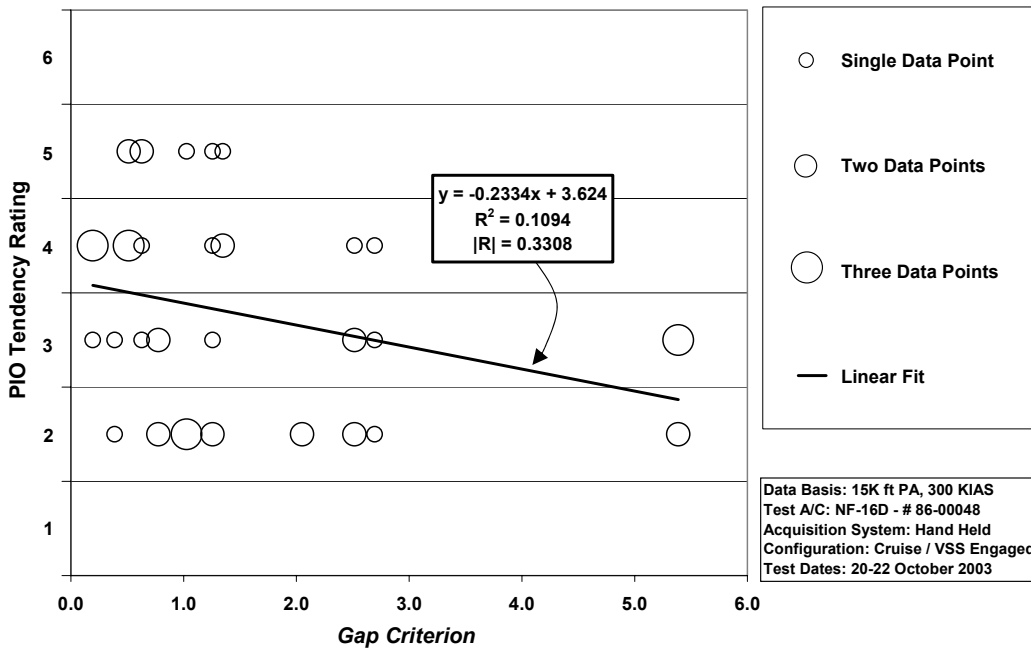


Figure 5-3. MAX GAP (VISTA) Phase 3 Discrete HUD Pitch Tracking Task Data

As in the previous analyses, the probability of a linear correlation existing for the data was investigated as described in Appendix C. The linear fit depicted on the plots displays this correlation.

Again, confidence level was used to determine if a relationship existed between PIOR and corresponding *Gap Criterion* values. A 95% confidence level was maintained as the threshold for justifiably acceptable correlation (Wheeler and Ganji, 1996:147). A table listing the linear correlation coefficient, minimum correlation coefficient and confidence level for both datasets of the flight test portion of Project MAX GAP is shown below.

Table 5-10. MAX GAP (VISTA) Correlation Confidence Levels

Dataset	Sample Size	95 % Confidence Minimum Correlation	Actual Linear Correlation	Actual Confidence Level
Phase 2 Sum-of-sines	71	0.233	0.400	99.95%
Phase 3 Discrete Pitch Tracking	46	0.291	0.331	97.53%

MAX GAP (VISTA) Best Curve Fit.

Multiple curve fits were attempted for these datasets as well. The same exponential, natural logarithmic, polynomial and power series interpolations were tried. The correlation coefficient of each fit was calculated and the results are listed below.

Table 5-11. MAX GAP (VISTA) Curve Fit Correlation Values

Dataset	Linear	Exponential	Logarithmic	2 nd Order Polynomial	Power Series
Phase 2 Sum-of-sines	0.400	0.372	0.414	0.430	0.399
Phase 3 Discrete Pitch Tracking	0.331	0.312	0.357	0.368	0.355

Yet again the second order polynomial curve fit gives the highest correlation values. But this curve fit still does not match well at higher *Gap Criterion* values. Just as in the preceding analyses, the natural logarithmic curve fit does a better job of endpoint matching while maintaining a relatively high correlation factor. Figures 5-4 and 5-5 show the data with this logarithmic curve fit.

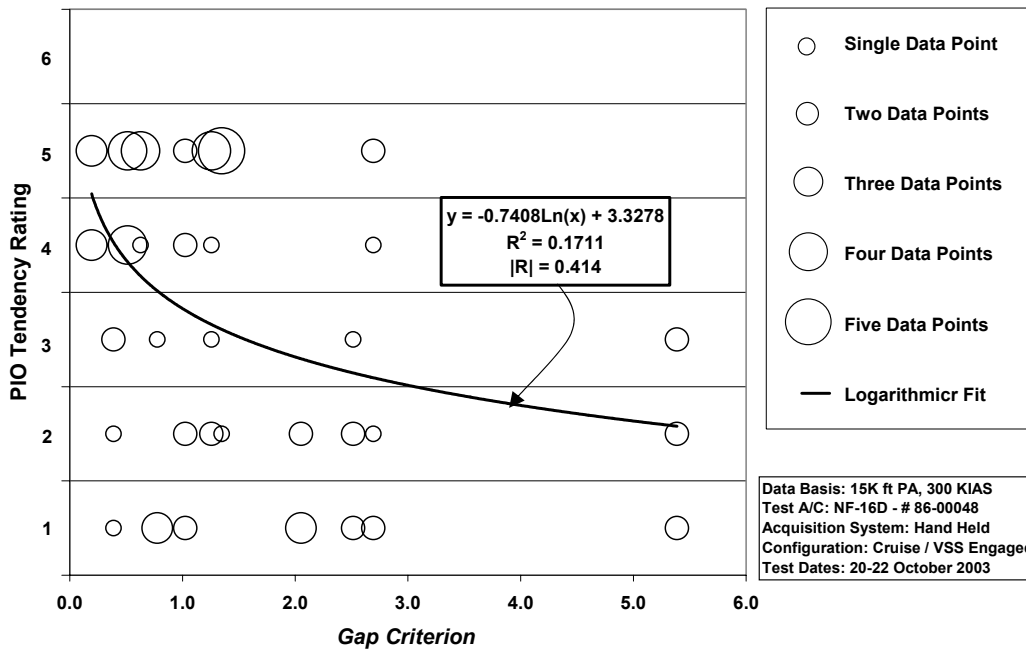


Figure 5-4. MAX GAP (VISTA) Phase 2 Sum-of-sines Task Data with Logarithmic Curve Fit

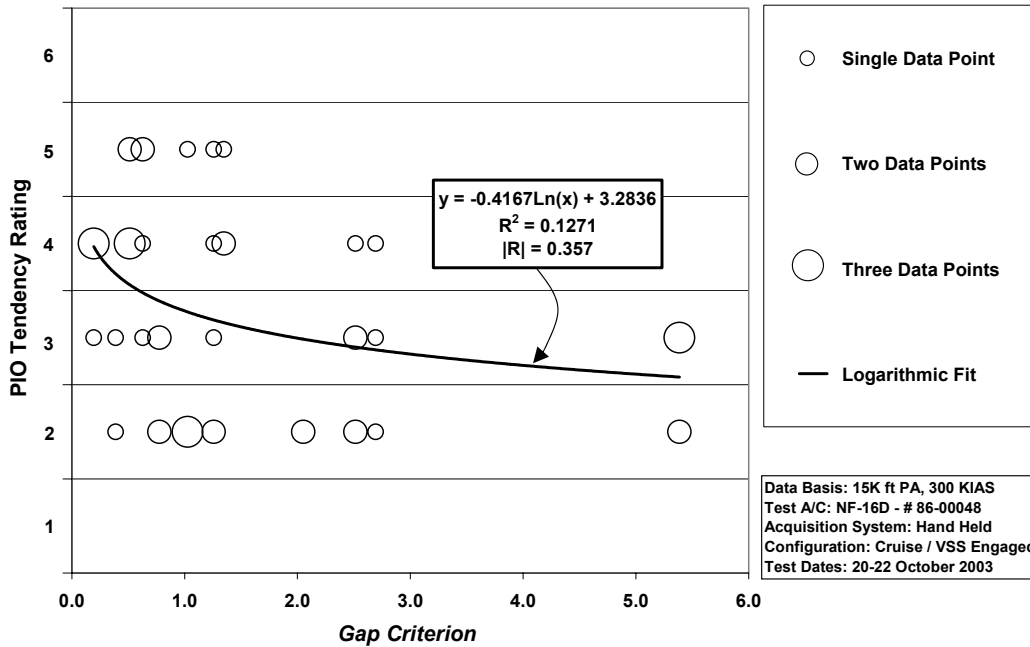


Figure 5-5. MAX GAP (VISTA) Phase 3 Discrete HUD Pitch Tracking Task Data with Logarithmic Curve Fit

MAX GAP (VISTA) Summary

Just as in the MAX GAP (LAMARS) analyses, each dataset shows correlation and each linear correlation confidence level is better than 95%. The HAVE PREVENT, HAVE OLOP, MAX GAP (LAMARS) and MAX GAP (VISTA) individually demonstrate the correlation between *Gap Criterion* and PIO tendency rating. To determine if the *Gap Criterion* can be broadly applied, a correlation within combined datasets must be accomplished.

In Chapter VI, the datasets are combined and the data are analyzed for correlation between the PIOR and the *Gap Criterion*.

VI. Analysis of Combined *Gap Criterion* Data

In the previous sections, correlation for individual datasets has been assessed and best fit curves and data correlation have been established. But, the *Gap Criterion* is supposed to be applied universally. The effects of combining datasets will now be examined. Datasets will be combined for Handling Qualities Phase, task and source. Finally, simulator and flight test results will be combined for each Handling Qualities phase and task. Combining Handling Qualities phases was not considered due to differences in pilot control techniques, specifically HQDT versus operational flying styles (Brown and others, 2002:21-18 to 21-19).

Figures 6-1 through 6-3 have all datasets obtained from LAMARS plotted together and Figure 6-4 and 6-5 show all VISTA data.

LAMARS Combined Datasets

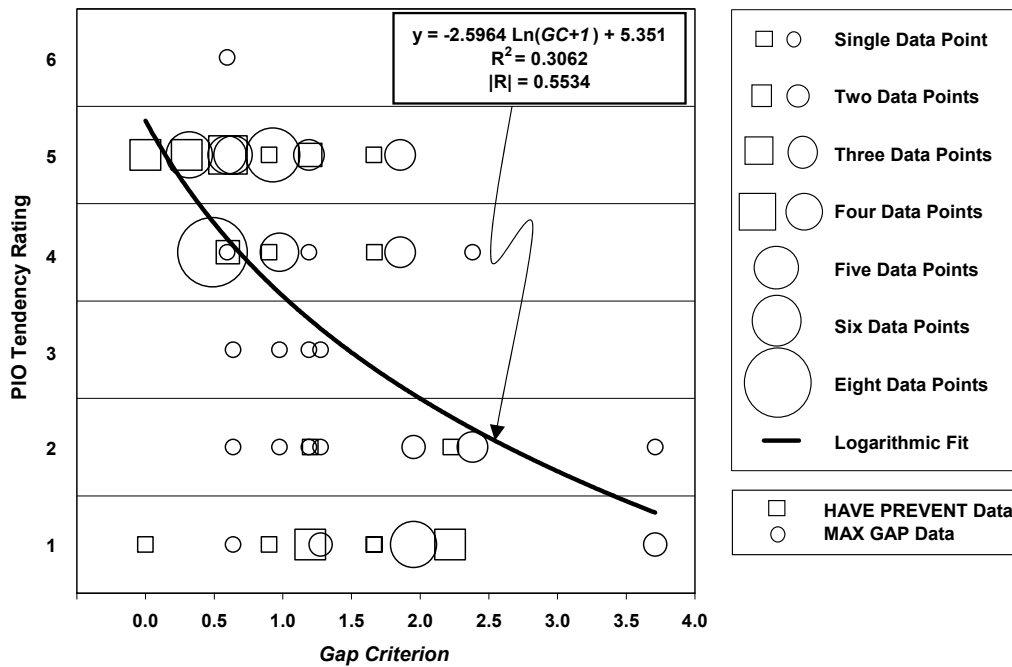


Figure 6-1. LAMARS Combined Phase2 Sum-of-sines Dataset

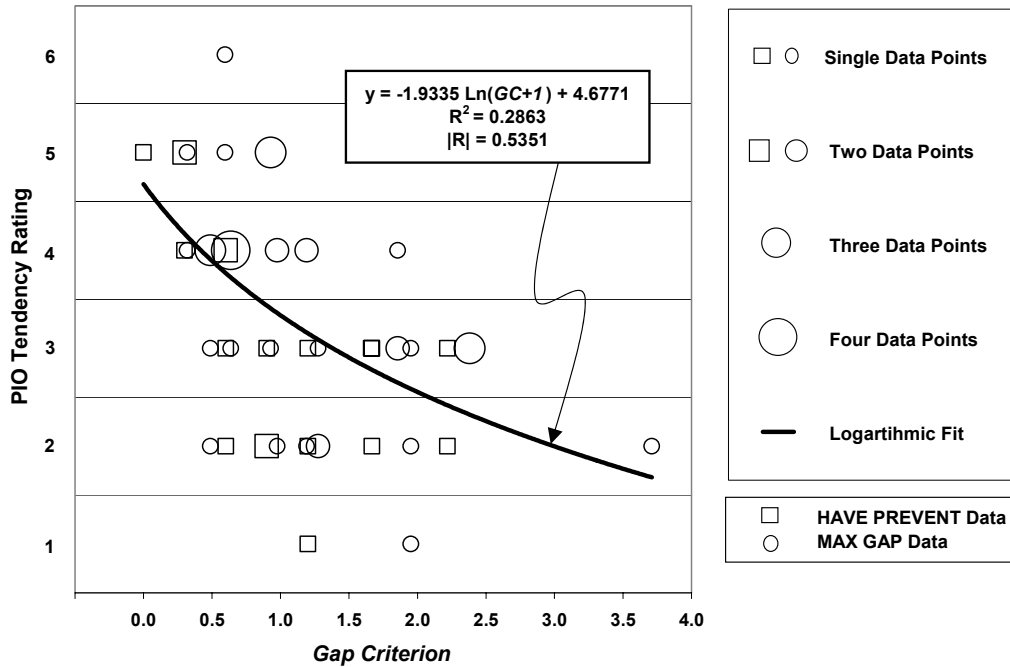


Figure 6-2. LAMARS Combined Phase 3 Discrete (HUD) Pitch-Tracking Dataset

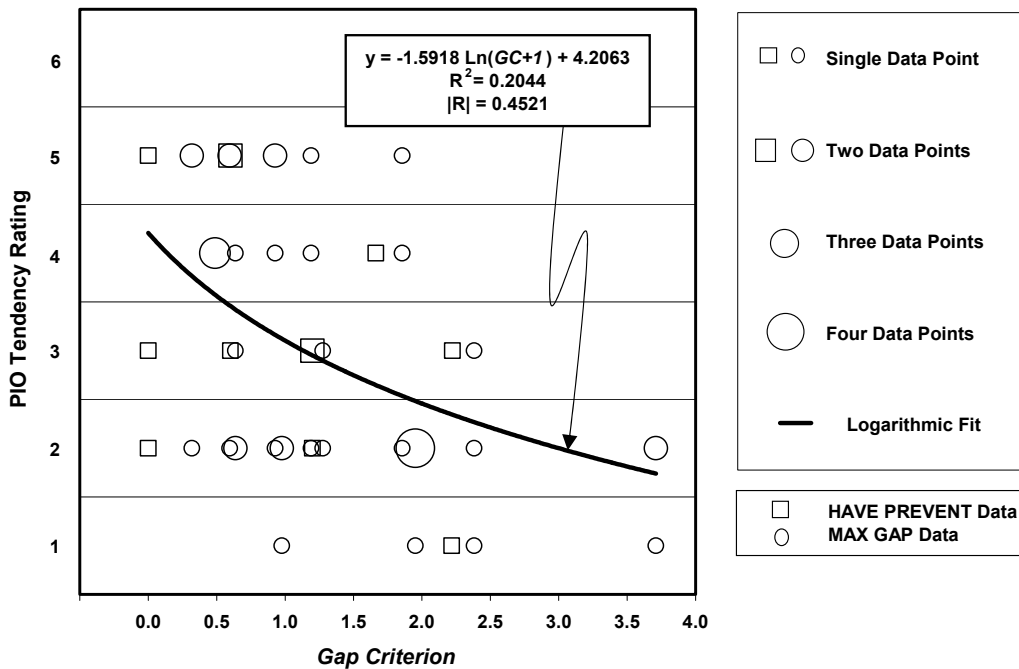


Figure 6-3. LAMARS Combined Phase 3 Target Tracking Dataset

VISTA Combined Datasets

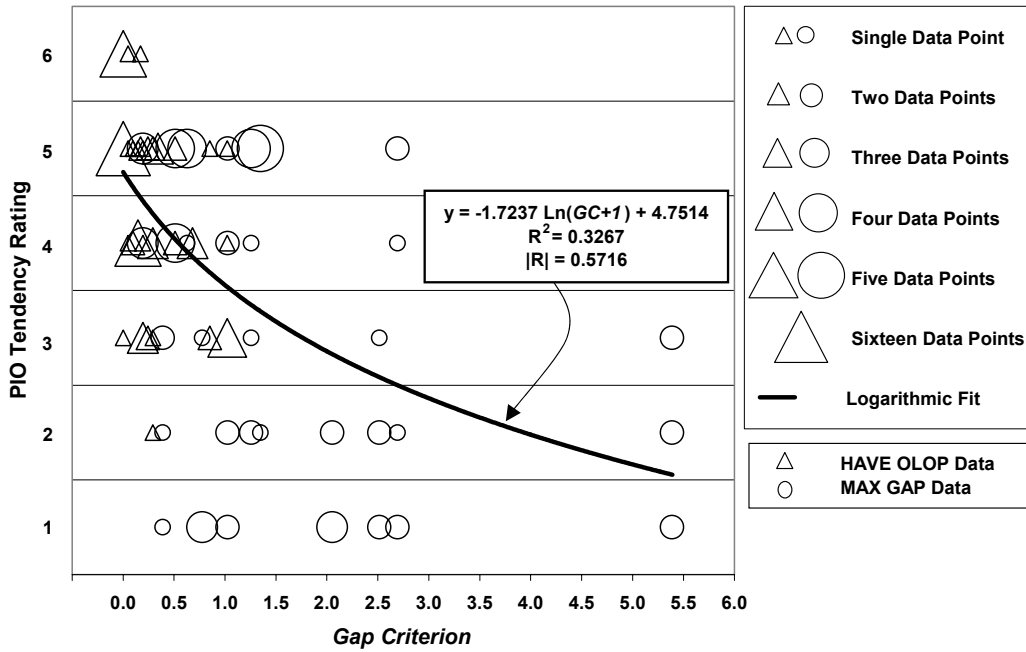


Figure 6-4. VISTA Combined Phase 2 Sum-of-sines Dataset

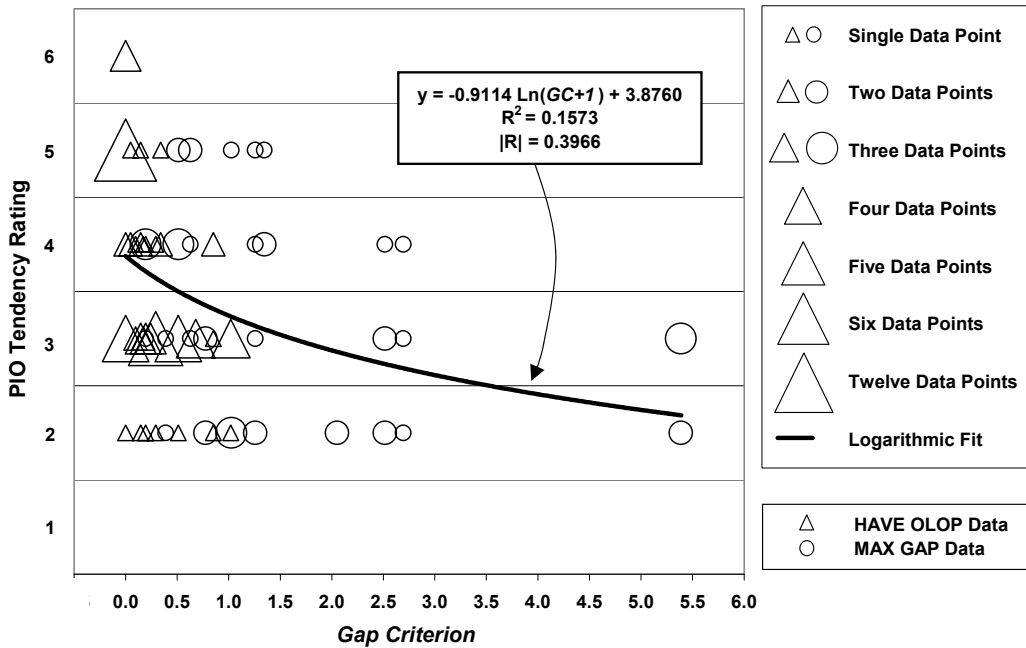


Figure 6-5. VISTA Combined Phase 3 Discrete (HUD) Pitch-Tracking Dataset

LAMARS and VISTA Combined Dataset Correlation

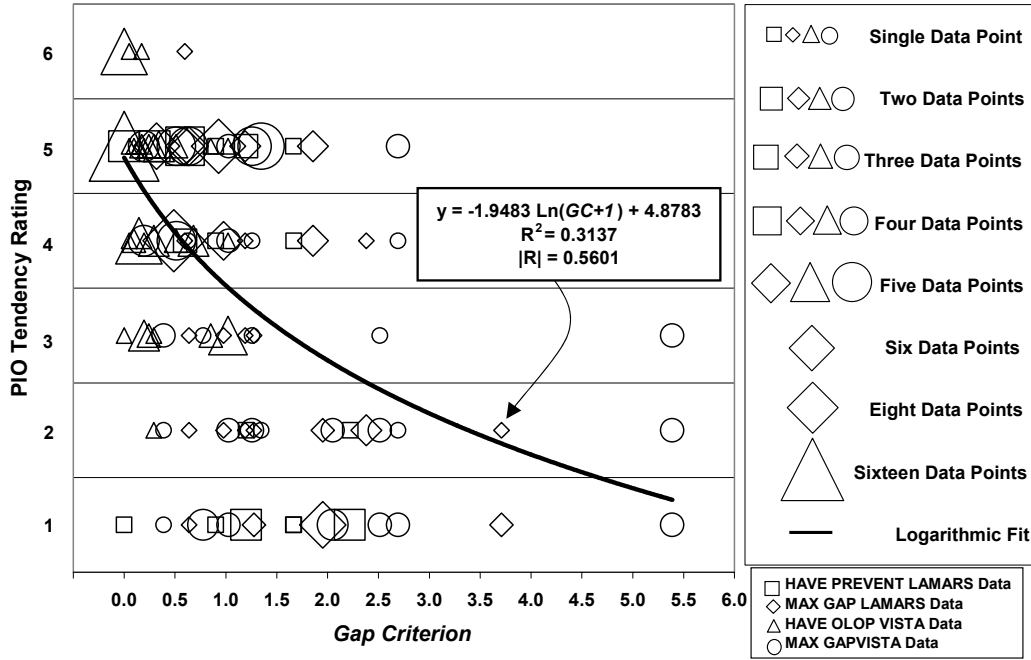


Figure 6-6. LAMARS and VISTA Combined Phase 2 Sum-of-sines Data

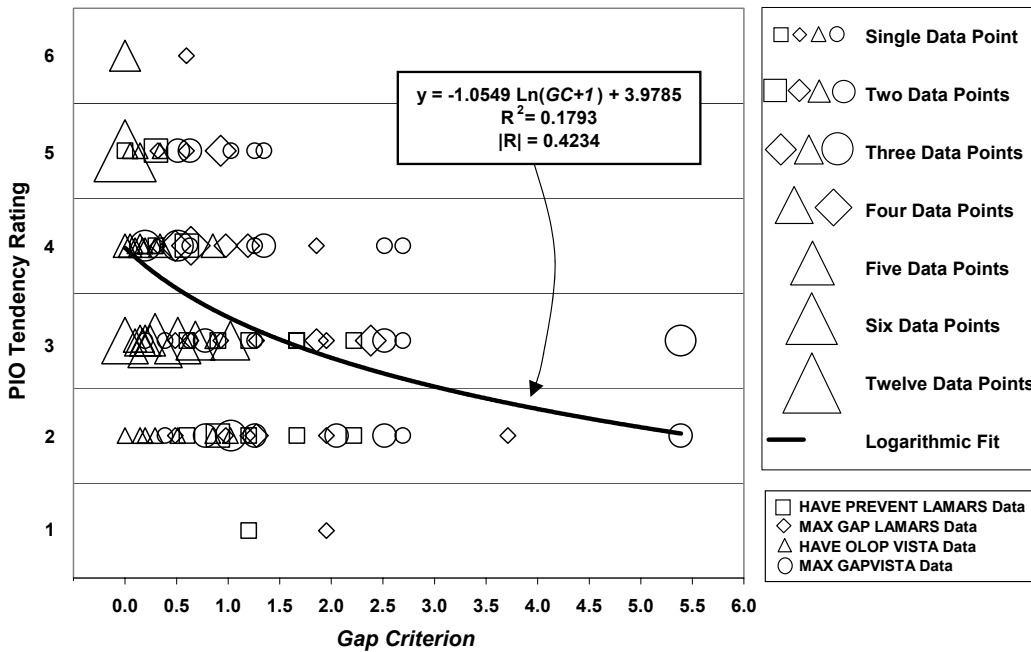


Figure 6-7. LAMARS and VISTA Combined Phase 3 Discrete Pitch-Tracking Data

Combined Dataset Analysis and Observations

Each combined dataset far exceeded a 95% confidence level that correlation existed. In fact, the lowest correlation confidence level was 99.95% for the LAMARS Combined Phase 3 Target Tracking. The logarithmic curve fits shown in the previous figures proved to be the best combination of high correlation factor and endpoint matching for both high and low *Gap Criterion* values.

Further inspection of the plots reveals some trends. From the PIO tendency scale shown in Figure 1-4 of Chapter I, a PIOR of 4, 5 or 6 represents a tendency for PIO while a PIOR of 1, 2 or 3 represents no tendency for PIO, though some undesirable motions are still possible. From the combined dataset figures in can be seen that PIOR rating is an inverse function of the *Gap Criterion*: High PIOR come at low *Gap Criterion* values and vice versa. Also, from these figures it can be seen that, in general, the majority of PIO tendency ratings 4, 5, and 6 occur at *Gap Criterion* values less than approximately 1.0 while PIO tendency ratings at *Gap Criterion* values above 1.0 tend to be non-PIO values of 1, 2 or 3. These two observations were more pronounced in the Phase 2 Sum-of-sines Tracking Task than in the Phase 3 tasks. This is possibly due to the high gain, high bandwidth piloting technique used in this task while the other tasks were more focused on task performances which required both high and low gains and bandwidths.

The *Gap Criterion* value of 1.0 also has physical significance. Consider a Type I solution in which $G(s)$ was such that ΔK_p approached zero. Then the *Gap Criterion* would simply be the amplitude to cause PIO divided by the maximum amplitude available and if this *Gap Criterion* equals 1.0 then the amplitude to cause PIO would be equal to the maximum amplitude available. Hence, any *Gap Criterion* value greater than

1.0 would require more actuator deflection than was available, thereby providing a natural limit to creating a PIO. In other words, if an amplitude of 35 degrees were required, with only 30 degrees available, it is readily apparent that a PIO cannot be achieved.

The relatively high correlation factors, especially for the Combined Phase 2 Sum-of-sine datasets indicate the potential for *Gap Criterion* validation and acceptance as a tool for predicting Category II PIO due to rate-limited actuators.

VII. Conclusions

In this study, a new criterion for predicting pilot-induced oscillation tendency rating due to rate-limited actuators was developed and correlated to datasets of these ratings. This criterion was called the *Gap Criterion*.

Two historical databases, Projects HAVE PREVENT and HAVE OLOP were selected to see if the *Gap Criterion* had merit. Most datasets were assessed with greater than 95% confidence that a correlation indeed existed. Further, a logarithmic curve fit was deemed best. Follow on testing in Project MAX GAP gathered more PIO tendency rating data to augment these earlier findings. These datasets also showed strong evidence of correlation and again found a logarithmic interpolation of the data worked well.

These datasets were combined for different tasks and sources to determine whether the *Gap Criterion* was universal in nature. This seemed to be the case with all combined datasets indicating greater than 99.95% confidence level that correlation existed between the PIOR and the *Gap Criterion*. Logarithmic curve fits again appeared superior with high relative correlation factors and good endpoint matching.

Further observations were made for the combined datasets. Based on the relative positions of a majority of the data, it was found that lower *Gap Criterion* values resulted in higher PIO tendency ratings and vice versa. Further, proper PIO represented by PIO tendency rating values of 4, 5 or 6 were clustered at *Gap Criterion* values of 1.0 or less while PIO tendency ratings of 1, 2 or 3, representing non-PIO, were more prevalent at *Gap Criterion* values greater than 1.0.

The *Gap Criterion* has merit. It should be used as a tool to predict and reduce incidents of Category II PIO due to rate-limited actuators during aircraft development.

Appendix A. Matlab/Simulink™ Code

This appendix lists the Matlab™ source code used to move the short period poles of the F-16 to desired locations and then determine the feedback gains for angle-of-attack and pitch rate necessary to augment the new bare aircraft dynamics and return them to suitable closed loop dynamics. A Simulink™ diagram is also shown and was used for the preceding process. The next code listing computes the *Gap Criterion* for various bare aircraft dynamics and rate limit choices.

Bare Aircraft Pole Placement

```
%Bare Aircraft Dynamics Bare Pole placement
%This matlab file will take the bare F-16 dynamics at 15,000 ft Pressure Altitude,
%300 KCAS and place the short period poles where I want them based
%on what I give for short period damping and natural frequency.

clear;clc;format short g; format compact
warning off

a = [-0.033104 0.14957 -0.3207 -0.56111;
     -0.015511 -1.2826 1 -0.0024621;
     0.008081 -4.0875 -1.7556 0.0012828;
     0 0 1 0]
b = [-0.5193;
     -0.05243;
     -11.085;
     0]
c = eye(4)
d = [0; 0; 0; 0]
%Input the Desired Short Period Damping Ratio and Short Period Natural Frequency for test case
%Example: MAX GAP LAMARS Case B zetasp = 0.61, omegansp = 2.34

zetasp = input('Short Period Damping Ratio:');
omegansp= input('Short Period Natural Frequency:');
sigma = zetasp*omegansp
omegad = omegansp*sqrt(1-zetasp^2)

%Compute P vector to "place" the poles for the desired Short Period Damping
%Ratio and Short Period Natural Frequency.
%Also, Phugoid pole locations are chosen as -0.017+/-0.074j
%(Phugoid Damping Ratio = 0.224, Phugoid Natural Frequency = 0.075928 rad/s)

P=[-.017+.074*j -.017-.074*j -sigma+omegad*j -sigma-omegad*j]

kinner=-1*place(a,b,P)
'ahat is a+b*kinner'
```

```

ahat=a+b*kinner
'eigenvalues of ahat'
eigenvalues = eig(ahat)
'natural frequencies and dampings of ahat'
[wnn,zz]=damp(ahat)
'(Phugoid Damping Ratio = 0.2239, Phugoid Natural Frequency = 0.075928 rad/s)'

[num,den]=ss2tf(ahat,b,c,d)
BareAcutLongDynamics=tf(num(4,:),den)
continuing = input('continue');

%The following are the phugoid and short period (sp1 & sp2) poles for the DESIRED
%(must be changed if desired closed loop characteristics are different)
%closed loop system using angle-of-attack (alpha) and pitch rate (q) feedback:

phugoid1=-.017+.074*j;phugoid2=-.017-.074*j;sp1=-2.2+2.22*j;sp2=-2.2-2.22*j

P2=[phugoid1 phugoid2 sp1 sp2]
K=place(ahat,b,P2)

%Find approximate values of Kq (call it Kqbase) and
%Kalpha (call it Kalphabase)
Kqbase=-K(1,3)
Kalphabase=-K(1,2)

%Find best Kq and Kalpha
%This is an iterative, graphical technique to find Kalpha and Kq that take the
%bare aircraft dynamics and change them into the desired closed loop dynamics
%The error function {E(ii)=abs(wn(3)-3.125)+4.439*abs(z(3)-.7)} is important
%in that it relates to the closed loop short period natural frequency desired (3.125)
%and the short period damping ratio desired (.7). The constant 4.439 is a weighting function
%so that frequency and damping ratio are considered equally (3.125/.7 = 4.439)

%This is to get a ballpark Kalpha and Kq

ii=1
for kq = Kqbase-1:.025:Kqbase+1;
    for kalpha = Kalphabase-1:.025:Kalphabase+1;
        Kqcounter(ii)= kq;Kacounter(ii)=kalpha;
        [A2,B2,C2,D2]=LINMOD('AugmentedDynamics',0);
        Yc=ss(A2,B2,C2,D2);
        [Yctfnum,Yctfden]=ss2tf(A2,B2,C2,D2);
        yctf=tf(Yctfnum,Yctfden);
        [wn,z]=damp(yctf);
        wnn(ii)=wn(3);zz(ii)=z(3);iii(ii)=ii;
        E(ii)=abs(wn(3)-3.125)+4.439*abs(z(3)-.7);
        ii=ii+1
    end
end

plot(iii,E)

grid on
grid minor

```

```

xx=input('what index?')
'kq',Kqcounter(xx)
'kalpha',Kacounter(xx)
Kqbase=Kqcounter(xx);
Kalphabase=Kacounter(xx);

%This is to get a more precise Kalpha and Kq

ii=1
for kq = Kqbase-.1:.0025:Kqbase+.1;
    for kalpha = Kalphabase-.1:.0025:Kalphabase+.1;
        Kqcounter(ii)= kq;Kacounter(ii)=kalpha;
        [A2,B2,C2,D2]=LINMOD('AugmentedDynamics',0);
        Yc=ss(A2,B2,C2,D2);
        [Yctfnum,Yctfden]=ss2tf(A2,B2,C2,D2);
        yctf=tf(Yctfnum,Yctfden);
        [wn,z]=damp(yctf);
        wnn(ii)=wn(3);zz(ii)=z(3);iii(ii)=ii;
        E(ii)=abs(wn(3)-3.125)+4.439*abs(z(3)-.7);
        ii=ii+1
    end
end

plot(iii,E)

grid on
grid minor
xx=input('what FINAL index?')

%Final results

kq=Kqcounter(xx)
kalpha=Kacounter(xx)
[A2,B2,C2,D2]=LINMOD('AugmentedDynamics',0);
Yss=ss(A2,B2,C2,D2);
[Ynum,Yden]=ss2tf(A2,B2,C2,D2)
Ytf=tf(Ynum,Yden)
damp(Ytf)

```

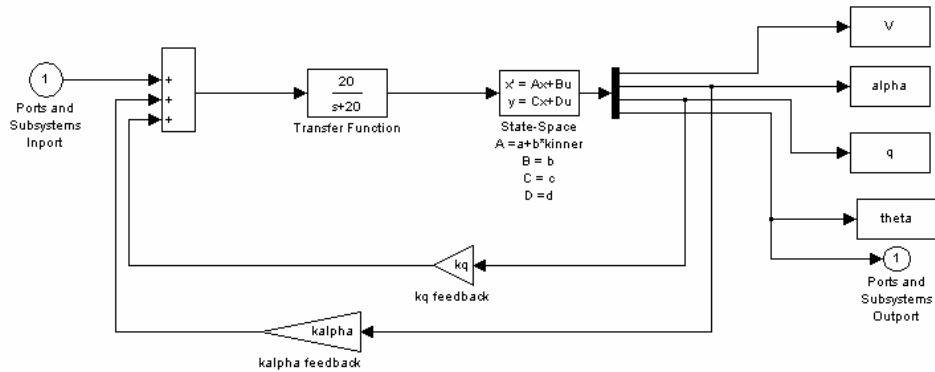


Figure A-1. Augmented Dynamics Simulink™ Model

Gap Criterion Computation

%This Matlab file will be used to take LAMARS Cases B, N, W and Y and compute the Gap Criterion
 % Maj Joel Witte
 % 04 Nov 03
 %This Matlab file takes the bare aircraft dynamics (Gc) and multiplies by the closed loop modified %Neal-Smith pilot model (Gp). Then the delta gain, gap (or ΔK_p), is calculated and kstar and omega %are determined.
 %Finally, the Gap Criterion is determined for each max actuator rate.

```
clear;clc;clf;format compact
```

```
figure(1)
```

```
%  

%The following are the parameters for the MAX GAP LAMARS evaluations.  

% Gc = bare aircraft dynamics  

%Gp = Neal-smith pilot model  

%G = bare aircraft dynamics convolved with the Neal-Smith Pilot Model  

%Choose which case by commenting/uncommenting the parameters  

%For example, currently Case B will be computed
```

```
%Case B
```

```
Gcb=tf([-11.08 -14.37 -0.5277],[1 2.889 5.578 0.2026 0.03157])  

Gpb=-.11483*tf([.32483 1],[.00001 1])*tf([5 1],[1 0],'iodelay',.25);  

G=Gcb*Gpb
```

```
%Case N
```

```
% Gcn=tf([-5.551e-015 -11.09 -14.37 -0.5277],[1 1.912 9.867 0.3439 0.05648])  

% Gpn=-.10919*tf([.32699 1],[.00001 1])*tf([5 1],[1 0],'iodelay',.25);  

% G=Gcn*Gpn
```

```
%Case W
```

```
% Gcw=tf([-3.553e-015 -11.09 -14.37 -0.5277],[1 8.512 22.48 0.8031 0.1279])  

% Gpw=-.15254*tf([.30311 1],[.00001 1])*tf([5 1],[1 0],'iodelay',.25);  

% G=Gcw*Gpw
```

```

%Case Y
%Gcy=tf([-6.217e-015 -11.08 -14.37 -0.5277],[1 4.21 5.53 0.2071 0.03103])
%Gpy= -.12528*tf([.31318 1],[.00001 1])*tf([5 1],[1 0],'iodelay',.25);
%G=Gcy*Gpy

W=LOGSPACE(log10(.1),log10(10),1000);

ii=0;
for kstarr=.1:.001:1;
    ii=ii+1;
    kstar(ii)=kstarr;
    mag_N(ii)=-20*log10(8*kstarr/(pi^2));
    ph_N(ii)=(180/pi)*acos(kstarr) - 180;
end

figure(1)
nichols(G,W)
grid on
hold on
plot(ph_N,mag_N,'r')
axis([-200 -70 -20 30])
grid on

w1=input('what freq (rad/s) range? Low end =')
w2=input('high end =')
W1=LOGSPACE(log10(w1),log10(w2),1000);
[mag_check1,phase_check1] = NICHOLS(G,W1);
mag_check=squeeze(mag_check1);
phase_check=squeeze(phase_check1);

check = polyfit(phase_check,mag_check,9)
swoosh = polyfit(ph_N,mag_N,9)

jj=1
for phase=-100:-.1:-170;
    checkmagdB(jj)=20*log10(polyval(check,phase));
    checkphase(jj)=phase;
    jj=jj+1;
end

jj=1;
for phase=-100:-.1:-170;
    swooshmag(jj)=polyval(swoosh,phase);
    swooshphase(jj)=phase;
    jj=jj+1;
end

dB=swooshmag-checkmagdB;

[Gap,index] = min(dB)

inc=10^(Gap/20)
nichols(G*inc,W)

```



```

hold on
axis([-200 -70 -20 30])
omega=input('just touchin omega')
[magtouch,phasetouch]=bode(G,omega)

ii=1;
for kstar=.1:.001:1;
    if ph_N(ii)>phasetouch
        kstar=kstar;
    end
    ii=ii+1;
end
kstar
maxdeg=30
%Compute Gap Criterion for rate limits 15 deg/sec, 30 deg/sec and 60 deg/sec
GapCriterion15=inc*(pi*15/(2*omega*kstar*maxdeg))
GapCriterion30=inc*(pi*30/(2*omega*kstar*maxdeg))
GapCriterion60=inc*(pi*60/(2*omega*kstar*maxdeg))

'done'

```

Appendix B. State Space Matrices for Project MAX GAP

This appendix lists the state space matrices for the F-16 dynamics as well as the bare aircraft dynamics of each case for Projects HAVE PREVENT, HAVE OLOP and MAX GAP.

F-16 Dynamics

$$\begin{aligned}
 a &= \begin{bmatrix} -0.033104 & 0.14957 & -0.3207 & -0.56111 \\ -0.015511 & -1.2826 & 1 & -0.002462 \\ 0.008081 & -4.0875 & -1.7556 & 0.001283 \\ 0 & 0 & 1 & 0 \end{bmatrix} & b &= \begin{bmatrix} -0.5193 \\ -0.05243 \\ -11.085 \\ 0 \end{bmatrix} \\
 c &= \begin{bmatrix} 1 & 0 & 0 & 0 \\ 0 & 1 & 0 & 0 \\ 0 & 0 & 1 & 0 \\ 0 & 0 & 0 & 1 \end{bmatrix} & d &= \begin{bmatrix} 0 \\ 0 \\ 0 \\ 0 \end{bmatrix}
 \end{aligned}$$

Modified Matrices

The following matrices are the pole placement results ($A = a + b \cdot kinner$).

HAVE PREVENT

Case A

$$A = \begin{bmatrix} -0.033094 & 0.069282 & -0.38266 & -0.56125 \\ -0.01551 & -1.2907 & 0.99374 & -0.002477 \\ 0.008304 & -5.8013 & -3.0782 & -0.001753 \\ 0 & 0 & 1 & 0 \end{bmatrix}$$

Case B

$$A = \begin{bmatrix} -0.033093 & 0.17889 & -0.3122 & -0.56093 \\ -0.01551 & -1.2796 & 1.0009 & -0.002444 \\ 0.008312 & -3.4615 & -1.5741 & 0.005109 \\ 0 & 0 & 1 & 0 \end{bmatrix}$$

Case C

$$A = \begin{bmatrix} -0.033114 & 0.3331 & -0.2587 & -0.56113 \\ -0.015512 & -1.2641 & 1.0063 & -0.002464 \\ 0.007874 & -0.16992 & -0.43222 & 0.00081 \\ 0 & 0 & 1 & 0 \end{bmatrix}$$

Case D

$$A = \begin{vmatrix} -0.033102 & 0.38576 & -0.20764 & -0.56119 \\ -0.015511 & -1.2588 & 1.0114 & -0.00247 \\ 0.008121 & 0.95415 & 0.65786 & -0.000441 \\ 0 & 0 & 1 & 0 \end{vmatrix}$$

HAVE OLOP

Case A

$$A = \begin{vmatrix} -0.035901 & -0.21367 & -0.22435 & -0.56209 \\ -0.015793 & -1.3193 & 1.0097 & -0.002562 \\ -0.051625 & -11.841 & 0.30117 & -0.019725 \\ 0 & 0 & 1 & 0 \end{vmatrix}$$

Case B

$$A = \begin{vmatrix} -0.033649 & 0.31011 & -0.23615 & -0.56149 \\ -0.015566 & -1.2664 & 1.0085 & -0.0025 \\ -0.003556 & -0.66055 & 0.04924 & -0.006762 \\ 0 & 0 & 1 & 0 \end{vmatrix}$$

Case C

$$A = \begin{vmatrix} -0.033422 & 0.20283 & -0.29951 & -0.56139 \\ -0.015543 & -1.2772 & 1.0021 & -0.00249 \\ 0.001303 & -2.9505 & -1.3034 & -0.004668 \\ 0 & 0 & 1 & 0 \end{vmatrix}$$

Case D

$$A = \begin{vmatrix} -0.033278 & 0.44459 & -0.21943 & -0.5614 \\ -0.015529 & -1.2528 & 1.0102 & -0.002491 \\ 0.004371 & 2.2099 & 0.40609 & -0.00486 \\ 0 & 0 & 1 & 0 \end{vmatrix}$$

MAX GAP (LAMARS)

Case B

$$A = \begin{vmatrix} -0.033384 & 0.17915 & -0.31228 & -0.56137 \\ -0.015539 & -1.2796 & 1.0009 & -0.002489 \\ 0.002102 & -3.456 & -1.5758 & -0.004294 \\ 0 & 0 & 1 & 0 \end{vmatrix}$$

Case N

$$A = \begin{vmatrix} -0.034932 & -0.080584 & -0.26522 & -0.56181 \\ -0.015696 & -1.3058 & 1.0056 & -0.002533 \\ -0.030946 & -9.0004 & -0.57123 & -0.013697 \\ 0 & 0 & 1 & 0 \end{vmatrix}$$

Case W

$$A = \begin{vmatrix} -0.032474 & -0.27041 & -0.57362 & -0.56097 \\ -0.015447 & -1.325 & 0.97446 & -0.002448 \\ 0.021525 & -13.052 & -7.1545 & 0.004179 \\ 0 & 0 & 1 & 0 \end{vmatrix}$$

Case Y

$$A = \begin{vmatrix} -0.032397 & 0.26148 & -0.37461 & -0.56107 \\ -0.01544 & -1.2713 & 0.99456 & -0.002458 \\ 0.023175 & -1.6987 & -2.9063 & 0.002109 \\ 0 & 0 & 1 & 0 \end{vmatrix}$$

MAX GAP (VISTA)

Case B

$$A = \begin{vmatrix} -0.033384 & 0.18062 & -0.31171 & -0.56137 \\ -0.015539 & -1.2795 & 1.0009 & -0.002489 \\ 0.002103 & -3.4248 & -1.5638 & -0.004301 \\ 0 & 0 & 1 & 0 \end{vmatrix}$$

Case N

$$A = \begin{vmatrix} -0.03532 & -0.068363 & -0.22347 & -0.56194 \\ -0.015735 & -1.3046 & 1.0098 & -0.002546 \\ -0.039218 & -8.7395 & 0.31992 & -0.016428 \\ 0 & 0 & 1 & 0 \end{vmatrix}$$

Case W

$$A = \begin{vmatrix} -0.032282 & 0.010816 & -0.48286 & -0.56098 \\ -0.015428 & -1.2966 & 0.98363 & -0.002449 \\ 0.02563 & -7.0493 & -5.2171 & 0.004129 \\ 0 & 0 & 1 & 0 \end{vmatrix}$$

Case Y

$$A = \begin{vmatrix} -0.032063 & 0.36636 & -0.36584 & -0.56099 \\ -0.015406 & -1.2607 & 0.99544 & -0.00245 \\ 0.030312 & 0.54004 & -2.7192 & 0.003902 \\ 0 & 0 & 1 & 0 \end{vmatrix}$$

Appendix C. Correlation Computation

Data Reduction and Analysis

The pre-computed *Gap Criterion* for the selected bare aircraft and rate limit configuration was plotted with the assigned PIO Tendency Rating. The confidence level of the data correlation was determined by computing a correlation coefficient, r_{xy} , shown in equation C-1 (Wheeler and Ganji, 1996:145-155).

$$r_{xy} = \frac{\sum_{i=1}^n (x_i - \bar{x})(y_i - \bar{y})}{\left[\sum_{i=1}^n (x_i - \bar{x})^2 \sum_{i=1}^n (y_i - \bar{y})^2 \right]^{1/2}} \quad (\text{C-1})$$

Where n is the number of data pairs and \bar{x} and \bar{y} are the mean values of x and y which were obtained from:

$$\bar{x} = \frac{\sum_{i=1}^n x_i}{n}, \quad \bar{y} = \frac{\sum_{i=1}^n y_i}{n} \quad (\text{C-2})$$

To determine if there is correlation to a certain degree of confidence, the absolute value of the correlation coefficient, r_{xy} , for n data pairs is compared to the minimum values of the correlation coefficient shown in Table C-1:

Table C-1. Minimum Values of the Correlation Coefficient for Confidence Level
(Wheeler and Ganji, 1996:147)

<i>n</i>	Confidence Level				
	80%	90%	95%	98%	99%
3	0.951	0.988	0.997	1.000	1.000
4	0.800	0.900	0.950	0.980	0.990
5	0.687	0.805	0.878	0.934	0.959
6	0.608	0.729	0.811	0.882	0.917
7	0.551	0.669	0.754	0.833	0.875
8	0.507	0.621	0.707	0.789	0.834
9	0.472	0.582	0.666	0.750	0.798
10	0.443	0.549	0.632	0.715	0.765
11	0.419	0.521	0.602	0.685	0.735
12	0.398	0.497	0.576	0.658	0.708
13	0.380	0.476	0.553	0.634	0.684
14	0.365	0.458	0.532	0.612	0.661
15	0.351	0.441	0.514	0.592	0.641
16	0.338	0.426	0.497	0.574	0.623
17	0.327	0.412	0.482	0.558	0.606
18	0.317	0.400	0.468	0.543	0.590
19	0.308	0.389	0.456	0.529	0.575
20	0.299	0.378	0.444	0.516	0.561
25	0.265	0.337	0.396	0.462	0.505
30	0.241	0.306	0.361	0.423	0.463
35	0.222	0.283	0.334	0.392	0.430
40	0.207	0.264	0.312	0.367	0.403
45	0.195	0.248	0.294	0.346	0.380
50	0.184	0.235	0.279	0.328	0.361
100	0.129	0.166	0.197	0.233	0.257
200	0.091	0.116	0.138	0.163	0.180

Appendix D. MAX GAP Histograms

The MAX GAP LAMARS and VISTA test histograms are contained in this appendix. These charts show the raw data collected and indicate which datapoints were considered outliers and omitted from the reduced dataset (Witte and others, 2003). Pilots 1, 2 and 3 were the same individual in each case.

MAX GAP (LAMARS) Histograms

Handling Qualities Phase 2 Sum-of-sines Task

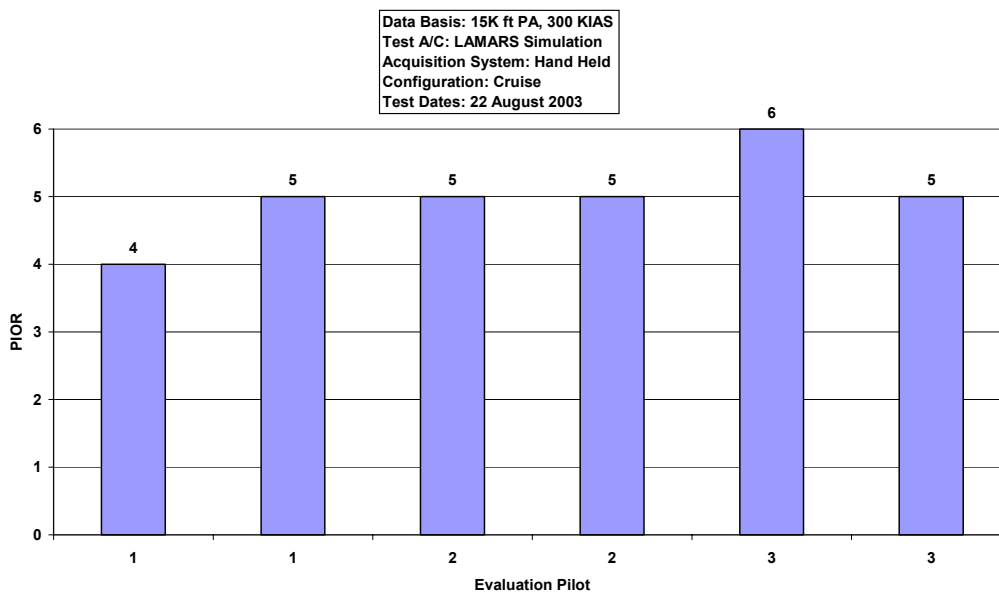


Figure D-1. LAMARS Phase 2 Sum-of-sines Data, Case B, 15 deg/sec

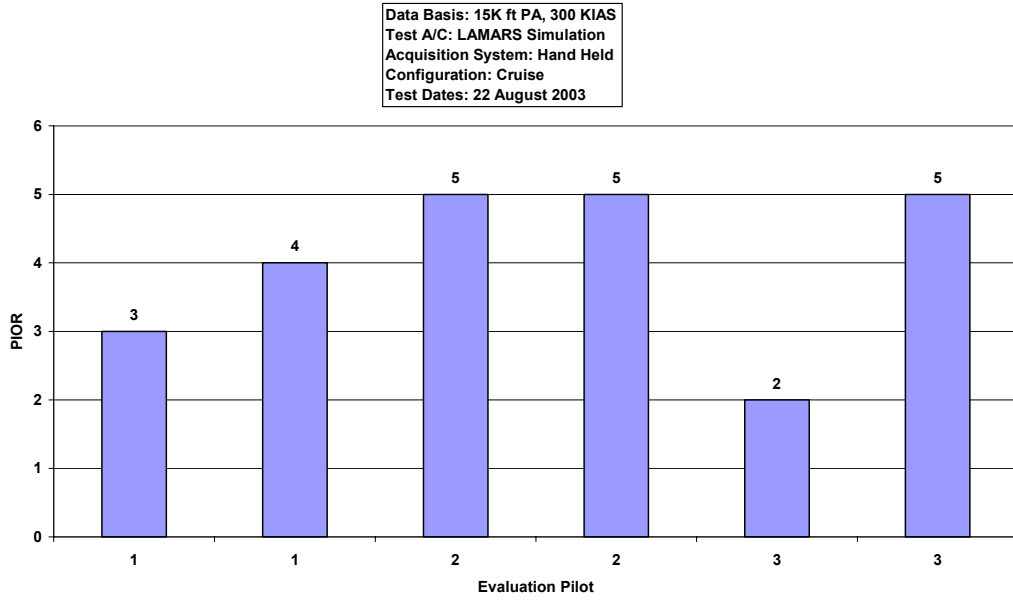


Figure D-2. LAMARS Phase 2 Sum-of-sines Data, Case B, 30 deg/sec

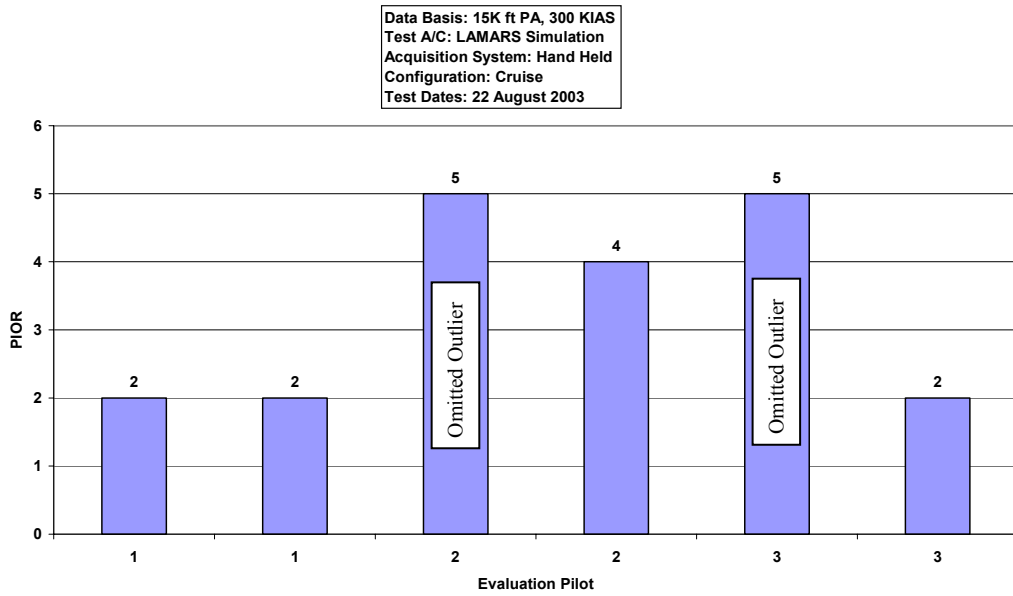


Figure D-3. LAMARS Phase 2 Sum-of-sines Data, Case B, 60 deg/sec

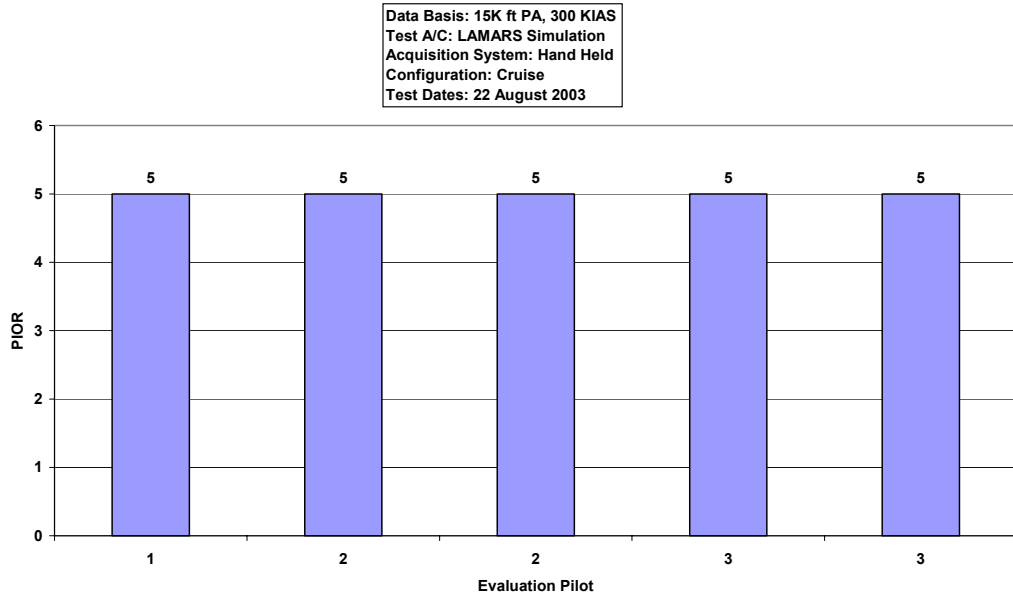


Figure D-4. LAMARS Phase 2 Sum-of-sines Data, Case N, 15 deg/sec

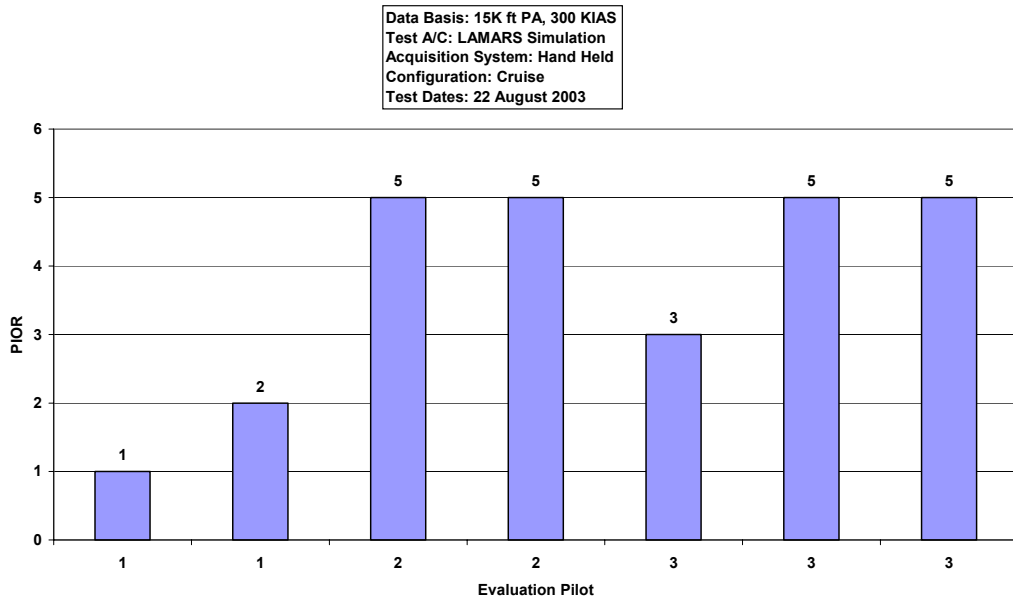


Figure D-5. LAMARS Phase 2 Sum-of-sines Data, Case N, 30 deg/sec

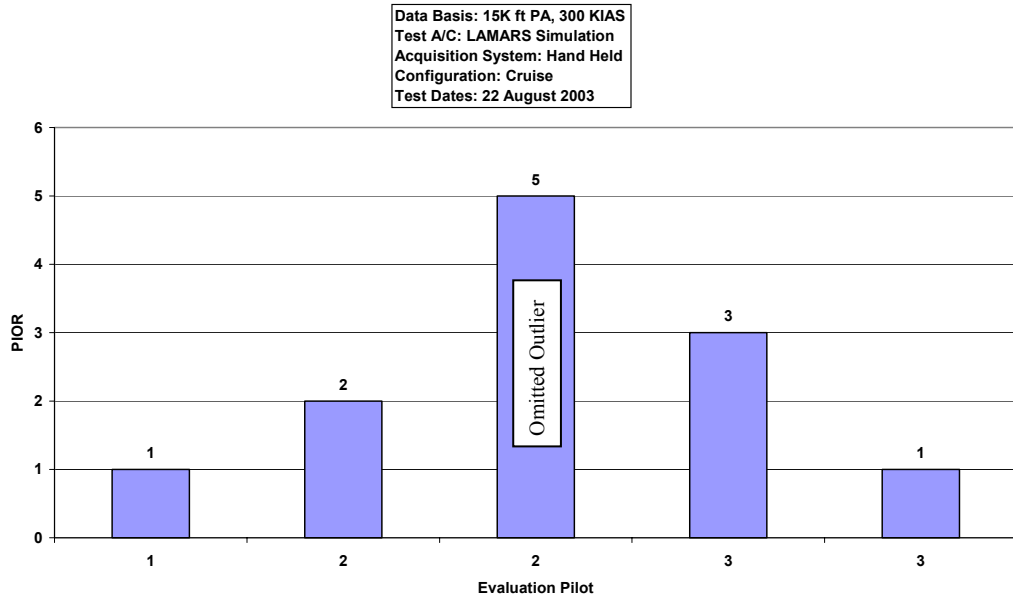


Figure D-6. LAMARS Phase 2 Sum-of-sines Data, Case N, 60 deg/sec

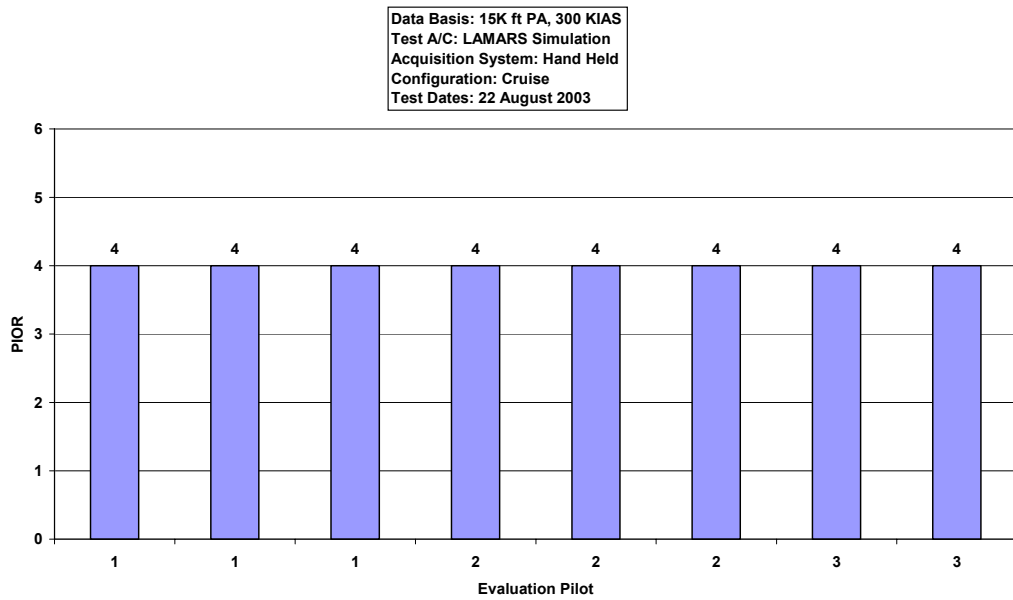


Figure D-7. LAMARS Phase 2 Sum-of-sines Data, Case W, 15 deg/sec

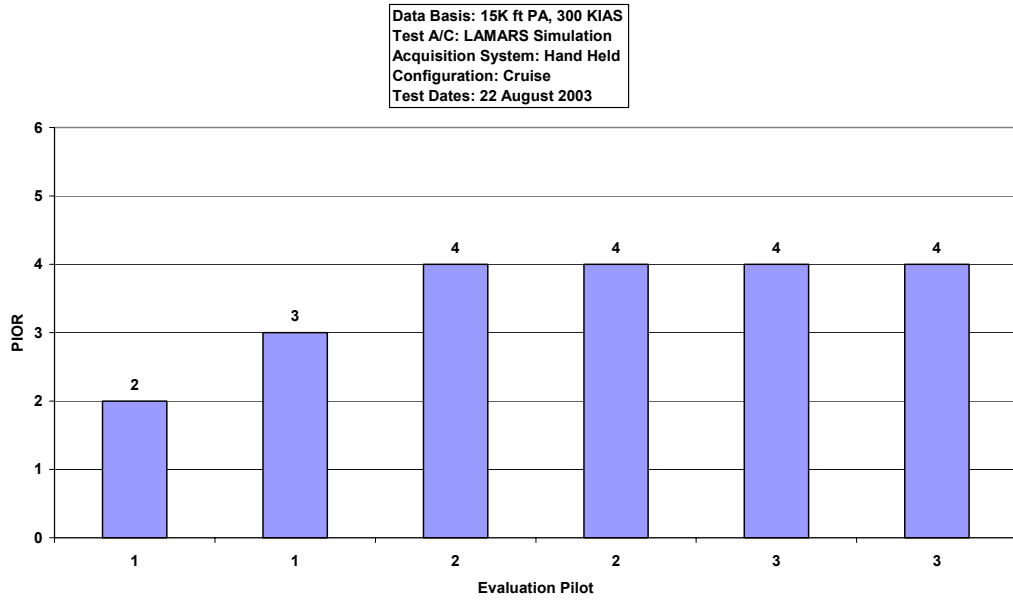


Figure D-8. LAMARS Phase 2 Sum-of-sines Data, Case W, 30 deg/sec

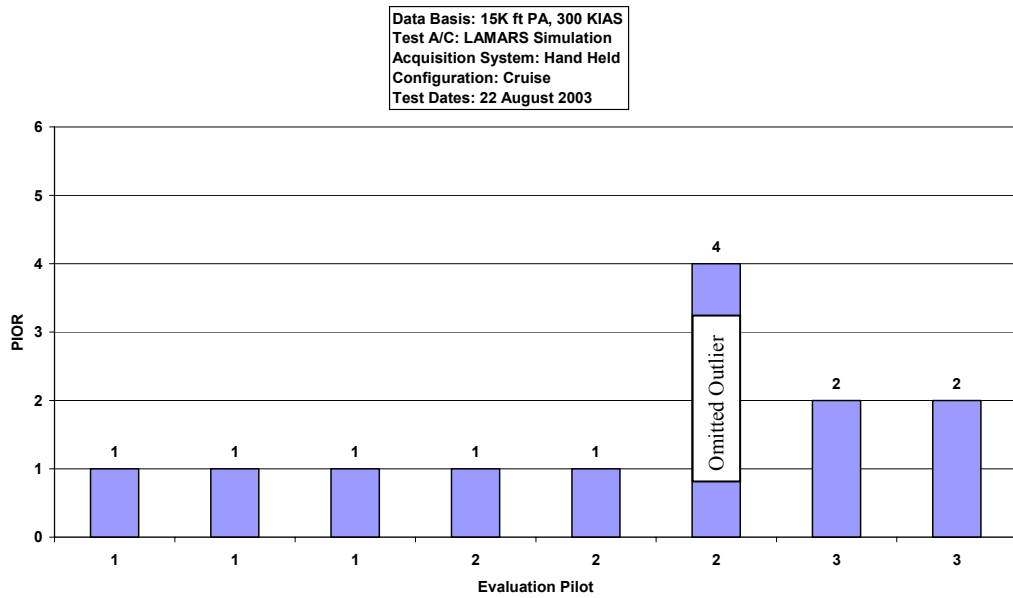


Figure D-9. LAMARS Phase 2 Sum-of-sines Data, Case W, 60 deg/sec

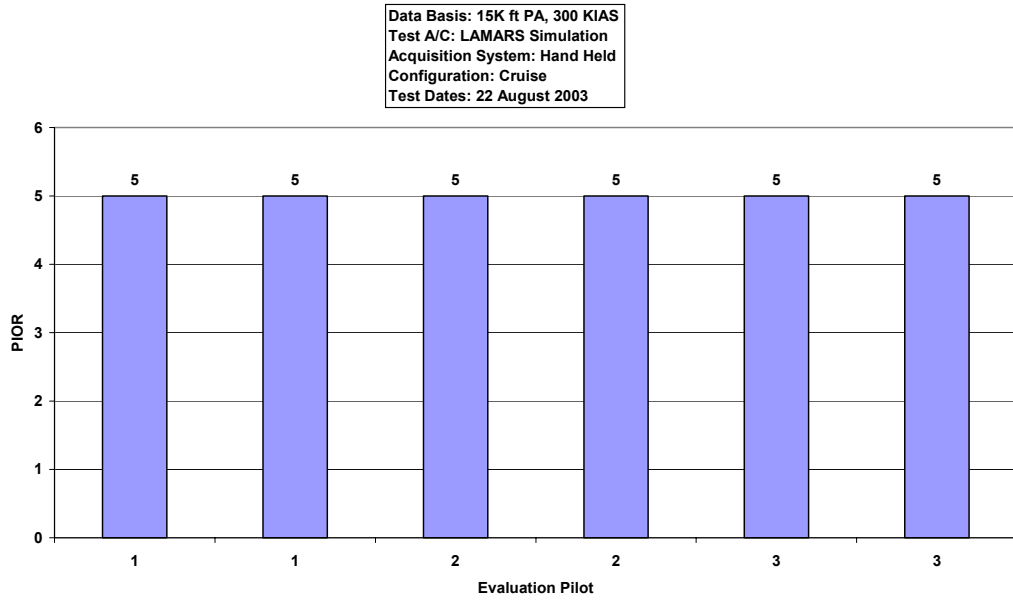


Figure D-10. LAMARS Phase 2 Sum-of-sines Data, Case Y, 15 deg/sec

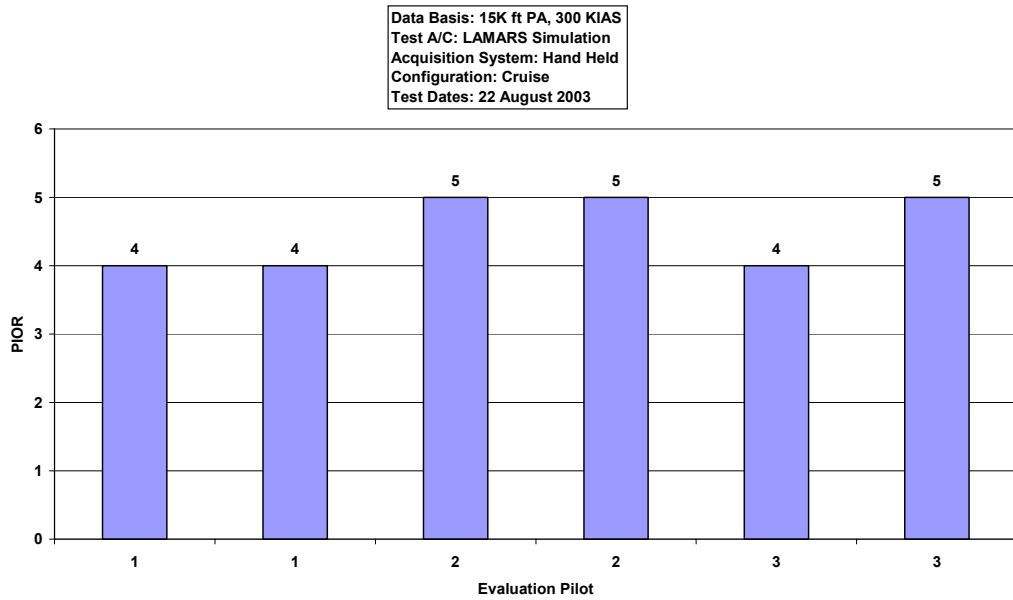


Figure D-11. LAMARS Phase 2 Sum-of-sines Data, Case Y, 30 deg/sec

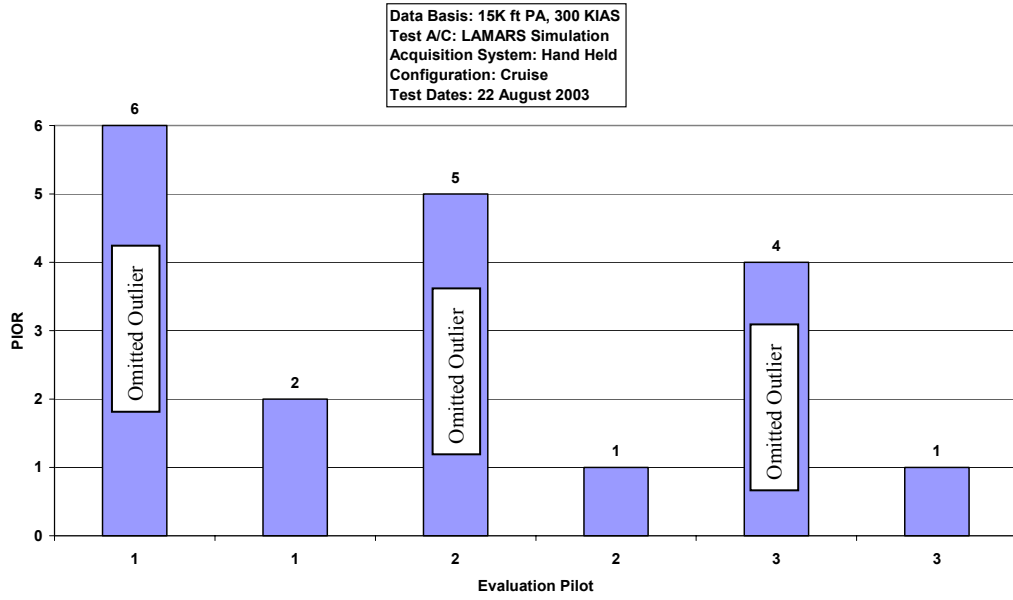


Figure D-12. LAMARS Phase 2 Sum-of-sines Data, Case Y, 60 deg/sec

Handling Qualities Phase 3 Discrete HUD Pitch Tracking Task

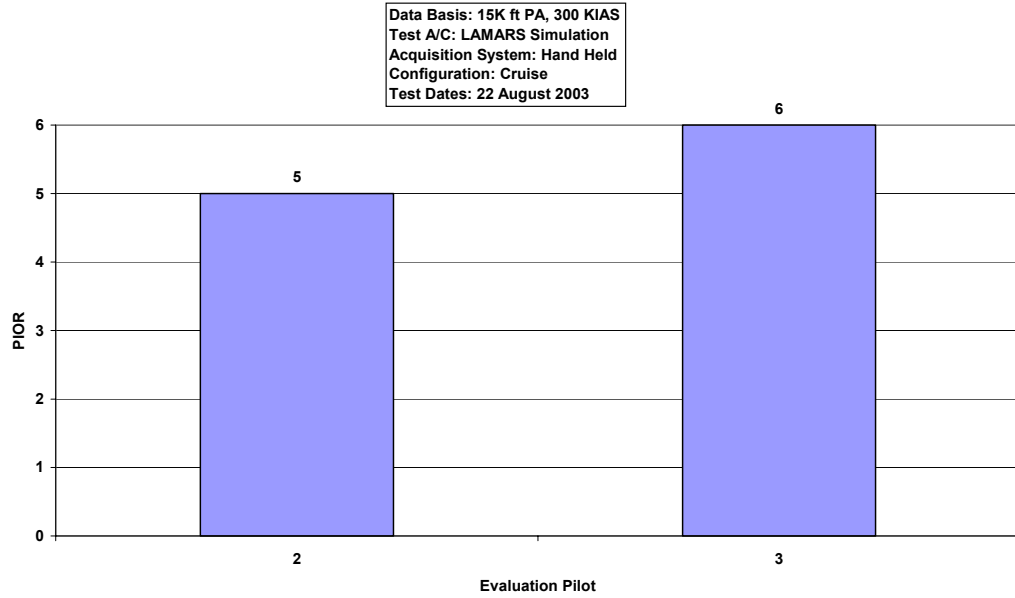


Figure D-13. LAMARS Phase 3 Discrete HUD Pitch Tracking Data, Case B, 15 deg/sec

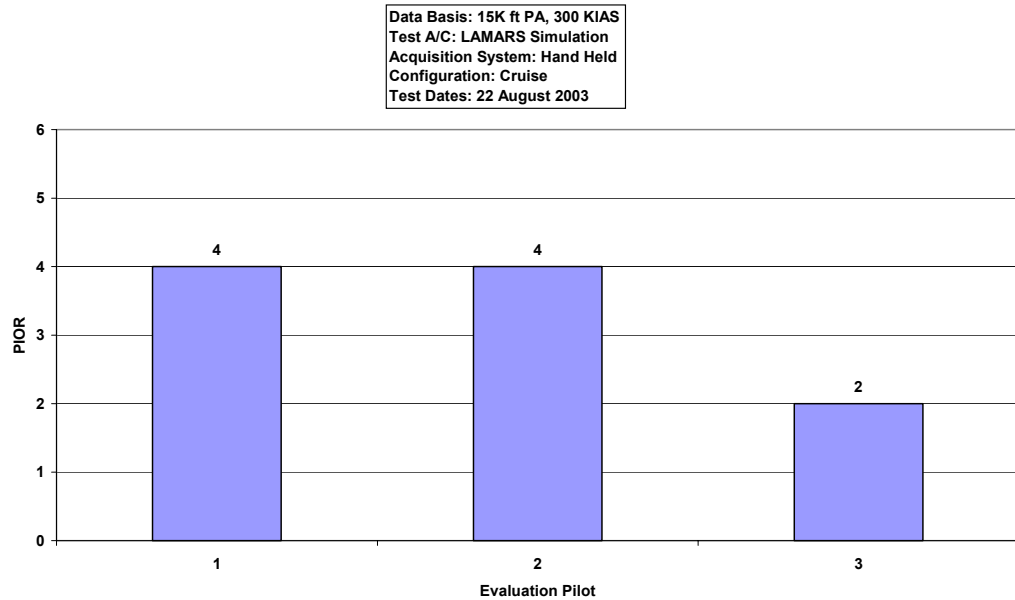


Figure D-14. LAMARS Phase 3 Discrete HUD Pitch Tracking Data, Case B, 30 deg/sec

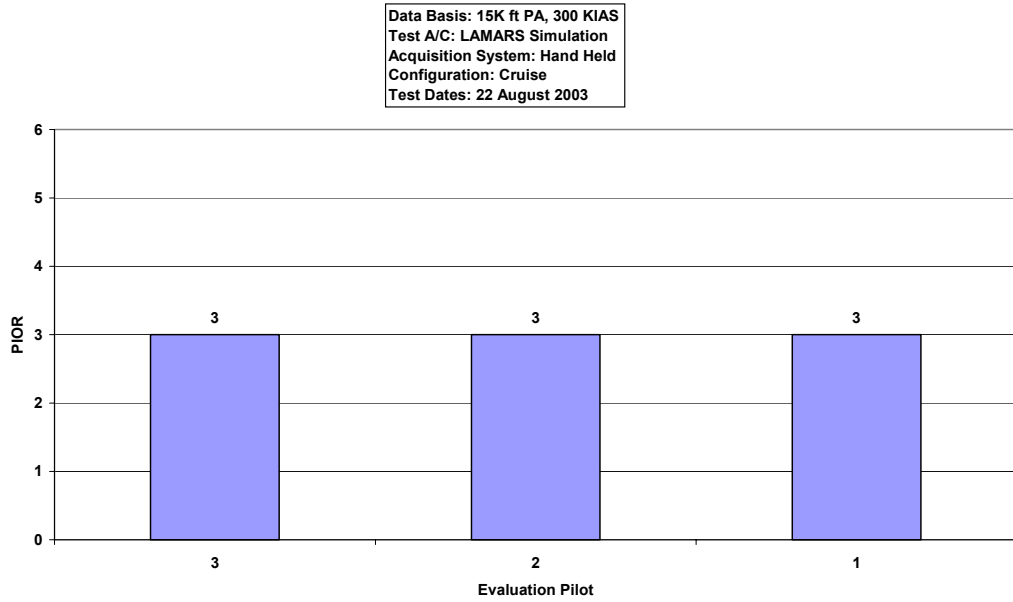


Figure D-15. LAMARS Phase 3 Discrete HUD Pitch Tracking Data, Case B, 60 deg/sec

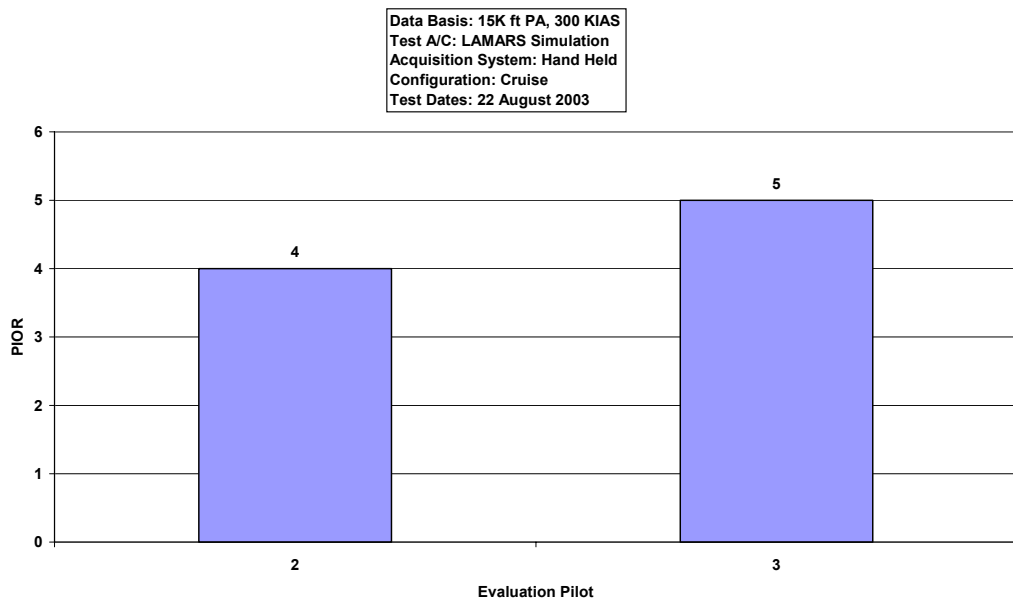


Figure D-16. LAMARS Phase 3 Discrete HUD Pitch Tracking Data, Case N, 15 deg/sec

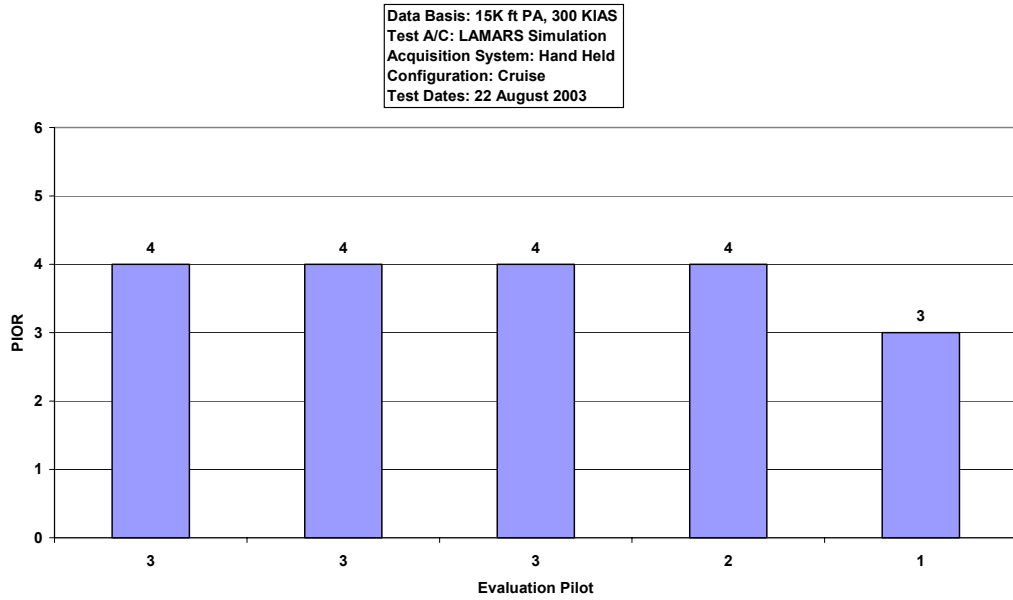


Figure D-17. LAMARS Phase 3 Discrete HUD Pitch Tracking Data, Case N, 30 deg/sec

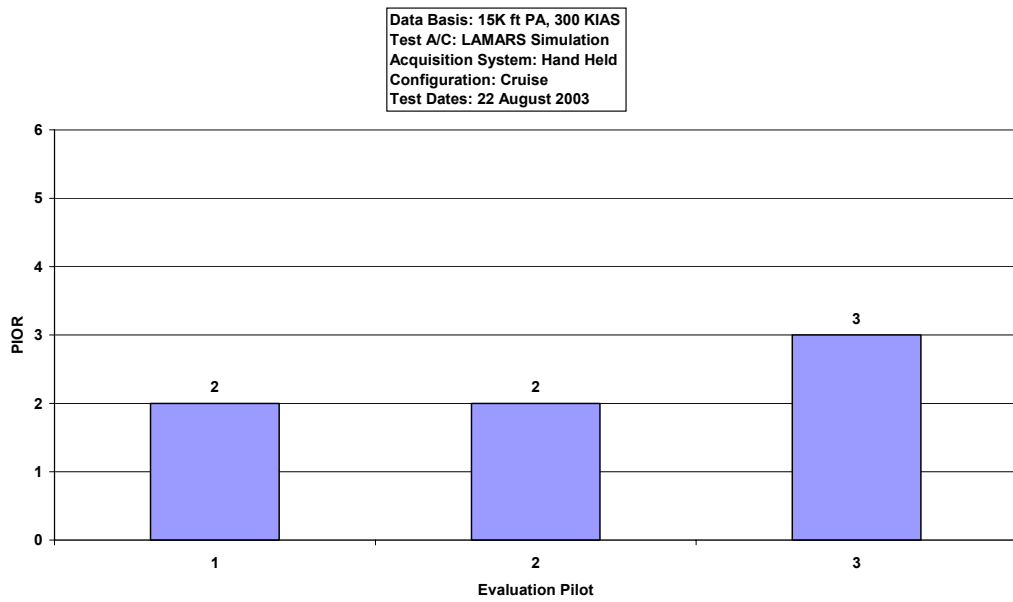


Figure D-18. LAMARS Phase 3 Discrete HUD Pitch Tracking Data, Case N, 60 deg/sec

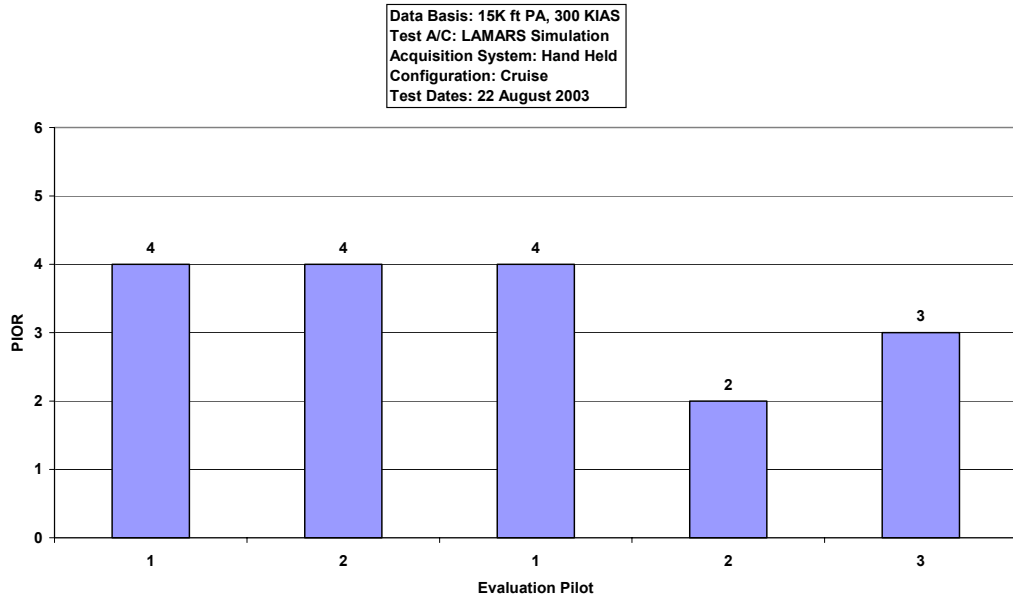


Figure D-19. LAMARS Phase 3 Discrete HUD Pitch Tracking Data, Case W, 15 deg/sec

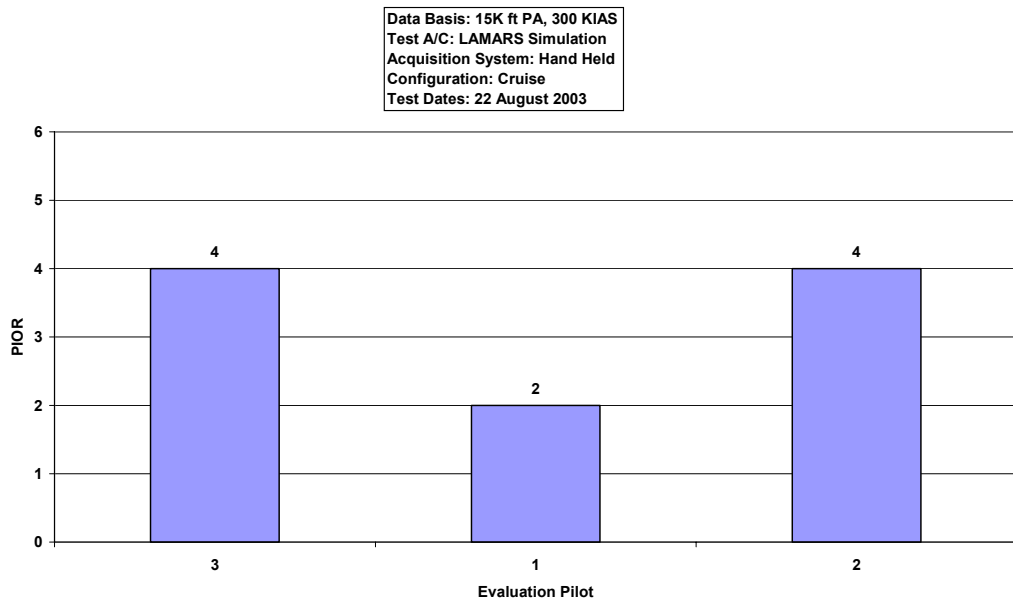


Figure D-20. LAMARS Phase 3 Discrete HUD Pitch Tracking Data, Case W, 30 deg/sec

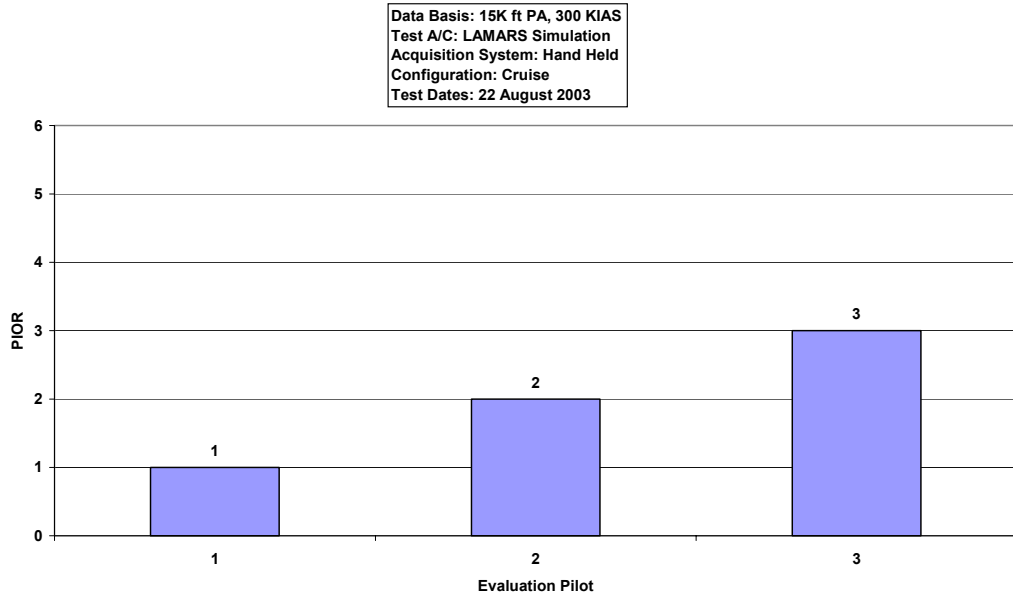


Figure D-21. LAMARS Phase 3 Discrete HUD Pitch Tracking Data, Case W, 60 deg/sec

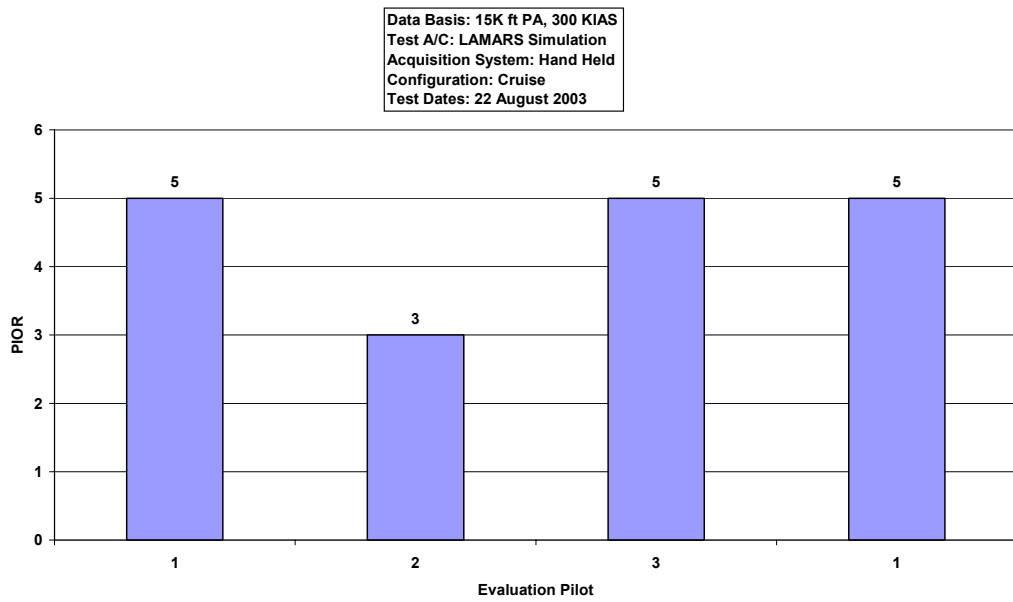


Figure D-22. LAMARS Phase 3 Discrete HUD Pitch Tracking Data, Case Y, 15 deg/sec

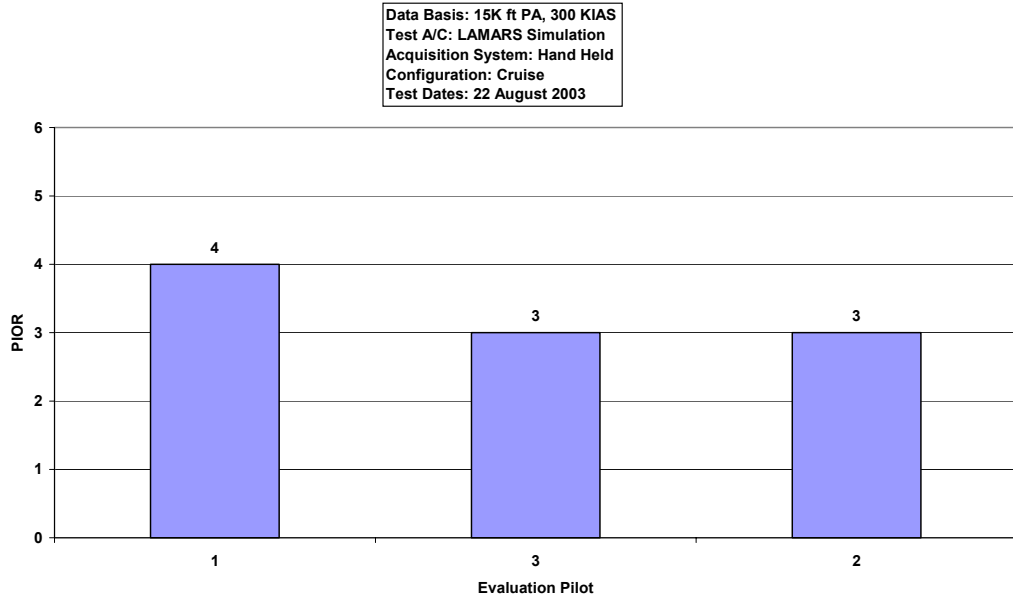


Figure D-23. LAMARS Phase 3 Discrete HUD Pitch Tracking Data, Case Y, 30 deg/sec

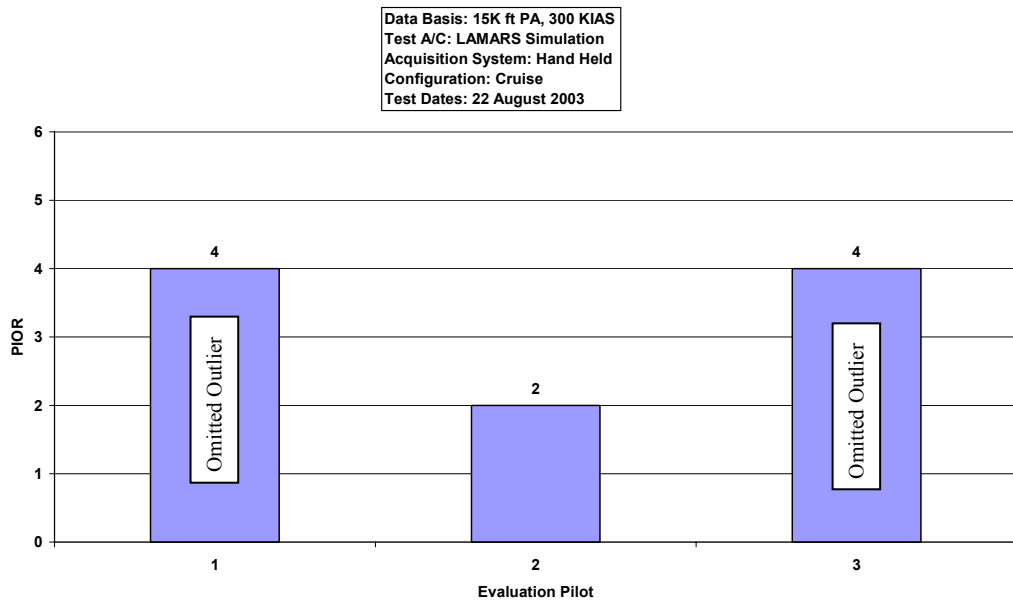


Figure D-24. LAMARS Phase 3 Discrete HUD Pitch Tracking Data, Case Y, 60 deg/sec

Handling Qualities Phase 3 Target Tracking Task

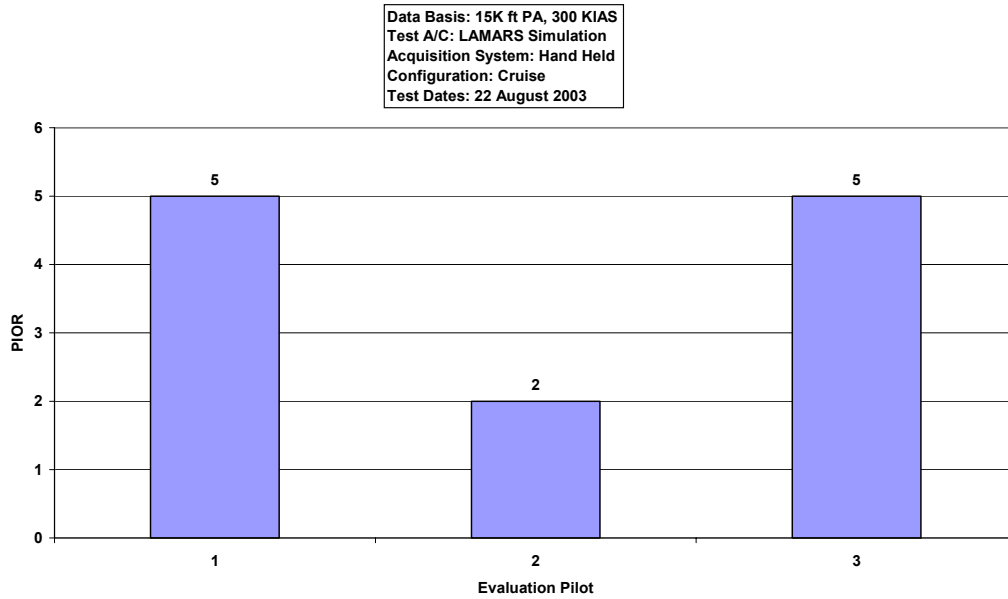


Figure D-25. LAMARS Phase 3 Target Tracking Data, Case B, 15 deg/sec

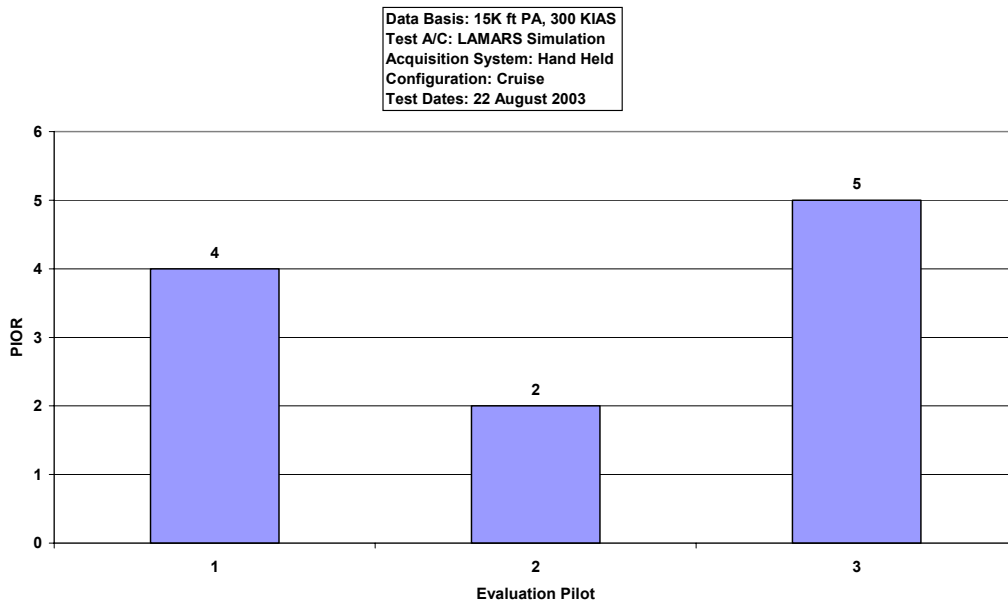


Figure D-26. LAMARS Phase 3 Target Tracking Data, Case B, 30 deg/sec

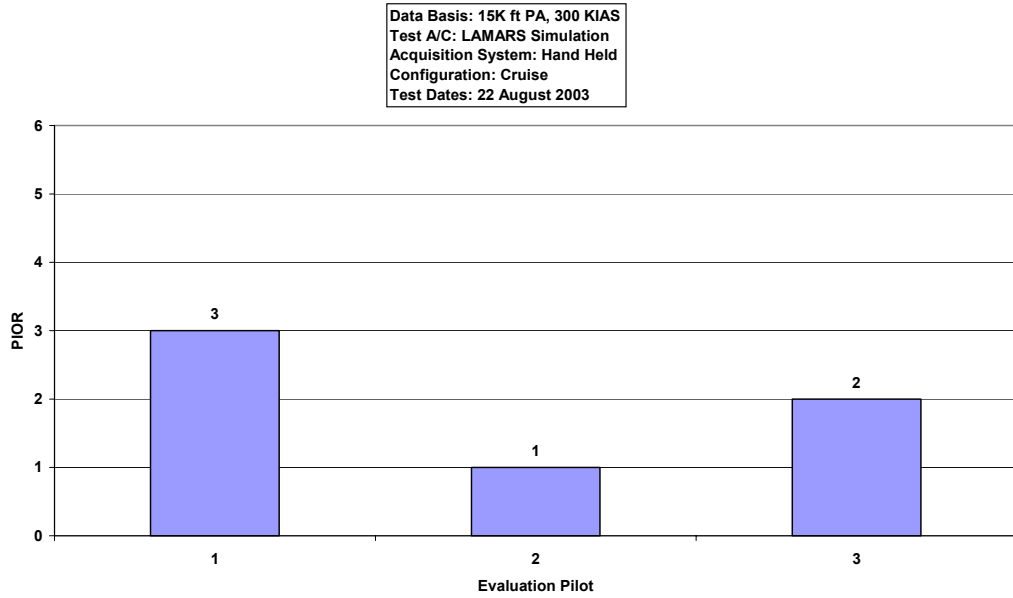


Figure D-27. LAMARS Phase 3 Target Tracking Data, Case B, 60 deg/sec

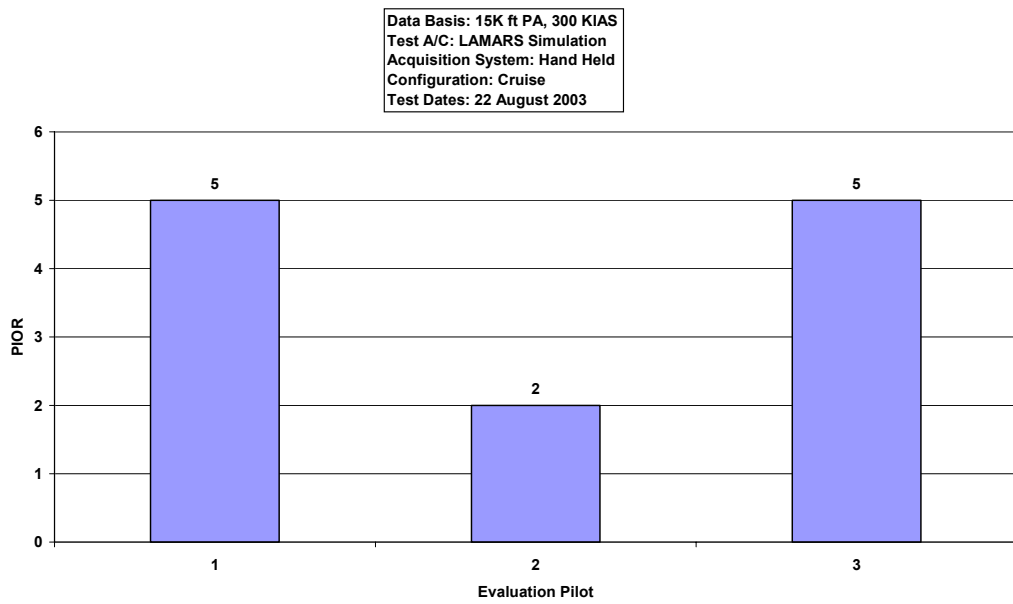


Figure D-28. LAMARS Phase 3 Target Tracking Data, Case N, 15 deg/sec

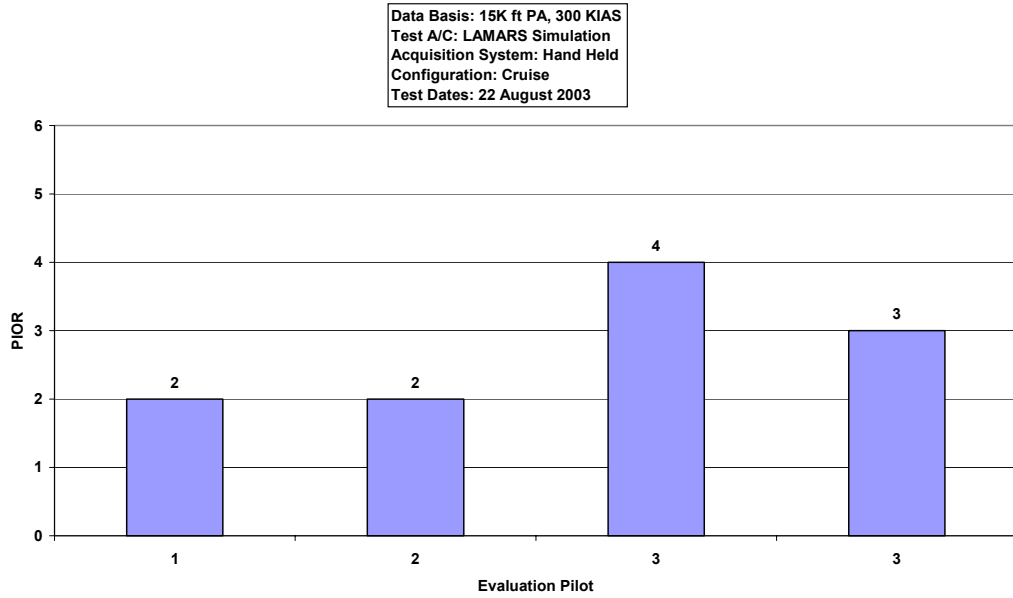


Figure D-29. LAMARS Phase 3 Target Tracking Data, Case N, 30 deg/sec

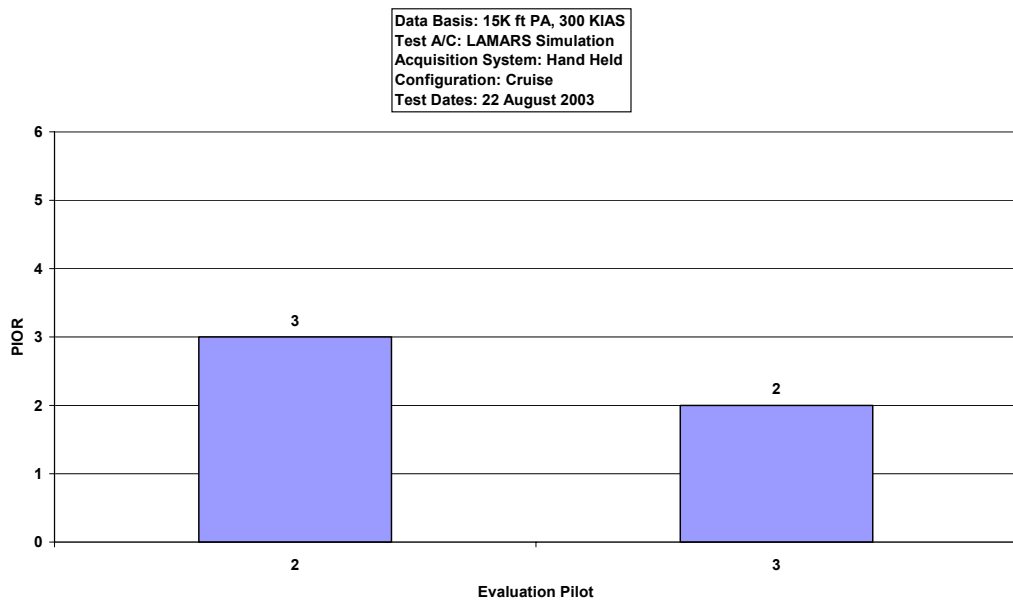


Figure D-30. LAMARS Phase 3 Target Tracking Data, Case N, 60 deg/sec

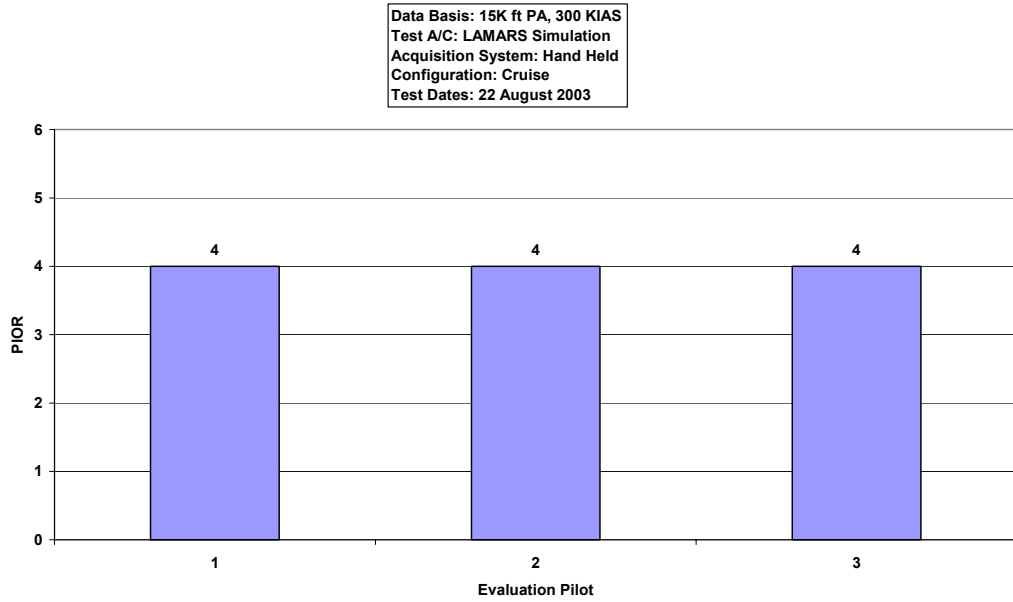


Figure D-31. LAMARS Phase 3 Target Tracking Data, Case W, 15 deg/sec

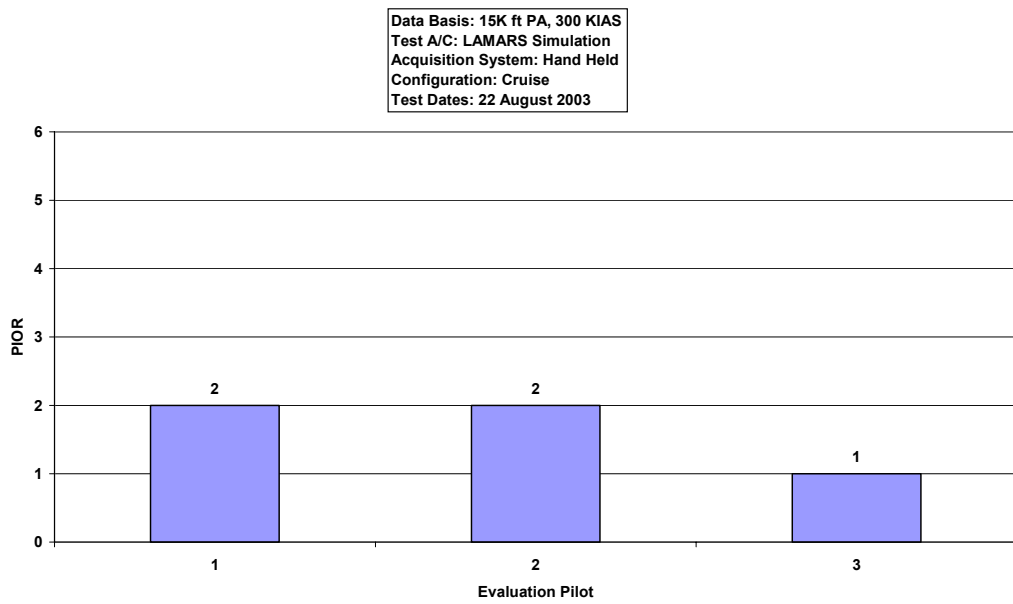


Figure D-32. LAMARS Phase 3 Target Tracking Data, Case W, 30 deg/sec

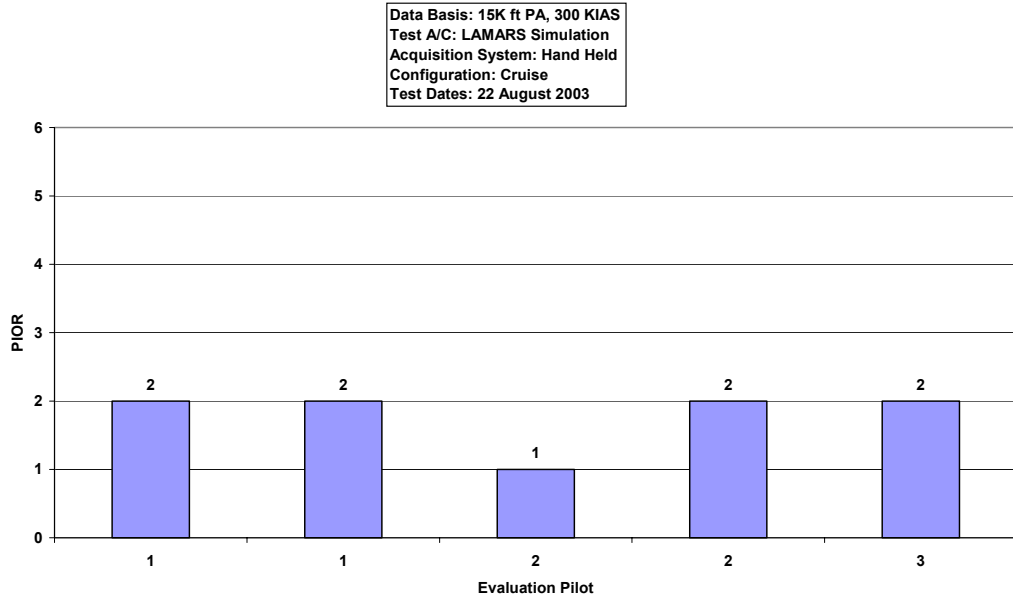


Figure D-33. LAMARS Phase 3 Target Tracking Data, Case W, 60 deg/sec

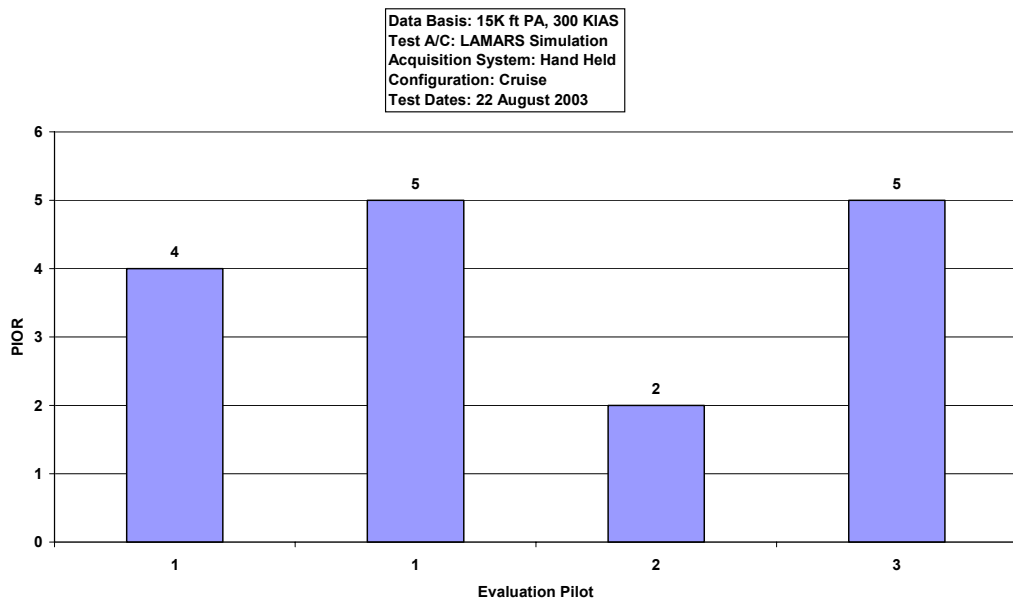


Figure D-34. LAMARS Phase 3 Target Tracking Data, Case Y, 15 deg/sec

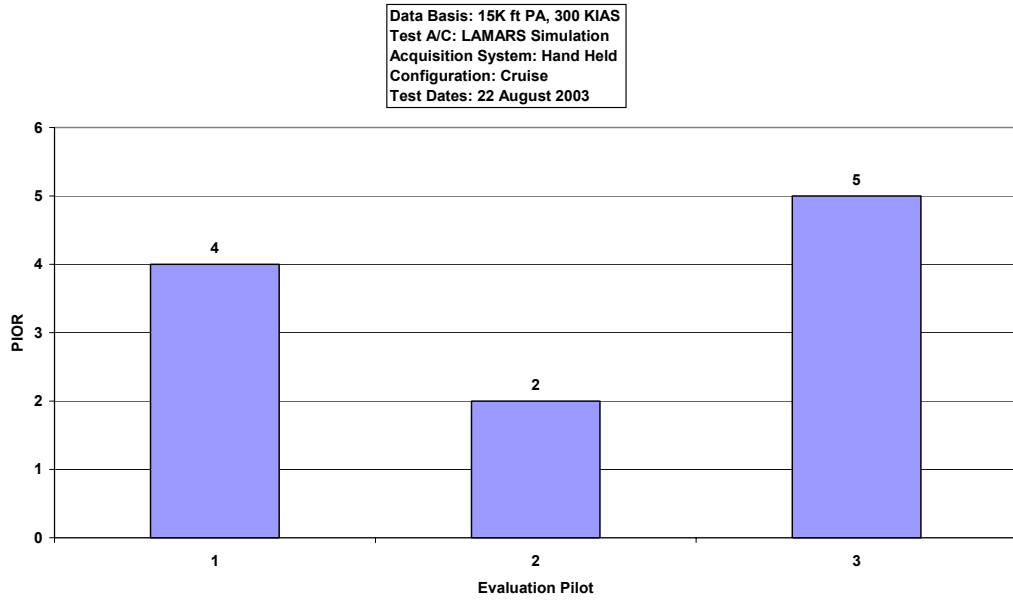


Figure D-35. LAMARS Phase 3 Target Tracking Data, Case Y, 30 deg/sec

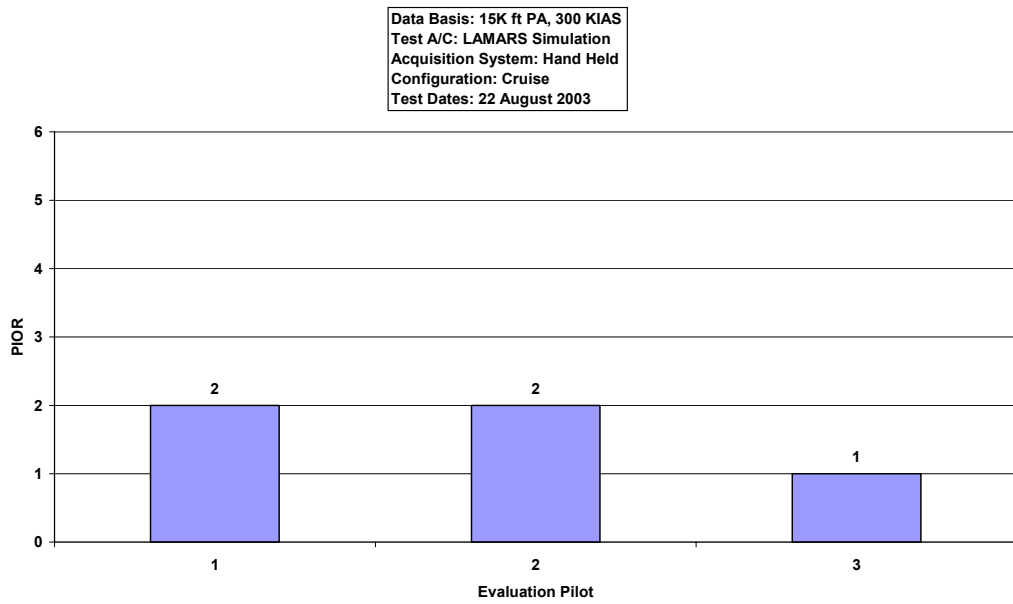


Figure D-36. LAMARS Phase 3 Target Tracking Data, Case Y, 60 deg/sec

MAX GAP (VISTA) Histograms

Handling Qualities Phase 2 Sum-of-sines Task

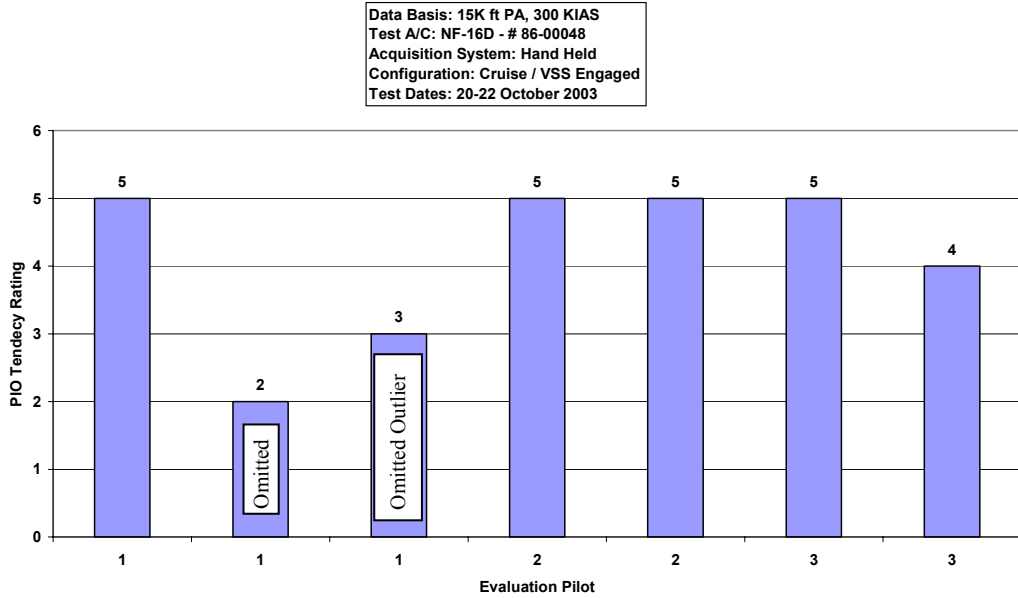


Figure D-37. VISTA Phase 2 Sum-of-sines Data, Case B, 15 deg/sec

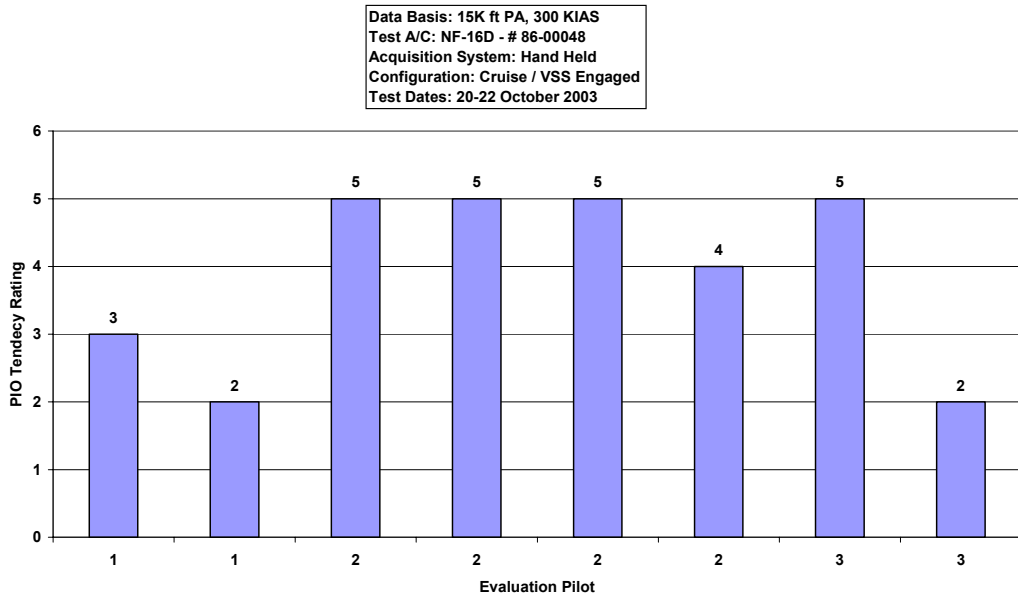


Figure D-38. VISTA Phase 2 Sum-of-sines Data, Case B, 30 deg/sec

Data Basis: 15K ft PA, 300 KIAS
 Test A/C: NF-16D - # 86-00048
 Acquisition System: Hand Held
 Configuration: Cruise / VSS Engaged
 Test Dates: 20-22 October 2003

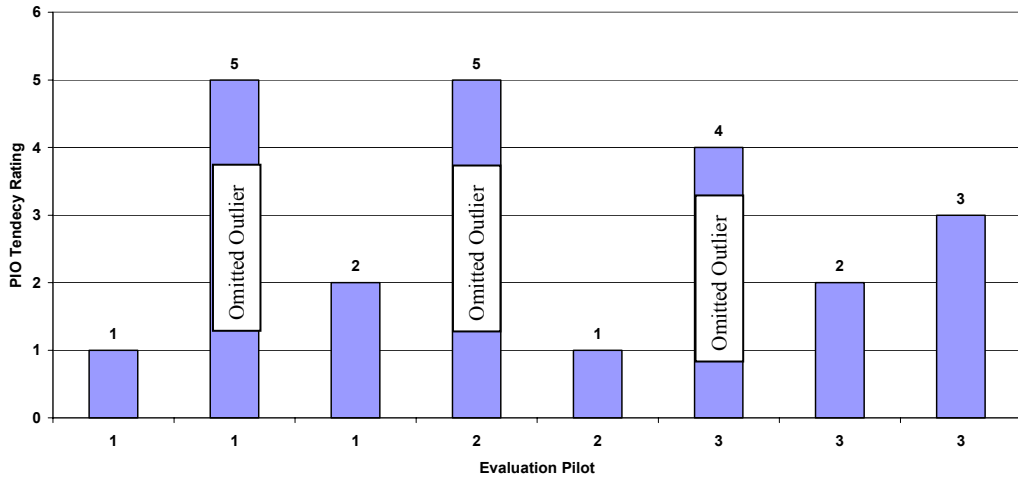


Figure D-39. VISTA Phase 2 Sum-of-sines Data, Case B, 60 deg/sec

Data Basis: 15K ft PA, 300 KIAS
 Test A/C: NF-16D - # 86-00048
 Acquisition System: Hand Held
 Configuration: Cruise / VSS Engaged
 Test Dates: 20-22 October 2003

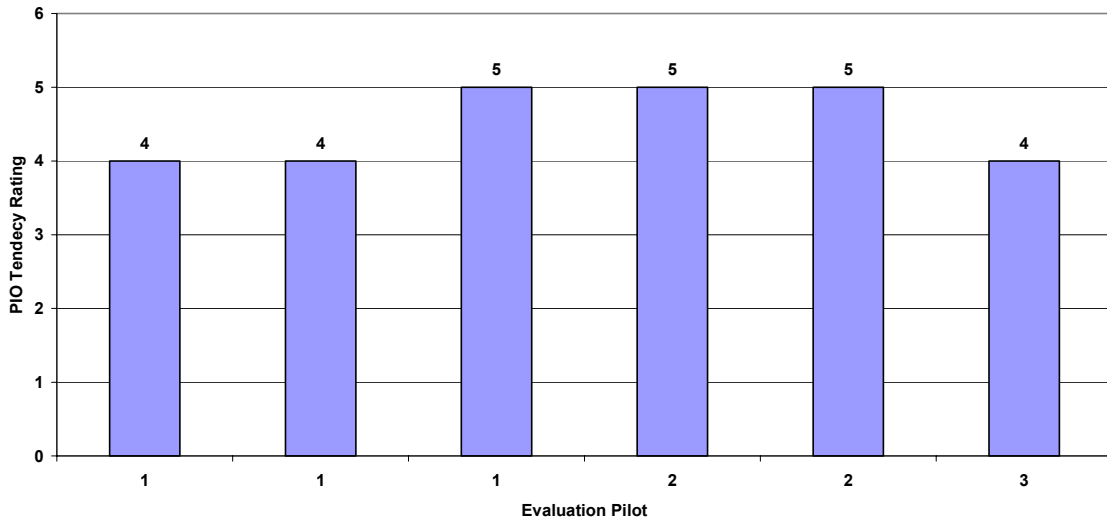


Figure D-40. VISTA Phase 2 Sum-of-sines Data, Case N, 15 deg/sec

Data Basis: 15K ft PA, 300 KIAS
 Test A/C: NF-16D - # 86-00048
 Acquisition System: Hand Held
 Configuration: Cruise / VSS Engaged
 Test Dates: 20-22 October 2003

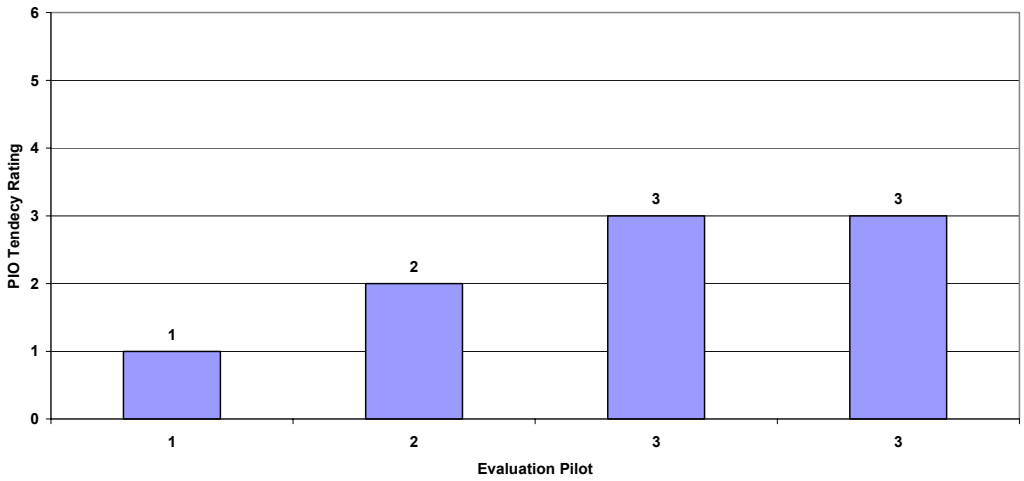


Figure D-41. VISTA Phase 2 Sum-of-sines Data, Case N, 30 deg/sec

Data Basis: 15K ft PA, 300 KIAS
 Test A/C: NF-16D - # 86-00048
 Acquisition System: Hand Held
 Configuration: Cruise / VSS Engaged
 Test Dates: 20-22 October 2003

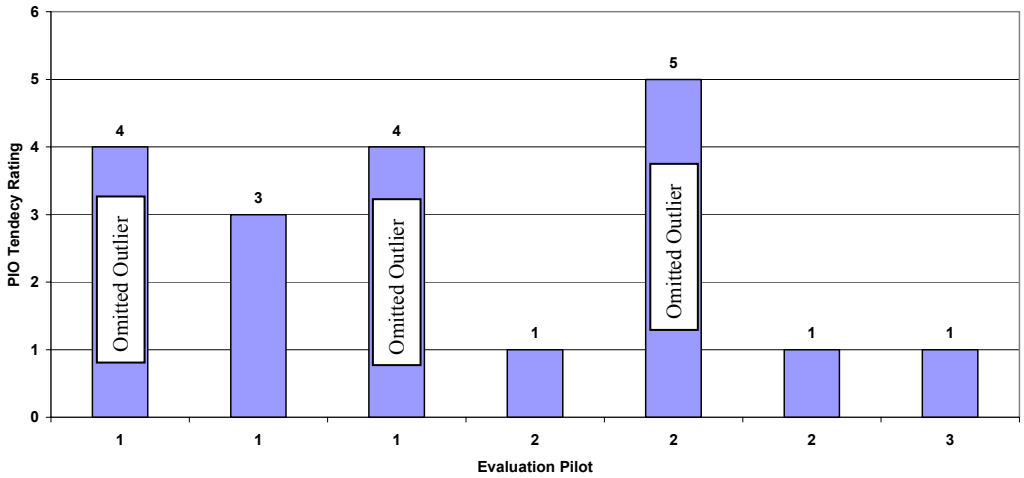


Figure D-42. VISTA Phase 2 Sum-of-sines Data, Case N, 60 deg/sec

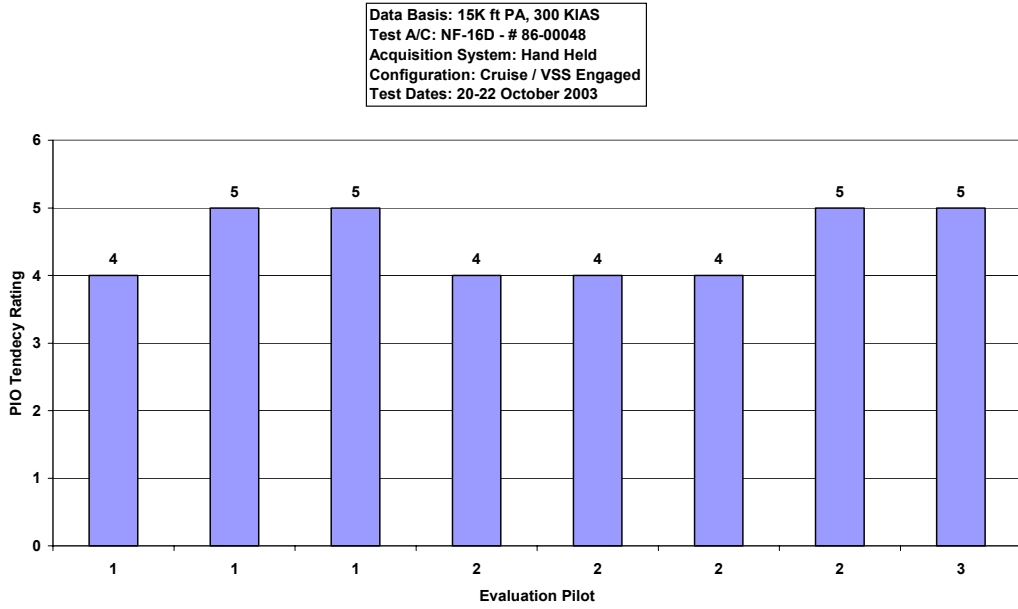


Figure D-43. VISTA Phase 2 Sum-of-sines Data, Case W, 15 deg/sec

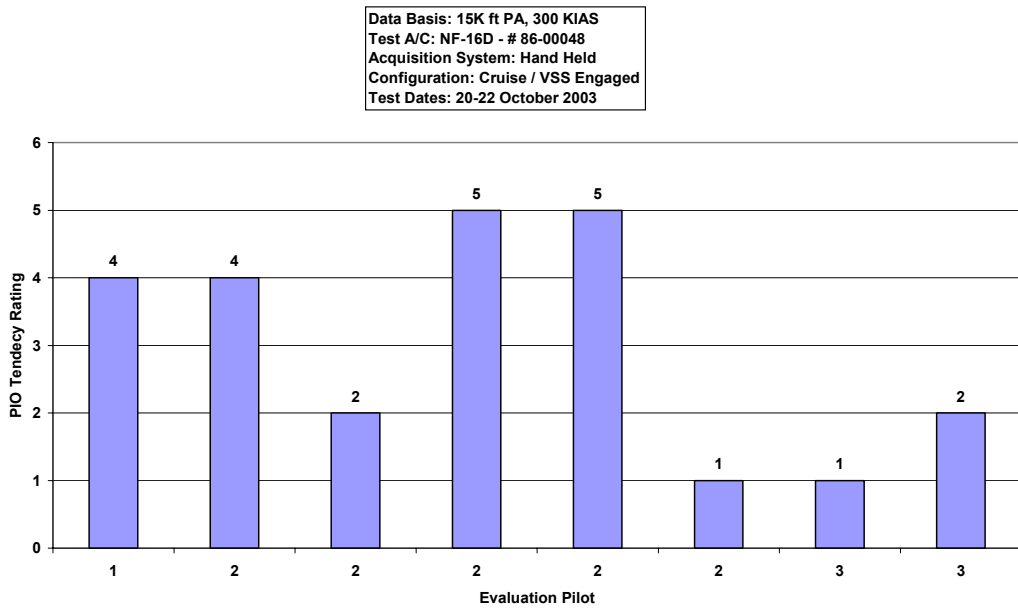


Figure D-44. VISTA Phase 2 Sum-of-sines Data, Case W, 30 deg/sec

Data Basis: 15K ft PA, 300 KIAS
 Test A/C: NF-16D - # 86-00048
 Acquisition System: Hand Held
 Configuration: Cruise / VSS Engaged
 Test Dates: 20-22 October 2003

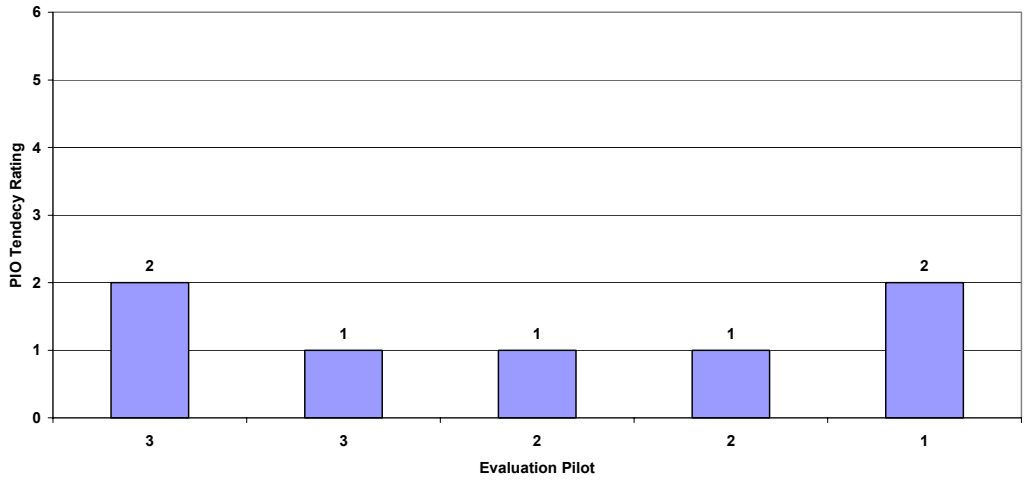


Figure D-45. VISTA Phase 2 Sum-of-sines Data, Case W, 60 deg/sec

Data Basis: 15K ft PA, 300 KIAS
 Test A/C: NF-16D - # 86-00048
 Acquisition System: Hand Held
 Configuration: Cruise / VSS Engaged
 Test Dates: 20-22 October 2003

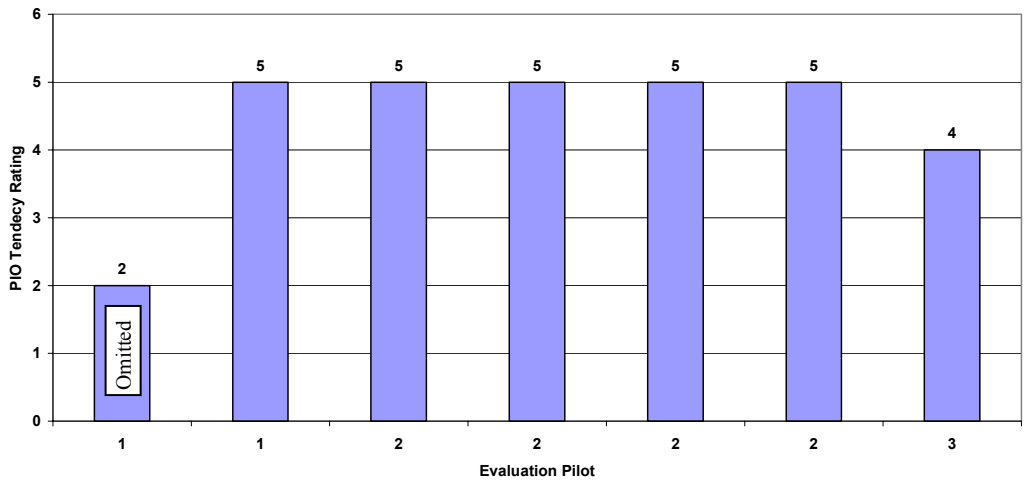


Figure D-46. VISTA Phase 2 Sum-of-sines Data, Case Y, 15 deg/sec

Data Basis: 15K ft PA, 300 KIAS
 Test A/C: NF-16D - # 86-00048
 Acquisition System: Hand Held
 Configuration: Cruise / VSS Engaged
 Test Dates: 20-22 October 2003

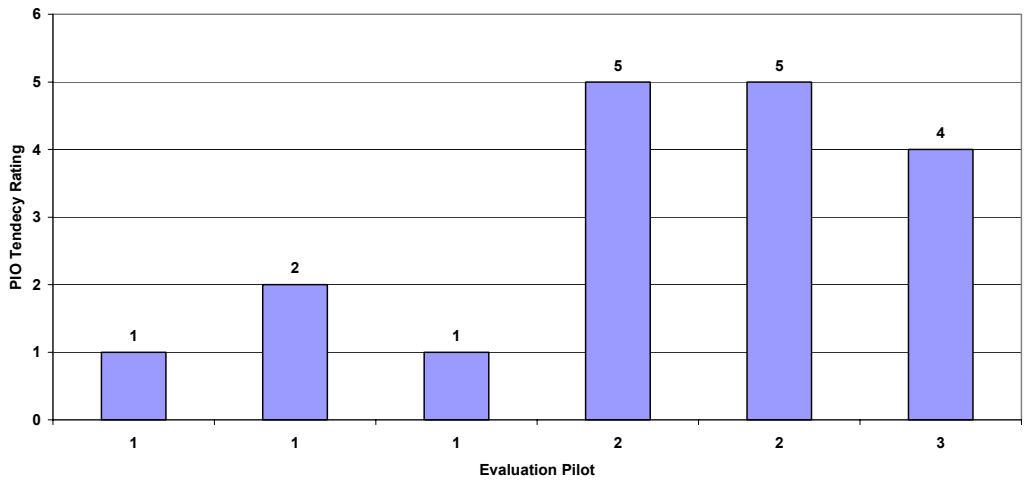


Figure D-47. VISTA Phase 2 Sum-of-sines Data, Case Y, 30 deg/sec

Data Basis: 15K ft PA, 300 KIAS
 Test A/C: NF-16D - # 86-00048
 Acquisition System: Hand Held
 Configuration: Cruise / VSS Engaged
 Test Dates: 20-22 October 2003

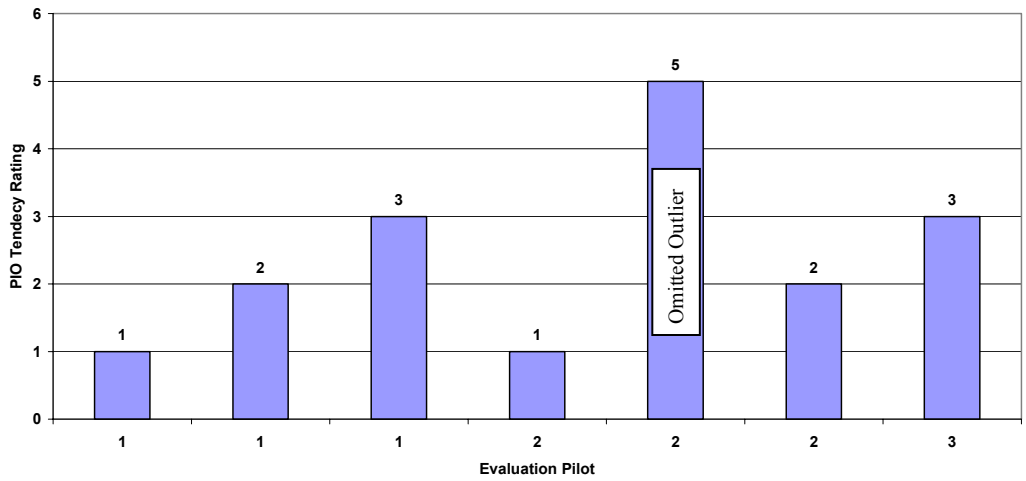


Figure D-48. VISTA Phase 2 Sum-of-sines Test Data, Case Y, 60 deg/sec

Handling Qualities Phase 3 Discrete HUD Pitch Tracking Task

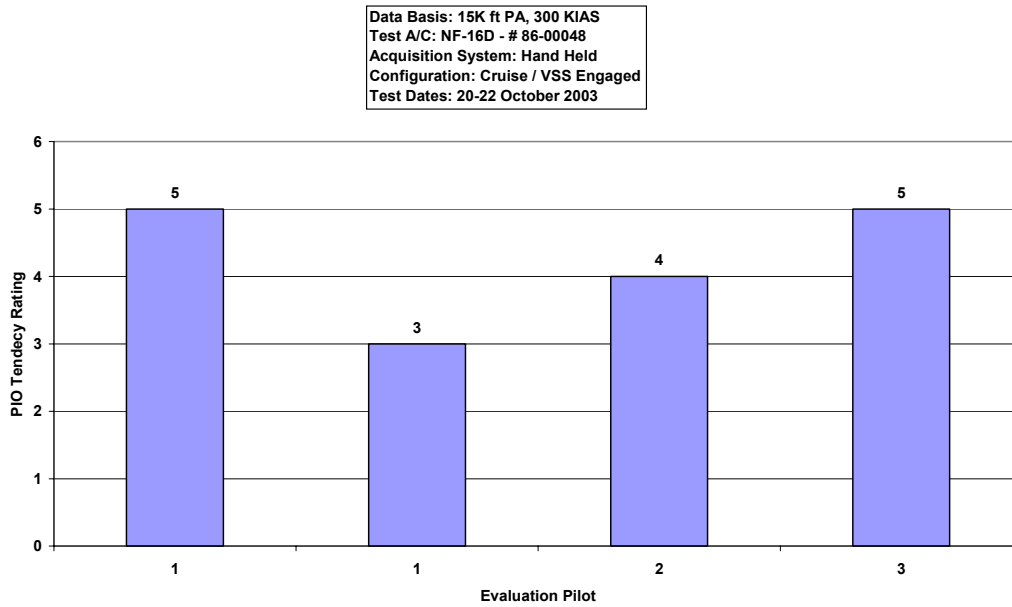


Figure D-49. VISTA Phase 3 Discrete HUD Pitch Tracking Data, Case B, 15 deg/sec

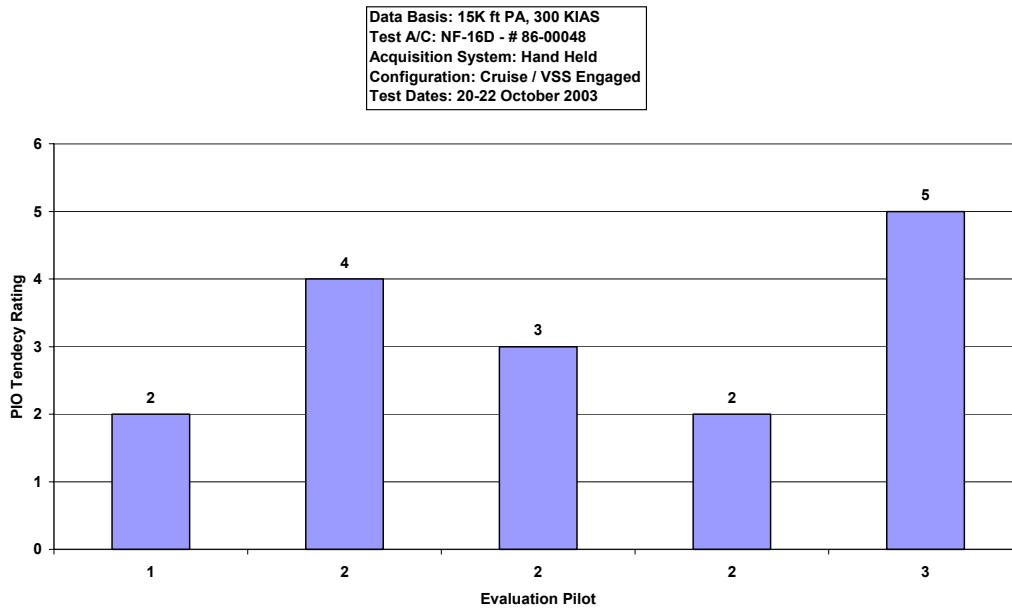


Figure D-50. VISTA Phase 3 Discrete HUD Pitch Tracking Data, Case B, 30 deg/sec

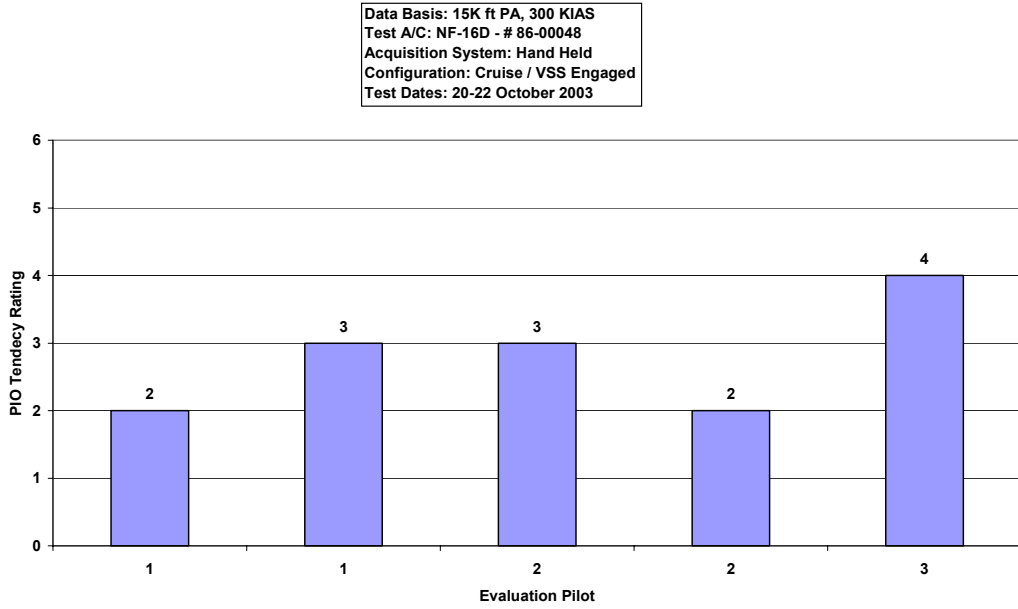


Figure D-51. VISTA Phase 3 Discrete HUD Pitch Tracking Data, Case B, 30 deg/sec

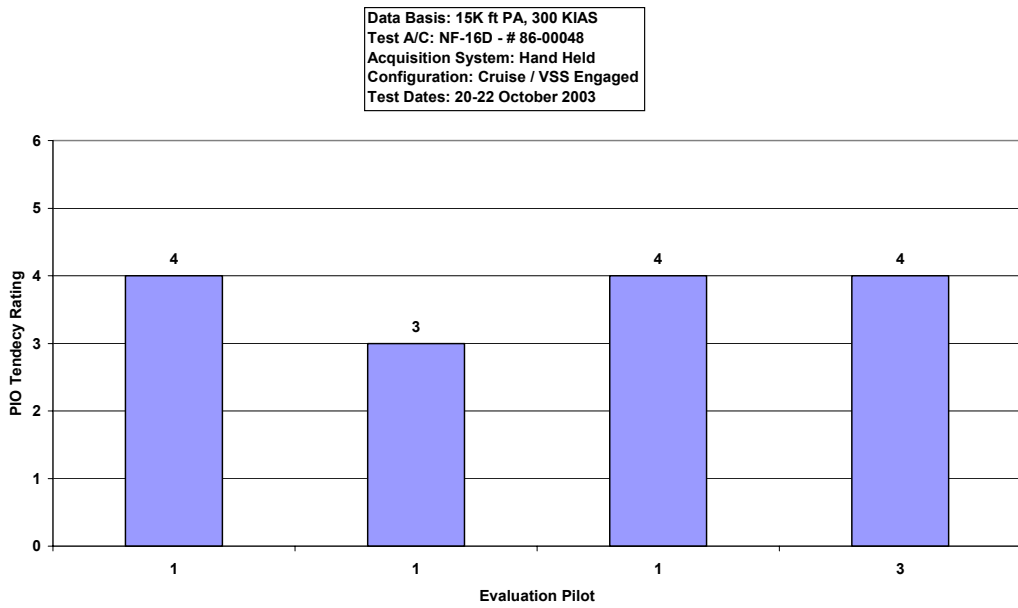


Figure D-52. VISTA Phase 3 Discrete HUD Pitch Tracking Data, Case N, 15 deg/sec

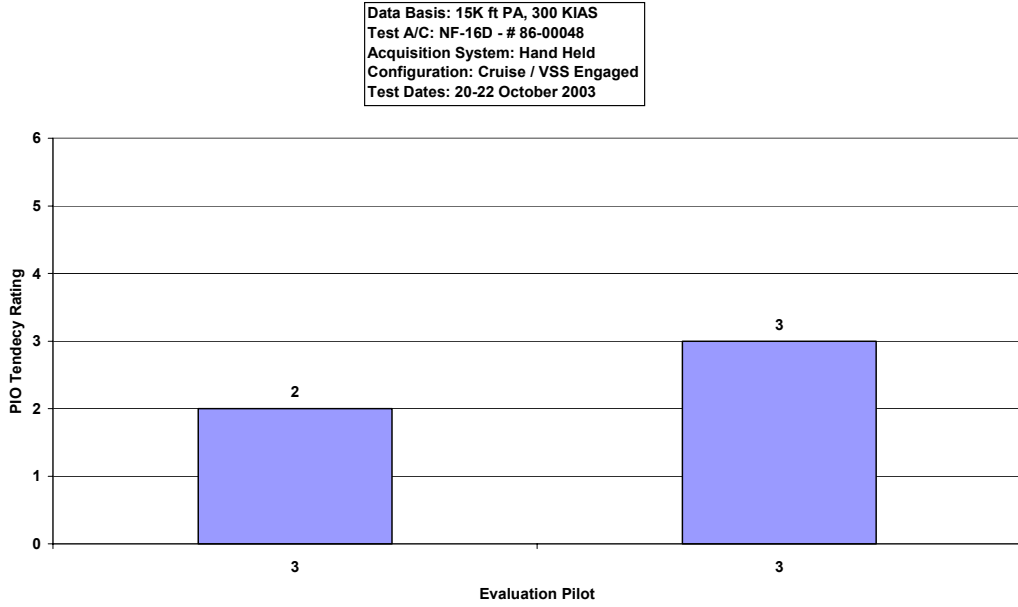


Figure D-53. VISTA Phase 3 Discrete HUD Pitch Tracking Data, Case N, 30 deg/sec

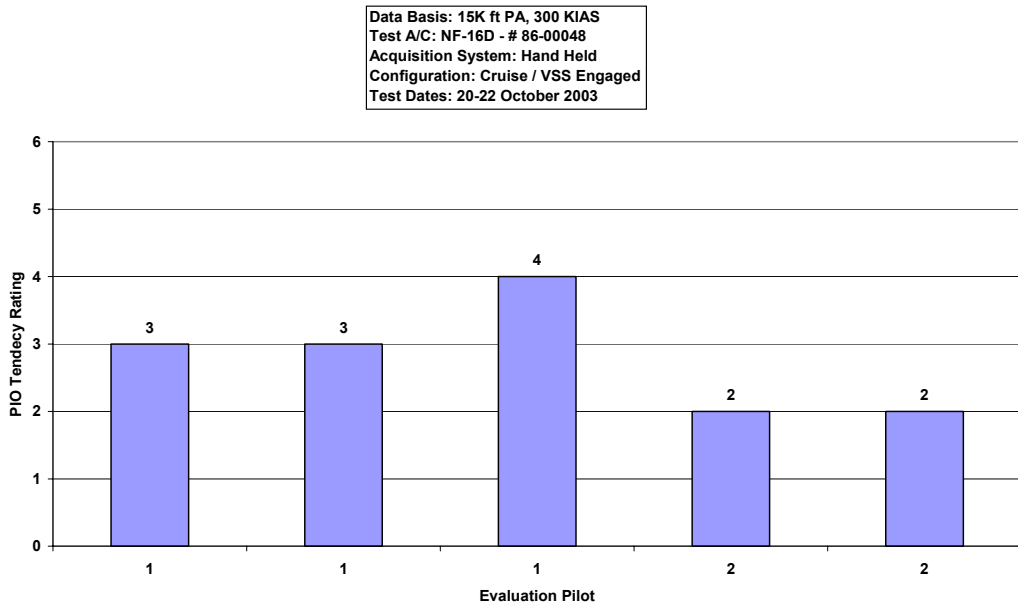


Figure D-54. VISTA Phase 3 Discrete HUD Pitch Tracking Data, Case N, 60 deg/sec

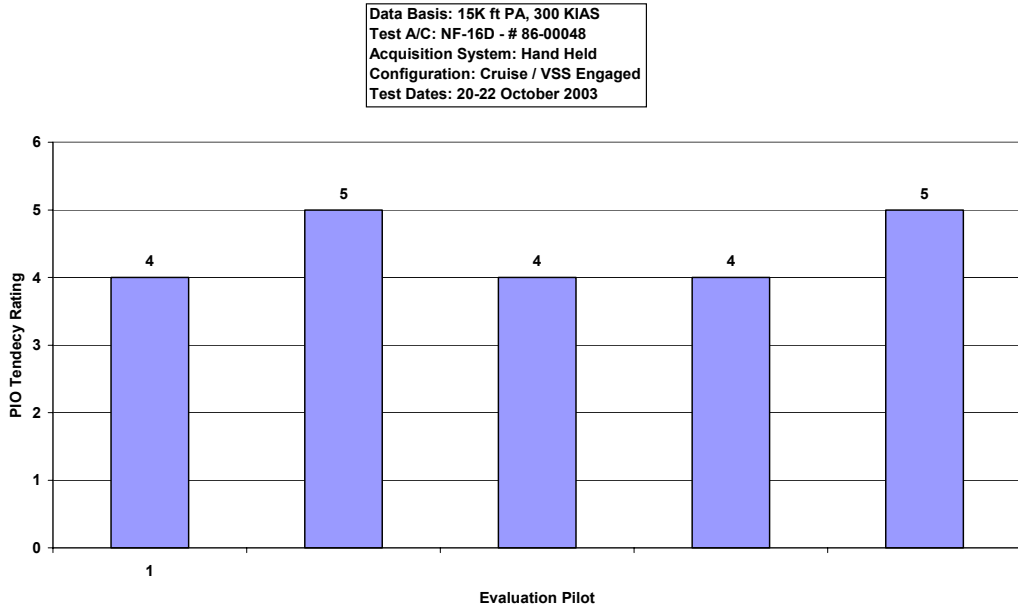


Figure D-55. VISTA Phase 3 Discrete HUD Pitch Tracking Data, Case W, 15 deg/sec

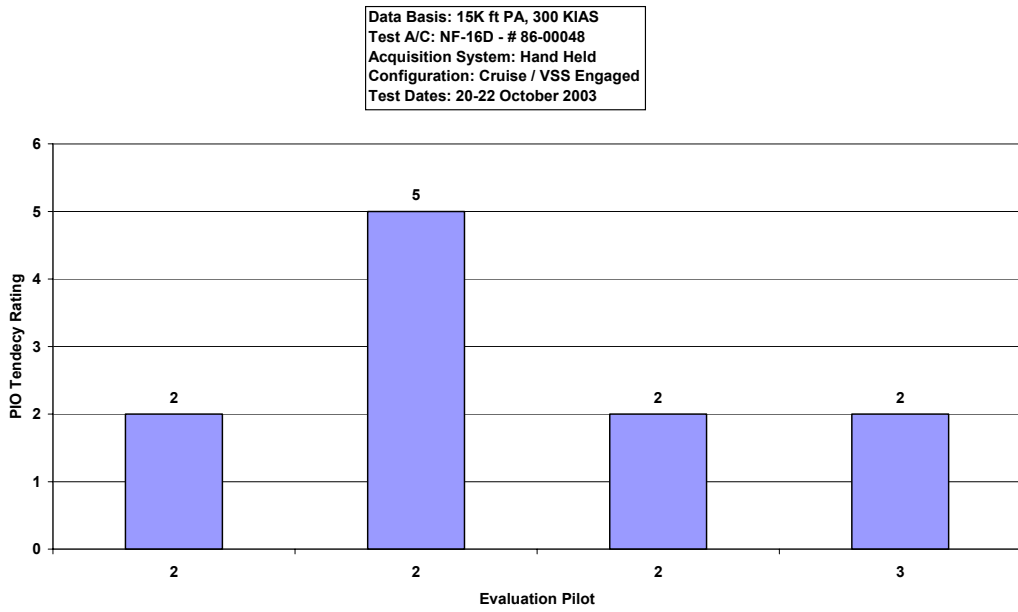


Figure D-56. VISTA Phase 3 Discrete HUD Pitch Tracking Data, Case W, 30 deg/sec

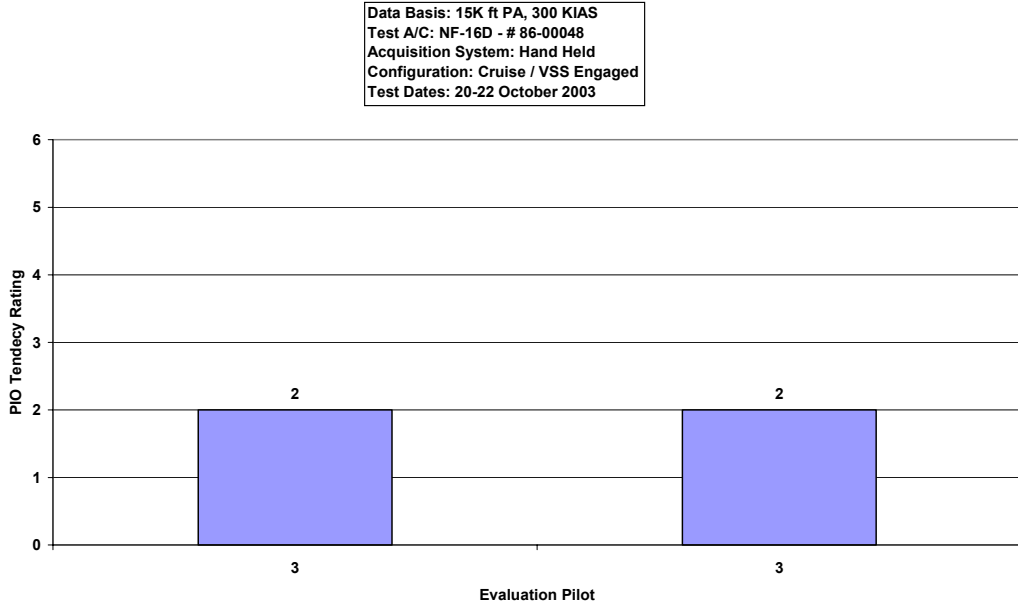


Figure D-57. VISTA Phase 3 Discrete HUD Pitch Tracking Data, Case W, 60 deg/sec

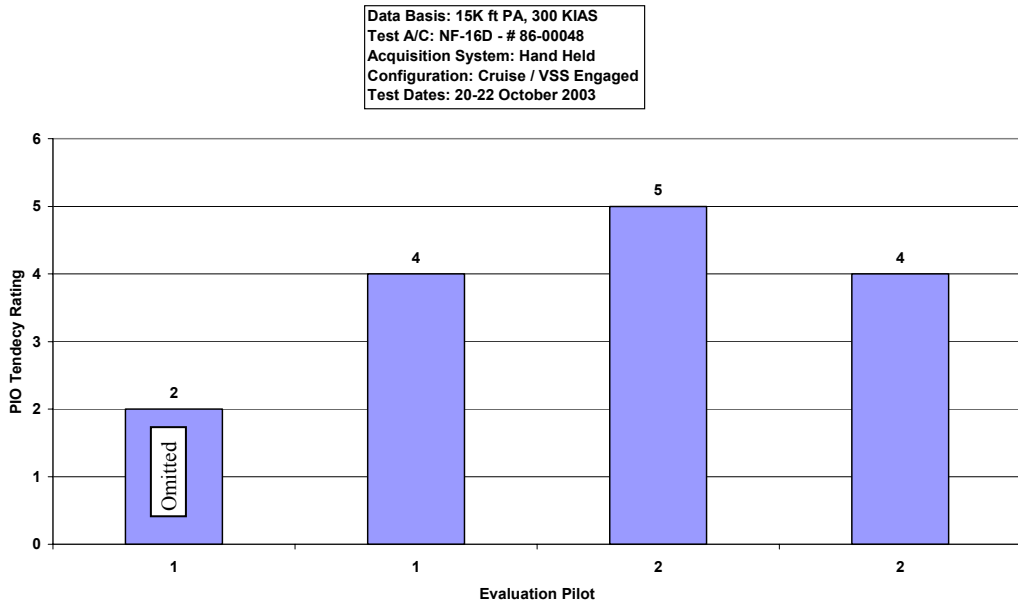


Figure D-58. VISTA Phase 3 Discrete HUD Pitch Tracking Data, Case Y, 15 deg/sec

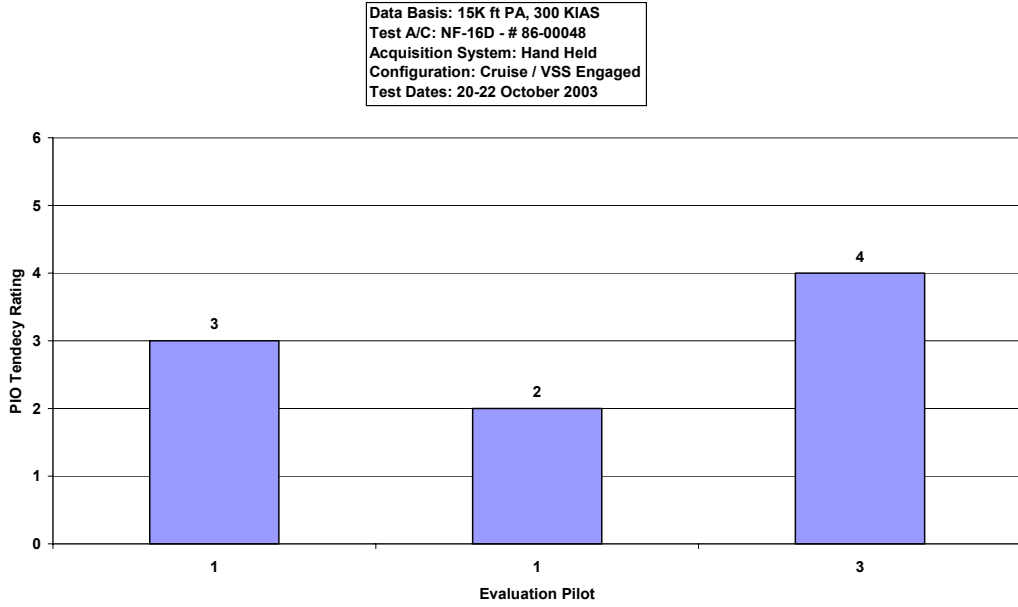


Figure D-59. VISTA Phase 3 Discrete HUD Pitch Tracking Data, Case Y, 30 deg/sec

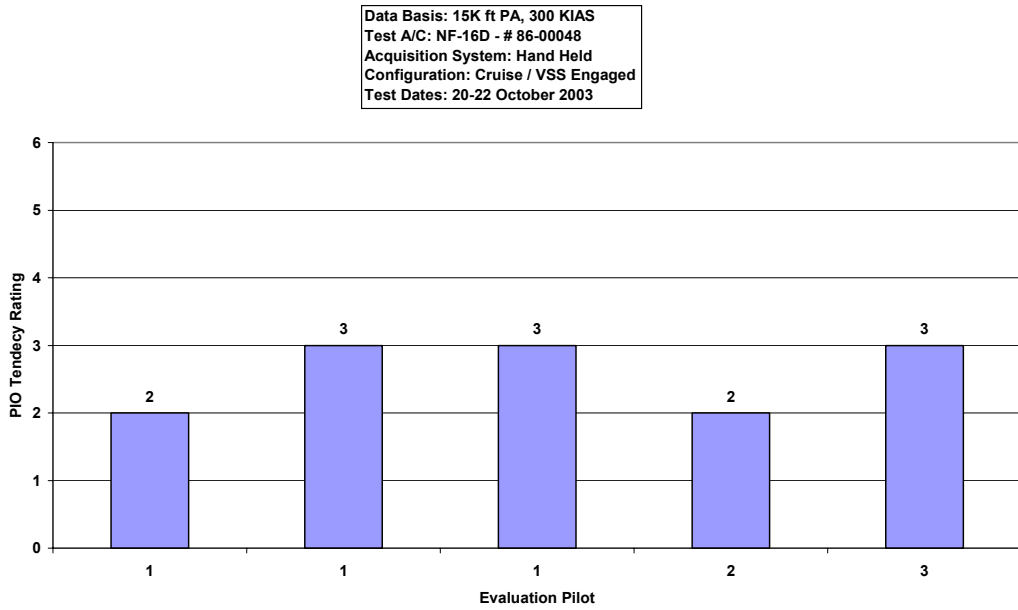


Figure D-60. VISTA Phase 3 Discrete HUD Pitch Tracking Data, Case Y, 60 deg/sec

Bibliography

- Ahlgren, Jan. *Report on the Accident Involving the JAS 39-1 Gripen February 2, 1989*. T1-1E-89. Government Accident Investigation Board (SHK), Sweden, March 1989.
- Anderson, Mark R. and Anthony B. Page. *Multivariable Analysis of Pilot-in-the-Loop Oscillations*. AIAA-95-3203-CP. Reston, VA: American Institute of Aeronautics and Astronautics, Inc., 1995.
- Brown, Frank and others. *Flying Qualities Testing*. Air Force Flight Test Center, Edwards AFB CA, 20 February 2002.
- Department of Defense. *Flying Qualities of Piloted Aircraft*. MIL-HDBK-1797. Washington: GPO, 19 December 1997.
- Dornheim, Michael A. "Boeing Corrects Several 777 PIOs," *Aviation Week and Space Technology*, 142 (19): 32–33 (1995).
- Doman, David B. and Lori Ann Foringer. *Interactive Flying Qualities Toolbox for Matlab, Version 2.0*. Computer Software. USAF Wright Laboratory, Flight Dynamics Directorate, Flight Control Division, Flying Qualities Section, Wright-Patterson AFB OH, August 1996.
- Duda, Holger. *Effects of Rate Limiting Elements in Flight Control Systems – A New PIO-Criterion*. AIAA-95-3204-CP. Reston, VA: American Institute of Aeronautics and Astronautics, Inc., 1995.
- Gilbreath, Greg and others. *A Limited Evaluation of a Pilot-Induced Oscillation Prediction Criterion (HAVE OLOP)*. AFFTC TIM-00-07. Air Force Flight Test Center, Edwards AFB, CA, December 2000.
- Gilbreath, Gregory P. *Prediction of Pilot-Induced Oscillations (PIO) Due to Actuator Rate Limiting Using the Open-Loop Onset Point (OLOP) Criterion*. MS Thesis, AFIT/GAE/ENY/01M-02, Graduate School of Engineering and Management, Air Force Institute of Technology (AU), Wright-Patterson AFB OH, March 2001.
- Hanley, James G. and others. *Comparison of Nonlinear Algorithms in the Prevention of Pilot-Induced Oscillations Caused by Actuator Rate Limiting (Project HAVE PREVENT)*. Air Force Flight Test Center, Edwards AFB CA, December 2002 (ADA410173).

- Hanley, James G. *A Comparison of Nonlinear Algorithms to Prevent Pilot-Induced Oscillations Caused by Actuator Rate Limiting*. MS thesis, AFIT/GAE/ENY/03-4. Graduate School of Engineering and Management, Air Force Institute of Technology (AU), Wright-Patterson AFB OH, March 2003 (ADA413992).
- Hodgkinson, John. *Aircraft Handling Qualities*. Reston, VA: American Institute of Aeronautics and Astronautics, Incorporated, 1999.
- Jensen, Clas and others. "JAS 39 Gripen EFCS: How to Deal with Rate Limiting." Unpublished report. SAAB, Sweden, Undated.
- Klyde, David H. and others. *Unified Pilot-Induced Oscillation Theory, Volume 1: PIO Analysis with Linear and Nonlinear Effective Vehicle Characteristics, Including Rate Limiting*. WL-TR-96-3028. Air Force Research Laboratories, Wright-Patterson AFB OH, December 1995.
- Liebst, Brad S. Class Handout, MECH 629, Aircraft Handling Qualities and Performance. Graduate School of Engineering and Management, Air Force Institute of Technology, Wright-Patterson AFB OH, July 2001.
- Liebst, Brad S. and others. "Nonlinear Pre-filter to Prevent Pilot-Induced Oscillations Due to Actuator Rate Limiting." *AIAA Journal of Guidance, Control, and Dynamics*, Vol. 25, No. 4: 740-747 (July 2002).
- MatlabTM /SimulinkTM*. Versions 6.1 and 6.5. Computer software. The Mathworks, Inc., Natick MA, 2001.
- McRuer, Duane T. *Pilot-Induced Oscillations and Human Dynamic Behavior*. NASA Contractor Report 4683. Hawthorne CA: Systems Technology, Inc., 1995
- Microsoft Excel*. Version 10.3506.3501 SP-1. Computer Software. Microsoft Corporation, Redmond WA, 2001.
- Mitchell, David G. and Roger H. Hoh. *Development of a Unified Method to Predict Tendencies for Pilot-Induced Oscillations*. WL-TR-95-3049. Air Force Research Laboratories, Wright-Patterson AFB OH, June 1995.
- Mitchell, David G. and David H Klyde. *A Critical Examination of PIO Prediction Criteria*. AIAA-98-4335. Reston, VA: American Institute of Aeronautics and Astronautics, Inc., 1998.
- Preston, Jeff D. and others. *Unified Pilot-Induced Oscillation Theory, Volume 2: Pilot-Induced Oscillation Criteria Applied to Several McDonnell Douglas Aircraft*. WL-TR-96-3029. Air Force Research Laboratories, Wright-Patterson AFB OH, December 1995 (ADB212157).

Slotine, Jean-Jacques E. and Weiping Li. *Applied Nonlinear Control*. Upper Saddle River, New Jersey: Prentice Hall, 1991.

Wheeler, Anthony J. and Ahmand R. Ganji. *Introduction to Engineering Experimentation*. Upper Saddle River, New Jersey: Prentice Hall, 1996.

Witte, Joel B. and others. *An Investigation Relating Longitudinal Pilot-induced Oscillation Tendency Ratings to Describing Function Predictions for Rate-limited Actuators (Project MAX GAP)*. Air Force Flight Test Center, Edwards AFB CA, December 2003.

Vita

Major Joel B. Witte was born in Ft Worth, Texas. He graduated from Burlison High School, Burlison, Texas in 1986. He earned a Bachelor of Science Degree in Aerospace Engineering from Texas A&M University in 1990.

After graduation, Major Witte entered Undergraduate Pilot Training at Reese AFB, Texas in January 1992. He received his wings one year later and was assigned to fly the C-27A at Howard AFB, Panama. His follow-on assignments included flying the C-141B and C-17A at Charleston AFB, South Carolina and McChord AFB, Washington. He has accumulated more than 2800 hours flying time.

Major Witte was selected for the joint Air Force Institute of Technology/USAF Test Pilot School program in February 2001 and began classes at AFIT in September. After graduation from AFIT/TPS, he will test Special Operations C-130s at Hurlburt Field, Florida.

Major Witte is a graduate of Test Pilot School, Class 03A – “The Centurions.”

REPORT DOCUMENTATION PAGE

Form Approved
OMB No. 074-0188

The public reporting burden for this collection of information is estimated to average 1 hour per response, including the time for reviewing instructions, searching existing data sources, gathering and maintaining the data needed, and completing and reviewing the collection of information. Send comments regarding this burden estimate or any other aspect of the collection of information, including suggestions for reducing this burden to Department of Defense, Washington Headquarters Services, Directorate for Information Operations and Reports (0704-0188), 1215 Jefferson Davis Highway, Suite 1204, Arlington, VA 22202-4302. Respondents should be aware that notwithstanding any other provision of law, no person shall be subject to a penalty for failing to comply with a collection of information if it does not display a currently valid OMB control number.

PLEASE DO NOT RETURN YOUR FORM TO THE ABOVE ADDRESS.

1. REPORT DATE (DD-MM-YYYY) 03-2004		2. REPORT TYPE Master's Thesis		3. DATES COVERED (From - To) Apr 2002 - Mar 2004	
4. TITLE AND SUBTITLE 5. AN INVESTIGATION RELATING LONGITUDINAL PILOT-INDUCED OSCILLATION TENDENCY RATING TO DESCRIBING FUNCTION PREDICTIONS FOR RATE-LIMITED ACTUATORS			5a. CONTRACT NUMBER		
			5b. GRANT NUMBER		
			5c. PROGRAM ELEMENT NUMBER		
			5d. PROJECT NUMBER		
6. AUTHOR(S) Witte, Joel B. Major, USAF			5e. TASK NUMBER		
			5f. WORK UNIT NUMBER		
			8. PERFORMING ORGANIZATION REPORT NUMBER AFIT/GAE/ENY/04-M16		
7. PERFORMING ORGANIZATION NAMES(S) AND ADDRESS(S) Air Force Institute of Technology Graduate School of Engineering and Management (AFIT/EN) 2950 P Street, Building 640 WPAFB OH 45433-7765			10. SPONSOR/MONITOR'S ACRONYM(S)		
9. SPONSORING/MONITORING AGENCY NAME(S) AND ADDRESS(ES) USAF TPS 220 Wolfe Ave Edwards AFB CA 93524 DSN: 527-3000					
11. SPONSOR/MONITOR'S REPORT NUMBER(S)			12. DISTRIBUTION/AVAILABILITY STATEMENT APPROVED FOR PUBLIC RELEASE; DISTRIBUTION UNLIMITED		
14. ABSTRACT The purpose of this study was to investigate pilot-induced oscillations (PIO) and determine a method by which PIO tendency rating could be predicted. In particular, longitudinal PIO in the presence of rate-limited actuators were singled out for examination. Sinusoidal input/triangular output describing function techniques using Nichols charts were used. A new criterion dubbed <i>Gap Criterion</i> was calculated for PIO sensitivity. This criterion consists of the product of pilot gain necessary to cause PIO and the normalized maximum amplitude of the commanded actuator. These results were paired with simulator and flight test PIO tendency rating data. The PIO rating scale used was the PIO tendency classification of MIL-HDBK-1797. This concept was applied to two historical test databases, HAVE PREVENT and HAVE OLOP. Additional PIO data was gathered in the Large Amplitude Multimode Aerospace Simulator (LAMARS) at the Air Force Research Laboratory (AFRL), Wright-Patterson AFB, Ohio and the USAF NF-16D Variable In-flight Stability Test Aircraft (VISTA) at Edwards AFB, California. Correlation between PIO tendency rating and <i>Gap Criterion</i> was determined for each dataset. Most datasets exceeded a confidence level of 95% that a correlation existed. Follow-on analysis for best curve fit was also accomplished with a logarithmic fit deemed best. Datasets were combined with success to demonstrate the universality of the <i>Gap Criterion</i> for correlating PIO tendency ratings.					
15. SUBJECT TERMS handling qualities pilot-induced oscillations pilot-induced oscillation prediction rate limiting flight controls					
16. SECURITY CLASSIFICATION OF:		17. LIMITATION OF ABSTRACT	18. NUMBER OF PAGES	19a. NAME OF RESPONSIBLE PERSON	
REPORT	ABSTRACT	c. THIS PAGE	UU	Dr Brad Liebst, AFIT ENY	
U	U	U	154	19b. TELEPHONE NUMBER (Include area code) (937) 255-3636, ext 4636	